Synthesis of pencil-beam antenna arrays with low dynamic range ratio of excitation coefficients

Vodvarka, Katarina

Doctoral thesis / Disertacija

2024

Degree Grantor / Ustanova koja je dodijelila akademski / stručni stupanj: **University of Zagreb, Faculty of Electrical Engineering and Computing / Sveučilište u Zagrebu, Fakultet elektrotehnike i računarstva**

Permanent link / Trajna poveznica: <https://urn.nsk.hr/urn:nbn:hr:168:560269>

Rights / Prava: [In copyright](#)/[Zaštićeno autorskim pravom.](#)

Download date / Datum preuzimanja: **2025-03-08**

University of Zagreb

FACULTY OF ELECTRICAL ENGINEERING AND COMPUTING

Katarina Vodvarka

SYNTHESIS OF PENCIL-BEAM ANTENNA ARRAYS WITH LOW DYNAMIC RANGE RATIO OF EXCITATION COEFFICIENTS

DOCTORAL THESIS

Zagreb, 2024

University of Zagreb

FACULTY OF ELECTRICAL ENGINEERING AND COMPUTING

Katarina Vodvarka

SYNTHESIS OF PENCIL-BEAM ANTENNA ARRAYS WITH LOW DYNAMIC RANGE RATIO OF EXCITATION COEFFICIENTS

DOCTORAL THESIS

Supervisor:

Professor Mladen Vučić, PhD

Zagreb, 2024

Sveučilište u Zagrebu

FAKULTET ELEKTROTEHNIKE I RAČUNARSTVA

Katarina Vodvarka

SINTEZA ANTENSKIH NIZOVA S USKOM GLAVNOM LATICOM I MALIM DINAMIČKIM RASPONOM POBUDNIH KOEFICIJENATA

DOKTORSKI RAD

Mentor:
Prof. dr. sc. Mladen Vučić

Zagreb, 2024.

About the supervisor

Mladen Vučić was born in Karlovac in 1965. He received Diploma Engineer, M.Sc. and Ph.D. degrees in electrical engineering from the University of Zagreb, Faculty of Electrical Engineering and Computing (FER), Zagreb, Croatia, in 1989, 1993 and 1999, respectively.

Since March 1989 he has been working at the Department of Electronic Systems and Information processing at FER. In 2001 he was promoted to an Assistant Professor, in 2006 to an Associate Professor, in 2011 to a Professor and in 2016 to a Full Professor. He led three scientific and one research project, and participated in four other projects funded by the Ministry of Science and Technology of the Republic of Croatia. Furthermore, he led one research project funded by the Croatian Science Foundation. He also participated in one EU FP7 project and one project funded by the European Regional Development Fund. He is a member of the Centre of Research Excellence for Data Science and Cooperative Systems. He published more than 60 papers in journals and conference proceedings in the area of circuit theory, analog and digital signal processing, optimization theory and applications, digital system design, and embedded systems.

Prof. Vučić is a member of IEEE and KoREMA. From 2013 to 2016 he served as the chair of *IEEE Circuits and Systems Chapter Croatia*. From 2016 to 2018 he was Head of the Department of Electronic Systems and Information Processing at FER. In 1997, he was awarded from the Ministry of Defence and the Ministry of Science and Technology of the Republic of Croatia by the *Annual award for scientific contribution to the development and strengthening of the defence system of the Republic of Croatia*. In 2019, he received the *Fran Bošnjaković* award from the University of Zagreb.

O mentoru

Mladen Vučić rođen je u Karlovcu 1965. godine. Diplomirao je, magistrirao i doktorirao u polju elektrotehnike na Sveučilištu u Zagrebu, Fakultetu elektrotehnike i računarstva (FER), 1989., 1993. odnosno 1999. godine.

Od ožujka 1989. godine radi na Zavodu za elektroničke sustave i obradbu informacija FER-a. Godine 2001. izabran je u znanstveno-nastavno zvanje docenta, 2006. u zvanje izvanrednog profesora, 2011. u zvanje redovitog profesora, a 2016. u zvanje redovitog profesora u trajnom izboru. Dosad je vodio tri znanstvenoistraživačka i jedan tehnologijski istraživačko razvojni projekt, te je sudjelovao na još četiri znanstvenoistraživačka projekta Ministarstva znanosti i tehnologije Republike Hrvatske. Vodio je jedan projekt koji je financiran od Hrvatske zaklade za znanost. Također, bio je istraživač na jednom EU FP7 projektu te na jednom projektu financiranom iz Europskog fonda za regionalni razvoj. Član je Znanstvenog centra izvrsnosti za znanost o podatcima i kooperativne sustave. Objavio je više od 60 radova u časopisima i zbornicima konferencija u području teorije električnih krugova, analogne i digitalne obrade signala, teorije i primjene optimizacijskih postupaka, dizajna digitalnih sustava te ugradbenih računalnih sustava.

Prof. Vučić član je udruga IEEE i KoREMA. Od 2013. do 2016. godine bio je predsjednik Odjela za električne krugove i sustave Hrvatske sekcije IEEE. Od 2016. do 2018. godine bio je predstojnik Zavoda za elektroničke sustave i obradbu informacija FER-a. 1997. godine dobio je *Godišnju nagradu za sveukupne znanstveno-istraživačke doprinose razvoju i jačanju sustava obrane Republike Hrvatske*, koju su zajednički dodijelili Ministarstvo obrane i Ministarstvo znanosti i tehnologije Republike Hrvatske. 2019. godine dobio je *Nagradu Fran Bošnjaković* koju je dodijelilo Sveučilište u Zagrebu.

Acknowledgement

I want to express my gratitude to my supervisor Mladen Vučić, for granting me the opportunity to pursue doctoral studies and for the significant time he invested in the work presented in this dissertation.

I would like to thank the committee members for taking the time to read my dissertation and for being on the committee.

Also, thanks to all the amazing colleagues I've met and worked with.

I would also like to thank my family, parents Mirjana and Josip, brother Luka, and sister Marina, for cheering for me throughout my studies.

In the end, I would like to thank my husband Mislav for his constant encouragement and support and for always believing in me.

Abstract

Antenna arrays used in modern communication systems are designed to satisfy several functional and implementation requirements. The former arise from the desired radiation pattern, requiring high beam efficiency, high directivity, low sidelobe level (SLL), etc. The latter are determined by real-world parameters of the beamforming networks, such as mutual coupling, dynamic range ratio (DRR) of excitation coefficients, etc. The best results are achieved if both requirements are simultaneously included in the array design. Such a design can be easily formulated as an optimization problem, with the positions and excitations of antenna elements playing the role of optimization variables. In this context, the dissertation considers the design of linear and planar pencil-beam antenna arrays with low dynamic range ratio of excitation coefficients. Three new methods are proposed.

The first method is based on convex optimization. It is suitable for the design of linear pencil beam arrays optimum in L_1 sense. The obtained arrays exhibit maximum SLL of approximately -21 dB for all array sizes, with the lobes that monotonically decrease as the angle increases. The DRR of excitation coefficients of these arrays increases linearly with the number of elements and generally takes low values.

The second method extends the design of L_1 pencil beams. The original convex optimization problem is here equipped with the constraints set on maximum dynamic range ratio and on maximum sidelobe level. Unfortunately, the obtained problem is not convex. For its solving, a global optimization method is developed. It utilizes global search based on branch and bound algorithm that employs convex optimization and feasibility test for tree pruning. The method supports independent control of DRR and SLL.

The third method is developed for the design of uniformly-excited unequally-spaced antenna arrays. The design of such arrays leads to nonlinear and nonconvex problems. For their solving, general-purpose methods for nonlinear optimization have been utilized. The application of these methods proved efficient in unconstrained and constrained design of linear and planar arrays with maximum beam efficiency and with maximum directivity. The proposed approach ensures fast convergence and enables very simple formulation of the design problems.

Keywords: antenna array, beam efficiency, branch and bound, convex optimization, directivity, dynamic range ratio, global optimization, L_1-norm, nonlinear optimization, pencil beam, unequally spaced array, uniform excitation.

Prošireni sažetak

Sinteza atenskih nizova s uskom glavnom laticom i malim dinamičkim rasponom koeficijenata

Moderni bežični komunikacijski sustavi zahtijevaju antenske nizove koji daju optimalne dijagrame zračenja. Neki od zahtjeva koje antenski nizovi korišteni u 5G mobilnim komunikacijama i u satelitskim sustavima moraju ispuniti su visoka učinkovitost glavne latice, velika usmjerenost, niske razine bočnih latica i jednostavnost pobudne mreže. Željeni dijagrami zračenja uobičajeno se ostvaruju korištenjem antenskih nizova s jednoliko razmaknutim i nejednoliko pobuđenim antenskim elementima. Međutim, nejednolika pobuda obično zahtijeva upotrebu pojačala s velikim dinamičkim rasponom koja rade na visokim frekvencijama, što rezultira skupim i složenim pobudnim mrežama. Stoga, kako bi se dobili željeni dijagrami zračenja uz korištenje jednostavnih pobudnih mreža, potrebno je dizajnirati antenske nizove s malim dinamičkim rasponom pobudnih koeficijenata. Jednostavnost pobudne mreže može se osigurati i korištenjem jedinične pobude na svim antenskim elementima te odabirom odgovarajućih pozicija elemenata. Na taj način dobivaju se željeni dijagrami zračenja uz najmanji mogući dinamički raspon koeficijenata. Navedeni ciljevi mogu se ostvariti upotrebom numeričke optimizacije. U praksi se koriste razni oblici dijagrama zračenja, npr. dijagrami s uskom glavnom laticom, sa širokom glavnom laticom, s više glavnih latica, itd. U ovoj disertaciji naglasak je stavljen na antenske nizove s uskom glavnom laticom. Glavna latica je u svim razmatranim slučajevima usmjerena okomito na os ili ravninu u kojoj se nalaze elementi niza. U takvim nizovima pobudni koeficijenti su realni brojevi.

Imajući spomenute zahtjeve na umu, cilj istraživanja provedenog u sklopu ove disertacije je unaprijediti postojeće te razviti nove metode za sintezu antenskih nizova s uskom glavnom laticom i malim dinamičkim rasponom pobudnih koeficijenata. U tom kontekstu provedeno istraživanje nudi sljedeći doprinos:

1. Sinteza linearnih antenskih nizova s uskom glavnom laticom i minimalnom L_1-normom temeljena na konveksnoj optimizaciji.

2. Metoda za globalnu optimizaciju linearnih antenskih nizova s uskom glavnom laticom, ograničenim dinamičkim rasponom pobudnih koeficijenata i minimalnom L_1-normom.

3. Metoda za dizajn antenskih polja s jednako pobuđenim nejednoliko razmaknutim antenskim elementima temeljena na optimizacijskim postupcima opće namjene.

Disertacija je podijeljena u sedam poglavlja. Prvo poglavlje je uvodno i opisuje strukturu disertacije. Drugo poglavlje opisuje antenske nizove te daje definiciju dijagrama zračenja.

Opisane su značajke dijagrama zračenja te implementacijski aspekti koje je potrebno uzeti u obzir prilikom dizajna nizova. U značajke dijagrama zračenja ubrajaju se bočne latice i njihove razine, širina glavne latice, usmjerenost te učinkovitost glavne latice. Implementacijski aspekti odnose se na dinamički raspon pobudnih koeficijenata te na prostorni razmještaj antena. Osim utjecaja na kompleksnost pobudnih mreža, dinamički raspon koeficijenata utječe i na elektromagnetsku spregu antenskih elemenata, koja ima negativan utjecaj na oblik dijagrama zračenja. Naime, poznato je da mali dinamički raspon koeficijenata smanjuje utjecaj elektromagnetske sprege. Smanjenje sprege moguće je postići i postavljanjem antenskih elemenata na odgovarajuće pozicije, pritom osiguravajući dovoljno veliki razmak između elemenata. Elementi u nizu mogu biti postavljeni tako da budu jednoliko ili nejednoliko razmaknuti. Kod antenskih nizova s jednoliko razmaknutim elementima, najčešće odabrani razmak je $\lambda/2$. Takav razmještaj omogućava upotrebu metoda za dizajn filtara s konačnim impulsnim odzivom (FIR) za izračun pobudnih koeficijenata antenskih elemenata. Nadalje, u takvim nizovima ne dolazi do pojave neželjenih bočnih latica. Kada su elementi u nizu nejednoliko razmaknuti, gubi se periodičnost pozicija. Na taj se način smanjuju razine neželjenih bočnih latice te se smanjuje utjecaj elektromagnetske sprege. Također, ako se pozicije uvedu u dizajn kao varijable, moguće je dobiti željeni dijagram zračenja korištenjem jedinične pobude.

Drugo poglavlje također sadrži pregled literature iz područja istraživanja. Navedene su dosad razvijene analitičke i optimizacijske metode za dizajn linearnih antenskih nizova s malim dinamičkim rasponom koeficijenata. Analitičke metode su brze i pouzdane, ali rijetko daju optimalne dijagrame zračenja u slučajevima kada je potrebno ograničiti dinamički raspon koeficijenata. S druge strane, optimizacija omogućava bolju kontrolu specifikacija dizajna te je zbog toga često upotrebljavana u dizajnu antenskih nizova. Optimizacijski problem koji sadrži ograničenja dinamičkog raspona koeficijenata je nekonveksan. Zbog toga su razvijene mnogobrojne metode s ciljem približavanja globalnom rješenju. Neke metode rješavaju relaksirani problem, npr. minimiziraju dinamički raspon podrazumijevajući da su svi koeficijenti isključivo pozitivni. Druge pristupaju originalnom problemu tako da ga pretvaraju u niz problema koji se rješavaju iterativno. Također, koriste se i evolucijski algoritmi, koji postaju sve popularniji za rješavanje nekonveksnih problema. Navedene metode nažalost ne garantiraju globalnost pronađenog rješenja. Jedina dosad razvijena metoda koja nudi globalno rješenje za problem minimizacije razine bočnih latica uz ograničen dinamički raspon koeficijenata temelji se na grananju i ograničavanju. Nadalje, u drugom poglavlju analizirane su i optimizacijske metode za dizajn rijetkih nizova s ograničenim dinamičkim rasponom, metode za dizajn nizova s nejednoliko razmaknutim elementima i malim dinamičkim rasponom koeficijenta te, konačno, metode za dizajn nizova s nejednoliko razmaknutim jednako pobuđenim elementima. Optimizacijski problemi koji sadrže pozicije elemenata kao varijable su izrazito nelinearni i nekonveksni. Tijekom godina predložene su mnoge metode za rješavanje takvih problema.

Međutim, niti jedna od njih ne daje globalno rješenje. Najveći dio istraživanja posvećen je pronalasku pozicija koje će dati minimalnu razinu bočnih latica, dok su ciljevi poput dobivanja maksimalne učinkovitosti glavne latice i maksimalne usmjerenosti manje zastupljeni u literaturi. Kod rješavanja ovih problema često se susreće ideja primjene Taylorove aproksimacije, što omogućava raspis originalnog problema u niz konveksnih problema koji se rješavaju iterativno. Osim toga, popularni su evolucijski algoritmi poput optimizacije rojem čestica, genetski algoritmi, optimizacija po uzoru na ponašanje sivih vukova i sl.

Budući da su u disertaciji predložene metode za dizajn antenskih nizova koje se temelje na optimizaciji, u trećem poglavlju dani su osnovni pojmovi vezani uz to područje te pregled odabranih optimizacijskih postupaka. Opisane su metode za konveksnu optimizaciju: linearno programiranje, kvadratno programiranje te optimizacija konveksne funkcije nad prostorom omeđenim stošcima drugog reda. Nadalje, opisane su dvije metode za nelinearnu optimizaciju. Prva metoda je kvazi-Newtonova metoda, koja se koristi za optimizaciju bez ograničenja, a druga je sekvencijalno kvadratno programiranje koje se može smatrati poopćenjem kvazi-Newtonove metode za slučaj optimizacije s ograničenjima. Na kraju poglavlja opisano je grananje i ograničavanje kao primjer metode za globalnu optimizaciju.

U četvrtom poglavlju predstavljena je sinteza linearnih antenskih nizova s uskom glavnom laticom i minimalnom L_1-normom temeljena na konveksnoj optimizaciji. Generalni optimizacijski problem koji opisuje dizajn linearnog antenskog niza s uskom glavnom laticom može se oblikovati kao minimizacija pogreške u području bočnih latica. Ta mjera pogreške često se izražava u obliku L_p-norme. Odabiri $p = 2$ i $p \to \infty$ često su zastupljeni u literaturi, a optimizacijski problemi koji koriste navedene vrijednosti su konveksni. Također, u tim slučajevima optimum se može izračunati i pomoću analitičkih izraza. Druge norme, poput L_1-norme, nisu zastupljene u dizajnu antenskih nizova. Nasuprot tome, u teoriji FIR filtara poznat je dizajn temeljen na L_1-normi. U usporedbi s L_2 optimalnim FIR filtrima, L_1 filtri imaju manju valovitost u području gušenja te nešto šire prijelazno područje. Uzimajući u obzir navedene značajke L_1 optimalnih FIR filtara, u disertaciji je predložena metoda za dizajn antenskih nizova koja se temelji na L_1-normi. Ova metoda rezultira dijagramima zračenja koji su pogodni za mnoge primjene.

Dizajn nizova s minimalnom L_1-normom izražen je kao problem optimizacije nad prostorom omeđenim stošcima drugog reda. Predstavljeni problem je konveksan te stoga navedeni postupak daje globalno rješenje. U disertaciji je opisani postupak primijenjen na dizajn antenskih nizova s raznim brojem elemenata. Nadalje, provedena je detaljna analiza dobivenih rezultata. Prvo je razmatran dizajn nizova s elementima koji su međusobno razmaknuti za $\lambda/2$. Dobiveni pobudni koeficijenti su pozitivni te imaju zvonoliku raspodjelu. Utvrđeno je kako se razina prve bočne latice ne mijenja značajno s porastom broja elemenata niza te da ona iznosi približno -21 dB. Razine ostalih bočnih latica padaju monotono s porastom kuta. Posljedično tome, dobiveni

nizovi imaju visoku učinkovitost glavne latice koja je uvijek viša od 98 %. Nadalje, dinamički raspon pobudnih koeficijenata linearno raste s porastom broja elemenata niza te generalno poprima male vrijednosti. Konačni primjer u četvrtom poglavlju pokazuje uspješnu primjenu predloženog L_1 dizajna u sintezi antenskih nizova s elementima postavljenim na predefinirane i nejednoliko razmaknute pozicije. U ovom slučaju, dobivaju se i negativne vrijednosti pobudnih koeficijenata.

Iako dinamički raspon pobudnih koeficijenta u nizovima s minimalnom L_1-normom generalno poprima male vrijednosti, u nekim aplikacijama one mogu biti veće od onih podržanih dostupnim sklopovljem. Da bi se taj problem riješio, u polazni L_1 dizajn potrebno je uključiti ograničenja dinamičkog raspona koeficijenta. Peto poglavlje predstavlja ovakav dizajn. Dodavanjem ograničenja na dinamički raspon koeficijenata optimizacijski problem postaje nekonveksan. Međutim, od ranije je poznato da je takav problem moguće globalno riješiti korištenjem metode grananja i ograničavanja, uz uvjet da su predznaci svih koeficijenata unaprijed poznati. Takav pristup primijenjen je u opisanom dizajnu. Dizajn je ilustriran primjerima, a dobiveni antenski nizovi i pripadajući dijagrami zračenja su analizirani. Utvrđeno je da ograničavanje dinamičkog raspona koeficijenata utječe na porast razine prve bočne latice. Takav porast može biti značajan i uglavnom je nepoželjan.

Preveliki porast razine prve bočne latice može se spriječiti dodavanjem ograničenja na maksimalnu razinu bočnih latica. Takva ograničenja su konveksna. No, zbog ograničenja dinamičkog raspona koeficijenata, i ovaj problem potrebno je riješiti upotrebom grananja i ograničavanja. Međutim, za pojedine kombinacije predznaka koeficijenata te za zadani dinamički raspon koeficijenata, željena razina bočnih latica se ne može postići. Tada je optimizacijski problem neizvediv. Ako se neizvedivi problem nađe u stablu za pretraživanje, ranije korištena metoda grananja i ograničavanja ne može uspješno obaviti pretraživanje i dati globalno rješenje. Zbog toga je u nastavku petog poglavlja predložena metoda grananja i ograničavanja s ugrađenim testom izvedivosti, koja globalno rješava problem optimizacije L_1 linearnih antenskih nizova s ograničenim dinamičkim rasponom pobudnih koeficijenata i ograničenom maksimalnom razinom bočnih latica. Metoda je uspješno primijenjena te su dizajnirani antenski nizovi s elementima razmaknutim za $\lambda/2$ i nizovi s nejednoliko razmaknutim, unaprijed zadanim, pozicijama elemenata. U prvom slučaju uočeno je su dobiveni koeficijenti često isključivo pozitivni i simetrični. Negativni i asimetrični koeficijenti pojavljuju se prilikom dizajniranja većih antenskih nizova s vrlo strogim zahtjevima postavljenim na dinamički raspon koeficijenata i maksimalnu razinu bočnih latica.

U šestom poglavlju predstavljen je dizajn linearnih i planarnih antenskih nizova s jednako pobuđenim nejednoliko razmaknutim elementima. Takav pristup osigurava minimalan dinamički raspon koeficijenata. Optimizacija pozicija provedena je s ciljem dobivanja maksimalne učinkovitosti glavne latice te maksimalne usmjerenosti. Budući da su takvi prob-

lemi nekonveksni i nelinearni, za njihovo rješavanje predloženi su optimizacijski postupci opće namjene. Prvo je razmatrana optimizacija bez ograničenja. Za takvu optimizaciju odabrana je kvazi-Newtonova metoda. Rezultati pokazuju da metoda brzo konvergira ka rješenju što omogućava brzo eksperimentiranje s raznim kriterijima. Također, promatrani problemi vrlo se lako prilagođavaju za rješavanje spomenutom metodom. U slučaju maksimizacije učinkovitosti glavne latice, u rješenju se mogu pojaviti elementi s malim međusobnim razmakom. S druge strane, kada je riječ o maksimizaciji usmjerenosti, svi elementi nalaze se na dovoljno velikim razmacima, što rezultira poboljšanjem usmjerenosti u odnosu na nizove s jednoliko razmaknutim elementima.

Sljedeći korak bio je dodavanje ograničenja u dizajn. Dodana su ograničenja na minimalni razmak između elemenata, na maksimalnu razinu bočnih latica i na maksimalnu veličinu niza. Za rješavanje takvih problema predloženo je sekvencijalno kvadratno programiranje. Ova metoda jedna je od najučinkovitijih metoda za nelinearnu optimizaciju s ograničenjima. U primjerima su pokazani razni nizovi, dobiveni optimizacijama s raznim kombinacijama navedenih ograničenja. Utvrđeno je da odabrana metoda konvergira za sve analizirane primjere, čak i u slučajevima kada je početna točka izvan izvedivog područja. Rezultati pokazuju da je s predloženom metodom moguće postići poboljšanje usmjerenosti i učinkovitosti glavne latice u usporedbi s postojećim metodama.

Sedmo, zaključno poglavlje ističe glavne rezultate provedenog istraživanja.

Ključni pojmovi: antenski niz, antenski niz s nejednoliko raspoređenim elementima, dinamički raspon pobudnih koeficijenata, globalna optimizacija, grananje i ograničavanje, jedinična pobuda, konveksna optimizacija, L_1-norma, nelinearna optimizacija, učinkovitost glavne latice, uska glavna latica, usmjerenost.

Contents

Chapter 1

Introduction

Continuously evolving wireless communication technologies and a growing number of wireless devices used in everyday life require efficient antenna arrays that produce optimum radiation patterns. In particular, high beam efficiency, high directivity, low sidelobe level, and simple feeding networks are the ultimate features of antenna arrays that are used in 5G mobile communications as well as in satellite systems. Consequently, new and efficient antenna architectures are constantly being developed. Desired radiation patterns can be achieved by using equally spaced arrays with amplitude-weighted excitation coefficients. However, amplitude weighting induces poor power efficiency and requires radio-frequency amplifiers with high dynamic range, which results in expensive and complicated feeding networks. Therefore, to achieve both the desired radiation pattern and simple feeding network a low excitations' dynamic range ratio is required.

Having the aforementioned requirements in mind, the objective of the research covered within this dissertation is to upgrade existing and develop new methods for the synthesis of pencil-beam antenna arrays with low dynamic range ratio of excitation coefficients. In this context, the conducted research offers the following contribution:

1. Synthesis of pencil-beam linear antenna arrays with minimum L_1-norm based on convex optimization.
2. Method for global optimization of pencil-beam linear antenna arrays with constrained dynamic range ratio of excitation coefficients and minimum L_1-norm.
3. Method for the design of antenna arrays with uniformly excited unequally spaced antenna elements based on general-purpose optimization methods.

The thesis is organized as follows. The second chapter introduces common concepts and figures of merit of antenna arrays. Furthermore, it brings an overview of state-of-the-art antenna array design methods, with an emphasis on pencil-beam design with low dynamic range ratio of excitation coefficients. In that sense, methods that minimize or constrain the dynamic range ratio are considered. In addition, the methods that utilize the unity dynamic range ratio and op-

timize antennas' positions are discussed. Since the design methods proposed in this dissertation are based on optimization, the third chapter briefly discusses optimization techniques relevant to the proposed research.

The fourth, fifth, and sixth chapters describe newly developed methods for the design of pencil-beam antenna arrays. In the fourth chapter, a method for convex optimization for the design of L_1 linear pencil beams is presented. The design examples provide insight into behavior of such pencil beams, for both the arrays with equally and unequally spaced elements.

In the fifth chapter, the design of L_1 pencil beams is extended with the constraints set on dynamic range ratio of excitation coefficients. Constraining the dynamic range ratio might cause deterioration in array's radiation pattern. To prevent this, the sidelobe level constraints are included in the design. Since the optimization problems involving constraints on dynamic range ratio are not convex, a global optimization method based on branch and bound is proposed for their solving.

The sixth chapter considers the optimization of uniformly-excited unequally-spaced arrays. The optimization problems that contain elements' positions playing the role of design variables are highly nonlinear and nonconvex. For their solving, the application of methods for nonlinear optimization is investigated. In particular, the design of arrays with maximum beam efficiency and the design of arrays with maximum directivity are considered. The optimization of linear and planar arrays is performed and several examples are provided.

Finally, the seventh chapter concludes the dissertation.

Chapter 2

Antenna Arrays

Antenna arrays are used in applications that require radiation patterns that are not achievable by single antenna element [1], [2], [3]. Such applications include radars [4], satellite comunications [5], [6], 5G communications [7], [8], microwave power transmission [9], [10], [11], radio astronomy [12], [13], medical treatments [14], etc. The main purposes of antenna arrays are spatial filtering and beamforming [15]. In both, the radiating field is appropriately shaped and directed.

The radiating field can be divided into three regions: reactive near-field, radiating near-field, and far-field region [1]. In the reactive near-field nonradiating effects dominate, and as the name suggests, it is encountered in the region immediately around the antenna. As the distance from the antenna increases, radiating near-field region is entered. Therein, radiating effects are encountered, however, angular field distribution is dependent on the distance from the antenna. Finally, far-field region begins after reaching an appropriate distance from the antenna, which usually equals several wavelengths. In this region, field distribution practically does not depend on the distance from the antenna. All array design methods discussed in this dissertation consider only radiation patterns in the far-field region.

Radiation pattern can have various shapes, forming wide beams, pencil beams, cosecant square beams, multiple beams, etc. Main focus of this dissertation is set to pencil beams. Such beams have the most of the energy concentrated in a narrow spatial angle.

When considering spatial layout of radiating elements, there are linear, planar, volumetric arrays, etc. Further classification is based on interelement spacing, covering equally and nonequally spaced arrays. All of the mentioned layouts, except volumetric arrays, are considered in this dissertation.

2.1 Far-Field Radiation Pattern

Consider a single antenna element placed at the *x*-axis of a coordinate system, as shown in Figure 2.1a. Its complex radiation pattern in the far-field region in the *xz*-plane, is given by [3]

$$F(\theta) = G(\theta)\alpha e^{j\beta} e^{j\frac{2\pi}{\lambda}\hat{\mathbf{r}}\cdot\vec{\mathbf{d}}} \tag{2.1}$$

where $G(\theta)$ is radiation pattern of the antenna element, θ is elevation angle, $\alpha e^{j\beta}$ is excitation signal with magnitude α and phase β, λ is the wavelength of transmitted signal, $\hat{\mathbf{r}}$ is unit vector in the direction $\vec{\mathbf{r}}$ which points to the observation point R, and $\vec{\mathbf{d}}$ is vector which points to the antenna element. Assuming

$$\hat{\mathbf{r}} = \hat{\mathbf{x}}\sin\theta + \hat{\mathbf{z}}\cos\theta, \tag{2.2}$$

and

$$\vec{\mathbf{d}} = x_a\hat{\mathbf{x}}, \tag{2.3}$$

where $\hat{\mathbf{x}}$ and $\hat{\mathbf{z}}$ are unit vectors and x_a is the abscissa of the antenna element, the far-field radiation pattern of a single antenna takes the form

$$F(\theta) = G(\theta)\alpha e^{j\beta} e^{j\frac{2\pi}{\lambda}x_a\sin\theta}. \tag{2.4}$$
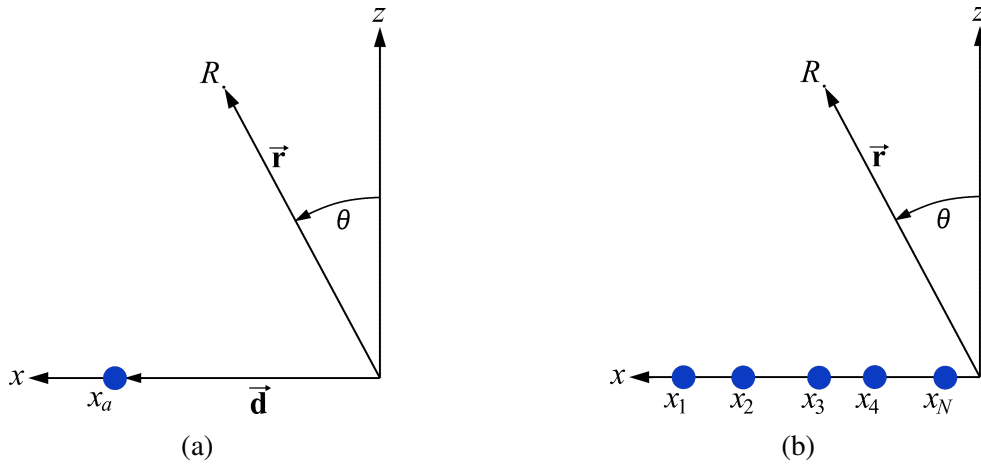
Figure 2.1: Single antenna element (a) and linear antenna array (b).

Next, consider the case where N antenna elements are placed along the *x*-axis, as shown in Figure 2.1b. Such configuration is called linear antenna array. The total radiated field of all elements can be obtained by using superposition. Assuming all elements have the same element pattern $G(\theta)$, far-field radiation pattern of a linear antenna array is given by

$$F(\theta) = G(\theta)\sum_{n=1}^{N}\alpha_n e^{j\beta_n} e^{j\frac{2\pi}{\lambda}x_n\sin\theta} \tag{2.5}$$

where x_n, α_n, and β_n, $n = 1, 2, ..., N$ represent elements' positions, magnitudes and phases. By denoting $a_n = \alpha_n e^{j\beta_n}$, $\mathbf{x} = [x_1, x_2, \ldots, x_N]^T$, and $\mathbf{a} = [a_1, a_2, \ldots, a_N]^T$, the expression in (2.5) can be written in a form

$$F(\mathbf{a}, \mathbf{x}, \theta) = G(\theta) \sum_{n=1}^{N} a_n e^{j\frac{2\pi}{\lambda} x_n \sin\theta} \tag{2.6}$$

Finally, if the array is composed of N antenna elements that are placed in the xy-plane, as illustrated in Figure 2.2, the configuration is called planar antenna array. In such a case, vector $\vec{\mathbf{d}}$ for each element is obtained as

$$\vec{\mathbf{d}} = x_a \hat{\mathbf{x}} + y_a \hat{\mathbf{y}}, \tag{2.7}$$

where x_a and y_a are abscissa and ordinate of antenna elements. The vector $\hat{\mathbf{r}}$ now takes the form

$$\hat{\mathbf{r}} = \hat{\mathbf{x}} \sin\theta \cos\varphi + \hat{\mathbf{y}} \sin\theta \sin\varphi + \hat{\mathbf{z}} \cos\theta. \tag{2.8}$$

where θ is elevation and φ is azimuth angle. The far-field radiation pattern of the array is given by

$$F(\mathbf{a}, \mathbf{x}, \mathbf{y}, \theta, \varphi) = G(\theta, \varphi) \sum_{n=1}^{N} a_n e^{j\frac{2\pi}{\lambda}(x_n \sin\theta \cos\varphi + y_n \sin\theta \sin\varphi)} \tag{2.9}$$

where $\mathbf{x} = [x_1, x_2, \ldots, x_N]^T$, $\mathbf{y} = [y_1, y_2, \ldots, y_N]^T$, $\mathbf{a} = [a_1, a_2, \ldots, a_N]^T$, and $G(\theta, \varphi)$ is the elements' radiation pattern.

If all coefficients have zero phases, i.e. $\beta_n = 0$, $n = 1, 2, \ldots, N$, the main beam is directed at the angle $\theta = 0$, which is perpendicular to the axis/plane at which the array is placed. Such arrays are called the broadside arrays. The phases, β_n, can be used to steer the beam away from the broadside. However, in this dissertation only broadside arrays are considered.

The summation terms in (2.6) and (2.9)

$$f(\mathbf{a}, \mathbf{x}, \theta) = \sum_{n=1}^{N} a_n e^{j\frac{2\pi}{\lambda} x_n \sin\theta} \tag{2.10}$$

and

$$f(\mathbf{a}, \mathbf{x}, \mathbf{y}, \theta, \varphi) = \sum_{n=1}^{N} a_n e^{j\frac{2\pi}{\lambda}(x_n \sin\theta \cos\varphi + y_n \sin\theta \sin\varphi)} \tag{2.11}$$

are called the array factors. Clearly, if elements in the array are isotropic radiators, i.e. $G(\theta, \varphi) = 1$, then the far-field radiation pattern is equivalent to the array factor. In this dissertation only arrays with isotropic elements are considered.

Note that the expressions (2.6) and (2.9) are obtained assuming antenna elements are ideal. In a real world, when multiple antennas are placed next to each other, element pattern of a single antenna is influenced by the radiation of other elements [1]. Such influence is known as mutual

coupling between antenna elements. In this dissertation only the array factors, i.e. the arrays with ideal isotropic elements will be considered.
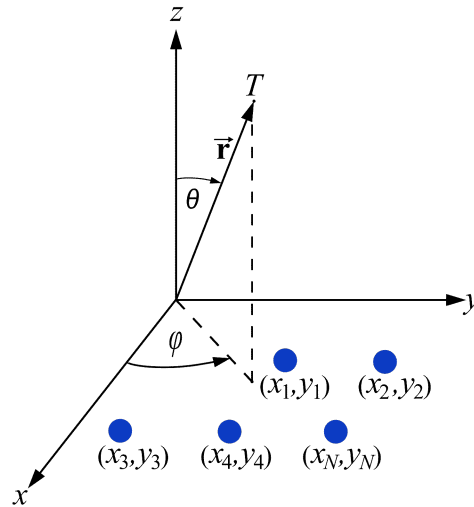
Figure 2.2: Planar antenna array.

2.2   Properties of Antenna Arrays

In antenna array design, attention should be paid on two sets of properties. First of them is related to the far-field radiation pattern, describing array's performances. The second describes implementation aspects.

2.2.1   Radiation Pattern

2.2.1.1   Radiation Pattern Lobes

The far-field radiation pattern of a pencil-beam array contains radiation lobes, namely, one main lobe and multiple side lobes.

Main lobe, or main beam, is the lobe with maximum radiated power. The width of the main lobe is described with two parameters: half-power beamwidth (HPBW) and first-null beamwidth (FNBW). HPBW is defined as a separation between angles at which the level of the main lobe is equal to -3 dB. It is often used to describe resolution capabilities, i.e. the ability to distinguish signals coming from two adjacent directions. FNBW is defined as an angular separation between the first nulls on the opposite sides of the main lobe [1].

Side lobes, or minor lobes, represent radiation in undesired directions [1]. The ratio of the power density in the largest side lobe and power density in the main lobe is called sidelobe level (SLL) [1]. Minimization of the sidelobe level is a common requirement in antenna array design.

2.2.1.2 Directivity

Directivity describes how effectively the antenna array directs energy in a specific direction [1]. It is defined as the ratio between the power density obtained in the observed direction and the average power density [1]. The maximum directivity occurs in the direction of the main lobe. If this direction is denoted as θ_{MB}, directivity of linear antenna array is given by

$$D = \frac{|f(\mathbf{a}, \mathbf{x}, \theta_{MB})|^2}{P_{tot}/4\pi}. \tag{2.12}$$

where P_{tot} is total radiated power. For planar array directivity is calculated by using array factor from (2.11).

2.2.1.3 Beam Efficiency

Beam efficiency (BE) is defined as the ratio between the power radiated within a main beam and the total radiated power [1], as in

$$BE = \frac{P_0}{P_{tot}}. \tag{2.13}$$

where P_0 is the power of the main beam. In some applications, such as the microwave power transmission, the term beam collection efficiency (BCE) is used rather than beam efficiency.

2.2.2 Implementation Aspects

2.2.2.1 Dynamic Range Ratio of Excitation Coefficients

The dynamic range ratio (DRR) of excitation coefficients is defined as the ratio of the coefficients' maximum and minimum absolute value, as in

$$DRR = \frac{\max\limits_{1 \le n \le N} \{|a_n|\}}{\min\limits_{1 \le n \le N} \{|a_n|\}}. \tag{2.14}$$

The excitations' DRR has a direct impact on the complexity and the cost of the arrays' feeding networks. The main components of a feeding network are amplifiers and phase shifters, which enable amplitude weighting and phase delay control at each antenna element [16]. Usually, the amplifiers that operate at high frequencies cover only a narrow dynamic range. Therefore, the coefficients with a low DRR relax the requirements set on the amplifiers. Additional benefit of a low DRR is better control of the mutual coupling between antenna elements [17]. Finally, a low DRR improves the power distribution between antenna elements [5], [9], which is important in microwave power transmission and satellite communications. Unfortunately, the

minimization of the sidelobe level requires a certain amount of coefficients' dynamics, since the uniformly excited arrays offer the sidelobe level of only -13.5 dB [1]. Therefore, a tradeoff between low DRR and specified SLL is often made in antenna array design.

2.2.2.2 Spatial Layout of Antenna Arrays

Antenna elements can be equally or unequally spaced. The positions at which antenna elements are placed greatly influence the array performance.

In equally spaced arrays, all neighboring antenna elements have the same interelement spacing. For broadside arrays, in order to avoid grating lobes, the interelement spacing should be less than λ. However, spacing should not be too small either, since mutual coupling effects increase with a decrease in the distances [1], [16]. Typical interelement spacing of equally spaced arrays is $\lambda/2$. Such spacing ensures the absence of aliasing and the obtained visible region coincides with the Nyquist band in signal processing theory [3]. This enables the application of methods for FIR-filter design in the design of antenna arrays.

In unequally spaced arrays the elements take arbitrary, usually nonequidstant, positions. The lack of periodicity reduces pattern's grating lobes, which allows increasing array's size or its sparsity [18], [19]. Moreover, non-uniform layout of antennas reduces the effects of mutual coupling [5]. Finally, introducing elements' positions as variables provides additional degrees of freedom (DOF) in the design. This allows obtaining specified radiation patterns with low-DRR or even uniform excitation coefficients [19], [20].

2.3 State-of-the-Art in Pencil-Beam Antenna Array Design

2.3.1 Linear Arrays with Low Dynamic Range Ratio

As elaborated in Section 2.2.2.1, the dynamic range ratio is often a bottleneck of arrays' implementation. Consequently, great efforts were made by scientific community to develop methods for the design of low-DRR antenna arrays. Design methods that incorporate DRR control can be divided into two main groups: analytic methods and optimization-based methods.

2.3.1.1 Design Based on Analytic Methods

Analytic methods are fast and robust. In the context of beamforming, they are usually based on windowing techniques and polynomial representations of either the array factor or the continuous current distribution of the array's aperture. There are several analytically obtained arrays that implicitly ensure low DRR, such as Dolph-Chebyshev [21], Taylor-Kaiser, Legendre, and Gaussian [22] arrays. However, there are not many analytic methods that explicitly take DRR into account.

Recently developed methods tackled this problem [23], [24], [25], [26], [27]. In [23] and [27], the excitation coefficients are obtained directly, by discretizing the appropriately modeled function that represents array's continuous current distribution. On the other hand, in [24] and [25], coefficients are obtained by applying inverese fast Fourier transform on the function representing the array factor. Majority of these methods provide minimum DRR for a specified sidelobe level [24], [25], [26]. Moreover, the method in [23] reduces the DRR by adjusting a control parameter that influences the DRR, which provides only indirect control of the DRR. Finally, in [27] the DRR is taken as an input parameter for the design. The arrays are designed to achieve minimum sidelobe level for a given DRR.

2.3.1.2 Design Based on Optimization Methods

Although analytic methods are straightforward, they rarely provide optimum beampatterns, especially when a low DRR is required. On the other hand, optimization offers exact control over design specifications and it has become a preferable choice in antenna array design.

The design of pencil beams can be considered as an optimization problem in which various specifications can be added, among which is the dynamic range ratio. There are two common approaches to controlling the DRR

- direct minimization of DRR
- incorporating DRR constraints into the design with some other objective function.

Either way, the optimization problem with DRR as a requirement is nonconvex. Therefore, it is difficult to solve globally. Namely, if the upper bound D is imposed on the value of DRR defined in (2.14), as in

$$\frac{\max_{1 \leq n \leq N} \{|a_n|\}}{\min_{1 \leq n \leq N} \{|a_n|\}} \leq D \tag{2.15}$$

then such constraint can be written as

$$|a_n| \leq Dt, \; n = 1, 2, \ldots, N \tag{2.16}$$

$$|a_n| \geq t, \; n = 1, 2, \ldots, N \tag{2.17}$$

$$t \geq 0 \tag{2.18}$$

where t is auxiliary variable. The constraint (2.17) is not convex. Consequently, numerous methods have been developed to approach the global solution of DRR-constrained problems as much as possible. These methods are either based on approximating the original problem by introducing relaxations into the design [28], [29], [30], or by using methods that solve the original problem approximately [17], [31], [32], [33], [34], [35].

Two simplest relaxations used in antenna array synthesis with the control of DRR are

- turning off the array elements whose amplitude is close to zero, as proposed in [29] and
- manual setting the magnitude of the element violating the required DRR to an appropriate value, as in [28].

Expectedly, such methods do not provide arrays with arbitrary DRR and may result in significant deterioration of the radiation patterns.

Another possible relaxation, proposed in [30], is to formulate the objective function as a difference between the maximum and the minimum value of excitation, as in

$$\underset{\mathbf{a}}{\text{minimize}} \quad \max|\mathbf{a}| - \min|\mathbf{a}| \tag{2.19}$$

assuming that all excitation coefficients take positive values. The resulting optimization problem is given by [30]

$$
\begin{aligned}
\underset{\mathbf{a}}{\text{minimize}} \quad & \max|\mathbf{a}| - \min|\mathbf{a}| \\
\text{subject to} \quad & \sum_{n=1}^{N} a_n = 1, \\
& |f(\mathbf{a}, \theta)| \leq \delta(\theta), \\
& \mathbf{a} \geq 0
\end{aligned}
\tag{2.20}
$$

where $\delta(\theta)$ is the upper bound of magnitude of array factor $f(\mathbf{a}, \theta)$. The problem (2.20) is convex and can be easily solved. In this way, the DRR is fully controlled. However, enforcing exclusively positive excitations reduces design freedom and consequently does not provide the best solution.

To solve the DRR minimization problem, approximate algorithms are often used. Such algorithms usually transform original problem into a problem suitable for solving with iterative methods, such as projection based algorithm [17], nonlinear optimization of penalty function [32], alternating direction method of multipliers (ADMM) [33], primal-dual method [34], and penalty dual decomposition [35]. All methods referred to reduce DRR while providing desired radiation pattern. Even though some of the listed methods, such as ADMM have supreme convergency properties [36], they cannot guarantee the globality of the solutions.

In addition to the aforementioned methods, which are deterministic, in [31] a genetic algorithm was used to perform simultaneous minimization of the difference between desired and obtained radiation pattern and the difference between desired and obtained DRR. The main advantage of genetic algorithms over deterministic algorithms is their ability to escape from local optimum, thus increasing the chance of finding the global solution. However, globality of the solution still cannot be guaranteed.

Recently, a method has been developed that globally solves the problems of minimization of SLL [37] and maximization of beam efficiency [38] of the arrays with constrained DRR. The

method referred to is based on branch and bound algorithm. It supports positive and negative coefficients. In addition, it works with DRRs as low as one. This method will be described in detail in Section 5.1.1 since the branch and bound algorithm is a base algorithm for the design of L_1 pencil beams with constrained DRR, which is presented in this dissertation.

2.3.2   Thinned Arrays with Low Dynamic Range Ratio

The term thinned arrays refers to the arrays obtained by eliminating certain elements from the equally spaced arrays. Array thinning can lead to arrays with average interelement spacing greater than $\lambda/2$. In such cases, as previously discussed in 2.2.2.2, thinned arrays can exhibit lower mutual coupling. Moreover, array manufacturing costs can be reduced, as radiation pattern specifications are met while utilizing fewer antenna elements. Finally, if such arrays also exhibit low DRR, these advantages become more prominent. Sometimes, thinned arrays are called sparse arrays.

There are many methods for the design of thinned arrays. However, very few of them perform array thinning and simultaneously incorporate the control of DRR. Such methods can be found in [39], [40], [41], [42].

In [39], [40] designs of planar arrays with arbitrary patterns are considered. The methods referred to can be applied to pencil beams as well, by an appropriate adjustment of the power pattern mask. Both methods are iterative and start with a fully populated array on a rectangular grid. The method in [39] is based on alternating projections technique. At each iteration scaling of the coefficients is performed according to the predefined bounds, and clipping of the coefficient whose magnitude is less than specified is performed. Furthermore, the method in [40] is based on convex relaxations. At each iteration, elements with small excitations' magnitudes are eliminated, similar to the method in [29]. Even though the methods [39] are [40] are efficient, they do not explicitly control the DRR. Design proposed in [42] utilizes convex optimization together with particle swarm optimization and genetic algorithm to synthesize sparse arrays with phase and amplitude control. The DRR is minimized in one of the steps of the algorithm by using formulation as in (2.19).

The method in [41] is an extension of the global optimization method from [37] for the case of thinned linear arrays. The method provides global solution to the problem of minimization of SLL with constrained DRR. Since the method allows zero excitations, additional reduction of SLL can be achieved compared to the case when only nonzero coefficients are allowed. Such behavior occurs because, in a DRR-constrained design, the coefficients that would naturally have low values would be pushed to higher values to satisfy the DRR constraints, which inevitably deteriorates the array factor. When such coefficients are allowed to take zero value, the deterioration is lower.

2.3.3 Unequally Spaced Arrays with Low Dynamic Range Ratio

Methods that simultaneously optimize positions and DRR of pencil-beam arrays are found in [43], [44]. In this way, number of degrees of freedom is increased since elements are allowed to move from their positions on predefined grid.

The work in [43] presents an iterative hybrid algorithm based on particle swarm optimization and second-order cone programming. This algorithm assumes all coefficients are positive. In each iteration, excitation coefficients are calculated by using second-order cone programming. Then, the element positions are updated by using particle swarm optimization.

The design proposed in [44] employs the density tapering method from [45] to find elements' positions assuming their excitation coefficients are uniform. The positions are calculated in a closed form. Then, excitations are evaluated by using the calculated positions and by taking into account DRR constraints and mutual coupling between antenna elements. The excitations are found by using alternating projection approach from [46]. The goal is to reduce the level of the side lobes. Only linear arrays are considered.

2.3.4 Unequally Spaced Uniformly Excited Arrays

The designs considering unequally-spaced arrays can be expressed as optimization problems. Unfortunately, problems containing elements' positions as design variables are highly nonlinear and nonconvex. Therefore, they are difficult to solve globally. Throughout the years such problems have been solved with numerous optimization-based methods. Even though these methods generally provide good results, the globality of the solutions cannot be guaranteed. Therefore, this is still an open problem in antenna array design.

A significant part of the research is focused on the control of the sidelobe level [4], [6], [20], [47], [48], [49], [50], [51], [52], [53], [54], [55], [56], [57], [58], [59], whereas the objectives such as maximization of beam efficiency [60], [61], [62], [63], [64], [65], [66], [67] or directivity [55], [65] [68] are less frequent. Moreover, many authors consider arrays with predefined excitation coefficients and optimize only elements' positions [4], [6], [20], [47], [48], [49], [50], [51], [52], [53], [54], [55], [56], [60], [61], [62], [63], [64], [65]. In this scenario, the most popular choice is uniform excitation, which is interesting because it ensures the lowest possible DRR. If the excitation coefficients are uniform, all amplifiers work under the same operating conditions which improves system's efficiency and enables the use of simple feeding networks. On the other hand, designs that include positions *and* excitations as variables can lead to better array performances. The examples of such designs can be found in [57], [58], [59], [66], [67]. However, the implementation of such arrays is more complex and expensive. Therefore, one of the emphases of this dissertation is on designing uniformly-excited unequally-spaced arrays.

The sidelobe level is one of the most important parameters of antenna arrays. Consequently, its minimization via unequal element spacing has been extensively studied. A popular approach in the minimization of SLL is to employ deterministic optimization based on convex optimization. Since the original problem is nonconvex, it is approximated by using Taylor expansion which leads to a sequence of convex problems that are solved iteratively. Such an approach was presented in [48]. At the kth iteration, array factor from (2.11) is linearized around current suboptimal solution $(\mathbf{x}_{k-1}, \mathbf{y}_{k-1})$. The linearization is achieved by exploiting the first-order Taylor approximation $e^{j\gamma} \approx 1 + j\gamma$, as in

$$f(\mathbf{a},\boldsymbol{\Delta}x,\boldsymbol{\Delta}y,\theta,\varphi) = \sum_{n=1}^{N} a_n e^{j\frac{2\pi}{\lambda}(x_n^{k-1}\sin\theta\cos\varphi + y_n^{k-1}\sin\theta\sin\varphi)}(1 + j\sin\theta\cos\varphi\Delta x + j\sin\theta\sin\varphi\Delta y)$$

(2.21)

where $\boldsymbol{\Delta}x$ and $\boldsymbol{\Delta}y$ are displacement vectors. The approximation is valid if $|\sin\theta\cos\varphi\Delta x| \ll 1$ and $|\sin\theta\sin\varphi\Delta y| \ll 1$. In this case, at the kth iteration $\boldsymbol{\Delta}x$ and $\boldsymbol{\Delta}y$ can be found by solving the problem

$$\begin{aligned} \underset{\boldsymbol{\Delta}x,\boldsymbol{\Delta}y}{\text{minimize}} \quad & \delta \\ \text{subject to} \quad & \max|f(\boldsymbol{\Delta}x,\boldsymbol{\Delta}y,\theta_s,\varphi_s)| \leq \delta, \quad (\theta_s,\varphi_s) \in S, \\ & |\boldsymbol{\Delta}x| \leq \varepsilon, \\ & |\boldsymbol{\Delta}y| \leq \varepsilon \end{aligned}$$

(2.22)

where δ is sidelobe level, S is the sidelobe region, and ε is the upper bound on changes in element locations. The problem (2.22) is convex and it can be solved by using second-order cone programming. Finally, new solution is obtained as

$$\mathbf{x}_k = \mathbf{x}_{k-1} + \boldsymbol{\Delta}x, \quad \mathbf{y}_k = \mathbf{y}_{k-1} + \boldsymbol{\Delta}y.$$

(2.23)

Similar approach was used in [53] where authors utilized second-order Taylor approximation and included constraints on minimum interelement spacing between the elements. Such constraints are crucial since they prevent elements from being too close to one another or from overlapping. The method referred to provided lower SLL values than did the method in [48].

Another approximation that leads to a sequence of convex problems is Chebyshev approximation used in [19]. Constraints on interelement spacing were also included in this design. For planar arrays these constraints are nonlinear and nonconvex, as in

$$(x_{ij}^k)^2 + (y_{ij}^k)^2 \geq d_{min}^2, \quad i \neq j$$

(2.24)

where k denotes iteration number, (x_{ij}^k) and (y_{ij}^k) are distances along x and y directions between ith and jth element, and d_{min} is minimum interelement spacing. In [19], linearized model of

these constraints is used, where linearization is performed around current suboptimal solution, (x_{ij}^{k-1}), (y_{ij}^{k-1}). Assuming

$$x_{ij}^k = x_{ij}^{k-1} + \Delta x_{ij}^k \qquad (2.25)$$

$$y_{ij}^k = y_{ij}^{k-1} + \Delta y_{ij}^k \qquad (2.26)$$

expression (2.24) becomes

$$(x_{ij}^{k-1})^2 + 2x_{ij}^{k-1}\Delta x_{ij}^k + (\Delta x_{ij}^k)^2 + (y_{ij}^{k-1})^2 + 2y_{ij}^{k-1}\Delta y_{ij}^k + (\Delta y_{ij}^k)^2 \geq d_{min}^2, \quad i \neq j \qquad (2.27)$$

If $\Delta x_{ij}^k \ll 1$ and $\Delta y_{ij}^k \ll 1$, $(\Delta x_{ij}^k)^2$ and $(\Delta y_{ij}^k)^2$ can be neglected, resulting in

$$x_{ij}^{k-1}\Delta x_{ij}^k + y_{ij}^{k-1}\Delta y_{ij}^k \geq \frac{d_{min}^2 - (x_{ij}^{k-1})^2 - (y_{ij}^{k-1})^2}{2}, \quad i \neq j \qquad (2.28)$$

For

$$\Delta x_{ij}^k = \Delta x_i^k - \Delta x_j^k \qquad (2.29)$$

$$\Delta y_{ij}^k = \Delta y_i^k - \Delta y_j^k. \qquad (2.30)$$

the constraints in (2.28) are linear.

In [19], [48], [53] elements' positions were optimized only for the broadside arrays. Consequently, such optimizations cannot provide optimum SLL when main beam is steered away from the broadside direction. The optimization of SLL for steered beams was considered in [54] and [4]. In [54], iterative convex optimization was performed, based on the approximations similar to those in [48], [19]. In [4], the method of moving asymptotes was used, which is a gradient-based method for nonlinear optimization. In addition to the aforementioned methods, popular choices for minimization of SLL are evolutionary methods such as differential evolution [47], [49], particle swarm optimization [51], and grey wolf optimization [56]. Deterministic techniques tailored for particular design problems were also considered [20], [6], [52], [55].

In some applications, as for example in microwave power transmission (MPT), the objective is to maximize beam collection efficiency of antenna array, whereas the SLL constraints serve as an additional protection requirement. The MPT systems are currently under consideration as one of the possible clean energy sources of the future. Popular methods for synthesis of maximum BCE arrays with predefined excitations are evolutionary algorithms such as particle swarm optimization [60], [62] and brain storm optimization [63]. The papers [60] and [62] considered the design of planar arrays, whereas in [63] only linear arrays were optimized. All of them had included constraints on maximum SLL, minimum interelement spacing, and max-

imum array size. Moreover, in [61] a simple deterministic method based on first-order Taylor approximation of objective function was presented for the optimization of linear arrays. However, this method had not include any constraints.

Chapter 6 of this dissertation considers maximization of beam (collection) efficiency. Constrained and unconstrained optimizations are presented that are based on nonlinear optimization [64], [65]. Examples that are provided therein show effectiveness of the proposed approach.

The arrays with high directivity are important in radar and satellite applications. In this context, arrays having minimum SLL and maximum directivity were synthesized in [55]. In the examples provided therein, arrays with large number of elements were considered that can be placed in geostationary orbit. Beam steering was also considered. Furthermore, directivity was maximized in [68] by using genetic algorithm.

In contrast to the customized method presented in [55], Chapter 6 considers constrained maximization of directivity by employing nonlinear optimization. The presented design includes constraints on the array size, interelement spacing, and sidelobe level.

Chapter 3

Optimization Methods

Optimization is the collection of techniques, methods, and algorithms that are used to find the optimal solution of a mathematically described problem [69]. It is often called programming, which originates from the 1940s when the term programming was used in the context of problem formulation and algorithm design [70].

A general optimization problem is formulated as finding the optimum vector $\mathbf{x}^*$ which yields the minimum value of objective function $f_0 : \mathbb{R}^N \to \mathbb{R}$, as in

$$
\begin{aligned}
\underset{\mathbf{x}}{\text{minimize}} \quad & f_0(\mathbf{x}) \\
\text{subject to} \quad & f_i(\mathbf{x}) \leq 0, \quad i = 1, 2, \ldots, I, \\
& f_j(\mathbf{x}) = 0, \quad j = 1, 2, \ldots, J,
\end{aligned}
\tag{3.1}
$$

where $\mathbf{x} = [x_1, x_2, \ldots, x_N]^{\mathrm{T}}$ is the vector of optimization variables, and functions f_i, $f_j : \mathbb{R}^N \to \mathbb{R}$, represent I inequality and J equality constraints. If the goal is to find the maximum value, the function $-f_0$ is minimized. All optimization problems considered in this dissertation will be formulated as minimization problems. If the problem does not impose any restrictions on $\mathbf{x}$, the constraints in (3.1) are omitted. Such a problem is known as unconstrained problem.

Various methods can be applied to solve the problem in (3.1), depending on the structure and properties of the objective function and constraints. These methods are categorized into several classes, covering convex optimization, nonlinear optimization, global optimization, etc.

Convex optimization is a class of optimization in which the objective function is convex and constraints define a convex set. A function is convex if (i) its domain is convex and (ii) the line segment connecting any two points of the corresponding function graph lies above the graph. Function domain, Ω, is convex if the line segment connecting any two points in Ω is completely contained in Ω. In a convex optimization problem, all local solutions are also global solutions [70]. Generally, if the problem at hand is recognized as a convex problem, it can be easily solved [71]. However, recognizing and formulating the problem in a convex form is not always an easy task.

If the problem contains nonlinear objective function or at least one nonlinear constraint, it can be solved by a method for nonlinear optimization. Such methods usually provide a local solution, whose globality can rarely be proved [70]. However, nonlinear optimization is a powerful tool that offers acceptable solution in many cases.

Many nonlinear optimization problems are multimodal, which means that they contain more than one local optimum. In such problems, the global solutions are found by using the methods for global optimization. Unfortunately, these methods often have a high computational complexity which can grow exponentially with the problem size. The class of global optimization includes deterministic methods such as exhaustive search and branch and bound, stochastic methods such as Monte Carlo method, and heuristic optimization, such as evolutionary methods (e.g. particle swarm optimization).

In the following sections, the methods that are used in this dissertation are briefly described.

3.1 Linear Programming

Problems where the objective function and the constraint functions are affine are called linear programs [71]. Linear programs are expressed as

$$\underset{\mathbf{x}}{\text{minimize}} \quad \mathbf{w}^{\mathrm{T}}\mathbf{x} + d \tag{3.2a}$$

$$\text{subject to} \quad \mathbf{Gx} \leq \mathbf{h}, \tag{3.2b}$$

$$\mathbf{Ax} = \mathbf{b} \tag{3.2c}$$

where $\mathbf{w} \in \mathbb{R}^N$, $\mathbf{G} \in \mathbb{R}^{M \times N}$, $\mathbf{A} \in \mathbb{R}^{P \times N}$, $\mathbf{h} \in \mathbb{R}^M$, $\mathbf{b} \in \mathbb{R}^P$, and $d \in \mathbb{R}$.

The intersections of halfspaces and hyperplanes defined by constraints (3.2b) and (3.2c) form a convex polytope. An example of such polytope is shown in Figure 3.1. Since the objective function is linear, the optimum solution of the program in (3.2) lies on a vertex of such polytope. Based on this property, the optimum can be found by using Dantzig's simplex method [71]. The simplex method starts the search for optimum at a vertex of the polytope and moves along its edges until the vertex with the optimum solution is found. It is clear that the more vertices the polytope contains, the more time-consuming the search becomes. This problem can be solved by using an interior point method [71]. Such method starts at a feasible point and follows a path inside the feasible region to reach the optimum. Therefore, interior point methods are more efficient in solving high-dimensional problems [69].
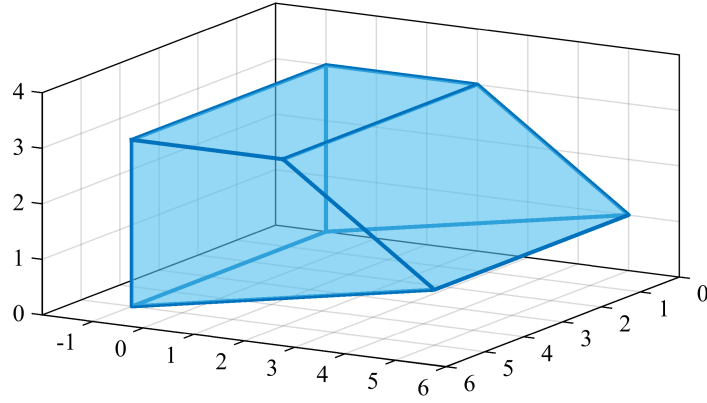
Figure 3.1: An example of convex polytope.

3.2 Quadratic Programming

Optimization problem that contains quadratic objective function and affine constraint functions is called quadratic programming (QP) problem [71]. Its form is given by

$$\begin{aligned} \underset{\mathbf{x}}{\text{minimize}} \quad & \frac{1}{2}\mathbf{x}^T\mathbf{W}\mathbf{x} + \mathbf{q}^T\mathbf{x} + r \\ \text{subject to} \quad & \mathbf{G}\mathbf{x} \leq \mathbf{h}, \\ & \mathbf{A}\mathbf{x} = \mathbf{b} \end{aligned} \tag{3.3}$$

where $\mathbf{W} \in \mathbb{R}^{N \times N}$ is positive semidefinite matrix, $\mathbf{q} \in \mathbb{R}^N$, $r \in \mathbb{R}$, $\mathbf{G} \in \mathbb{R}^{M \times N}$, $\mathbf{A} \in \mathbb{R}^{P \times N}$, $\mathbf{h} \in \mathbb{R}^M$, and $\mathbf{b} \in \mathbb{R}^P$. The quadratic program is convex. Therefore, it is often used as a base for solving general nonlinear optimization problems [69].

3.3 Second-Order Cone Programming

A second-order cone program (SOCP) is formulated as [72]

$$\underset{\mathbf{x}}{\text{minimize}} \quad \mathbf{w}^T\mathbf{x} \tag{3.4a}$$

$$\text{subject to} \quad \|\mathbf{A}_i\mathbf{x} + \mathbf{b}_i\| \leq \mathbf{c}_i^T\mathbf{x} + d_i, \quad i = 1, 2, \dots, M, \tag{3.4b}$$

where $\mathbf{w} \in \mathbb{R}^N$, $\mathbf{A}_i \in \mathbb{R}^{(P_i-1) \times N}$, $\mathbf{b}_i \in \mathbb{R}^{(P_i-1)}$, $\mathbf{c}_i \in \mathbb{R}^N$, $d_i \in \mathbb{R}$, M is the number of constraints, and $\|\cdot\|$ denotes the Euclidian norm. The constraints in (3.4b) are called second-order cone constraints. They are equivalent to

$$\begin{bmatrix} \mathbf{A}_i \\ \mathbf{c}_i^T \end{bmatrix} x + \begin{bmatrix} \mathbf{b}_i \\ d_i \end{bmatrix} \in C_i \tag{3.5}$$

where C_i represents a second-order cone (Lorentz or ice cream cone) of dimensions P_i. An example of second-order cone for $P_i = 3$ is shown in Figure 3.2. The second-order cone program is convex.

All addressed convex problems, LP, QP and SOPC, can be solved by using known convex optimization tools such as SeDuMi [73], MOSEK [74], CVX [75], YALMIP [76], etc.
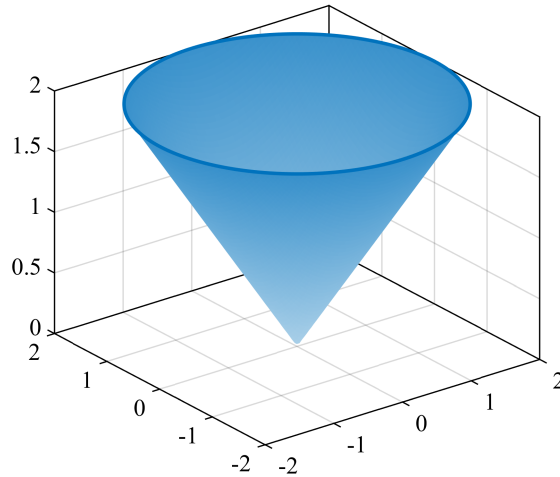
Figure 3.2: An example of second-order cone for $P_i = 3$.

3.4   Quasi-Newton Method

Quasi-Newton is a variant of the Newton method, which is one of basic optimization techniques used for unconstrained optimization. The Newton method uses first- and second-order partial derivatives of the objective function $f(\mathbf{x})$. The first-order derivative (gradient) provides information about the direction of the steepest ascent, whereas the second-order derivative (Hessian) provides information about the function's curvature. Therefore, in the Newton method, an objective function is modeled as the quadratic approximation of the Taylor series calculated at the point $(\mathbf{x}, \boldsymbol{\delta})$, where $\boldsymbol{\delta} = [\delta_1, \delta_2, \dots, \delta_N]^{\mathrm{T}}$ is the change of $\mathbf{x}$, as in

$$f(\mathbf{x}, \boldsymbol{\delta}) \approx f(\mathbf{x}) + \boldsymbol{\delta}^{\mathrm{T}} \mathbf{g}(\mathbf{x}) + \frac{1}{2} \boldsymbol{\delta}^{\mathrm{T}} \mathbf{H}(\mathbf{x}) \boldsymbol{\delta} \tag{3.6}$$

where the gradient, $\mathbf{g}(\mathbf{x})$, and the Hessian matrix, $\mathbf{H}(\mathbf{x})$, are given by

$$\mathbf{g}(\mathbf{x}) = \nabla f(\mathbf{x}) = \left[\frac{\partial f}{\partial x_1} \ \frac{\partial f}{\partial x_2} \ \cdots \ \frac{\partial f}{\partial x_N} \right]^{\mathrm{T}}, \tag{3.7}$$

$$\mathbf{H}(\mathbf{x}) = \nabla^2 f(\mathbf{x}) = \begin{bmatrix} \dfrac{\partial^2 f}{\partial x_1 \partial x_1} & \dfrac{\partial^2 f}{\partial x_1 \partial x_2} & \cdots & \dfrac{\partial^2 f}{\partial x_1 \partial x_N} \\[2ex] \dfrac{\partial^2 f}{\partial x_2 \partial x_1} & \dfrac{\partial^2 f}{\partial x_2 \partial x_2} & \cdots & \dfrac{\partial^2 f}{\partial x_2 \partial x_N} \\[2ex] \vdots & & \ddots & \vdots \\[2ex] \dfrac{\partial^2 f}{\partial x_N \partial x_1} & \dfrac{\partial^2 f}{\partial x_N \partial x_2} & \cdots & \dfrac{\partial^2 f}{\partial x_N \partial x_N} \end{bmatrix}. \tag{3.8}$$

The objective function is minimized iteratively. At the kth iteration, the value of $\boldsymbol{\delta}_k$ that minimizes $f(\mathbf{x}, \boldsymbol{\delta})$ is found by solving the equation

$$\nabla f(\mathbf{x}_k, \boldsymbol{\delta}_k) = \mathbf{g}(\mathbf{x}_k) + \mathbf{H}(\mathbf{x}_k)\boldsymbol{\delta}_k = 0, \tag{3.9}$$

resulting in

$$\boldsymbol{\delta}_k = -\mathbf{H}^{-1}(\mathbf{x}_k)\mathbf{g}(\mathbf{x}_k). \tag{3.10}$$

To find a point which minimizes the objective function in the direction of $\boldsymbol{\delta}_k$, a line search is applied in the form

$$\alpha_k = \arg\min_{\alpha} f(\mathbf{x}_k + \alpha\boldsymbol{\delta}_k), \tag{3.11}$$

where α_k determines the step length. New point, $\mathbf{x}_{k+1}$, is obtained as

$$\mathbf{x}_{k+1} = \mathbf{x}_k + \alpha_k\boldsymbol{\delta}_k \tag{3.12}$$

and the objective function is updated as

$$f_{k+1} = f(\mathbf{x}_{k+1}). \tag{3.13}$$

Iterative procedure described in (3.10), (3.11), (3.12), (3.13) is repeated until the step length or the gradient magnitude reaches specified tolerances ε_1, ε_2, as in

$$\|\alpha_k\boldsymbol{\delta}_k\| \leq \varepsilon_1 \tag{3.14}$$

and

$$\|\mathbf{g}_k\| \leq \varepsilon_2. \tag{3.15}$$

The above procedure utilizes gradient and Hessian of the objective function. However, their analytic expressions are often unavailable. In such situations, they are estimated by using finite difference computation of partial derivatives, as in

$$\frac{\partial f}{\partial x_n} \approx \frac{f(\mathbf{x} + \mathbf{d}_n) - f(\mathbf{x})}{d} = f'_n(\mathbf{x}), \quad n = 1, 2, \ldots, N, \tag{3.16}$$

$$\frac{\partial^2 f}{\partial x_n \partial x_m} \approx \frac{f'_n(\mathbf{x} + \mathbf{d}_m) - f'_n(\mathbf{x})}{d}, \quad n = 1, 2, \ldots, N,\ m = 1, 2, \ldots, N, \tag{3.17}$$

where d is difference step size, and vectors

$$\mathbf{d}_q = [0, \ldots, 0, d, 0, \ldots, 0]^\mathrm{T}, \quad q = m, n \tag{3.18}$$

contain the value d as the qth element.

The finite difference computation of Hessian matrix requires a large number of function evaluations, which increases the algorithm's complexity. To reduce this complexity the quasi-Newton methods have been developed. Instead of Hessian matrix, these methods utilize its approximations. Several formulas for this approximation have been developed, such as Davidon-Fletcher-Powell (DFP) and Broyden-Fletcher-Goldfarb-Shanno (BFGS) formula [77]. The latter is very efficient and widely used.

In BFGS method, search direction in (3.10) is obtained as

$$\boldsymbol{\delta}_k = -\mathbf{B}_k^{-1}(\mathbf{x}_k)\mathbf{g}(\mathbf{x}_k). \tag{3.19}$$

At the beginning, $\mathbf{B} = \mathbf{I}$ is set. In the subsequent iterations, $\mathbf{B}$ is updated based on function values and gradient obtained in current and previous iterations, as in

$$\mathbf{B}_{k+1} = \mathbf{B}_k + \frac{\boldsymbol{\gamma}\boldsymbol{\gamma}^\mathrm{T}}{\boldsymbol{\gamma}^\mathrm{T}\mathbf{s}} - \frac{\mathbf{B}_k\mathbf{s}\mathbf{s}^\mathrm{T}\mathbf{B}_k}{\mathbf{s}^\mathrm{T}\mathbf{B}_k\mathbf{s}}, \tag{3.20}$$

where

$$\boldsymbol{\gamma} = \mathbf{g}_{k+1} - \mathbf{g}_k, \tag{3.21}$$

and

$$\mathbf{s} = \mathbf{x}_{k+1} - \mathbf{x}_k. \tag{3.22}$$

3.5 Sequential Quadratic Programming

Sequential quadratic programming (SQP) is a class of methods for solving nonlinear optimization problems. They are considered to be the most effective methods for constrained nonlinear optimization [70]. As the name suggests, SQPs are iterative and they can be considered as a generalization of the quasi-Newton method adapted for constrained optimization. Detailed analysis of the SQP algorithms is given in [69]. Nevertheless, the most important parts are provided hereafter.

Consider the following constrained optimization problem

$$\begin{aligned}
\underset{\mathbf{x}}{\text{minimize}} \quad & f(\mathbf{x}) \\
\text{subject to} \quad & a_i(\mathbf{x}) = 0, \quad i = 1, 2, \ldots, I, \\
& c_j(\mathbf{x}) \geq 0, \quad j = 1, 2, \ldots, J
\end{aligned} \tag{3.23}$$

where I and J are the numbers of equality and inequality constraints. The objective and constraint functions in (3.23) are nonlinear.

The Lagrangian of the problem in (3.23) is given by

$$\mathcal{L}(\mathbf{x}, \boldsymbol{\lambda}, \boldsymbol{\mu}) = f(\mathbf{x}) - \mathbf{a}^{\mathrm{T}}(\mathbf{x})\boldsymbol{\lambda} - \mathbf{c}^{\mathrm{T}}(\mathbf{x})\boldsymbol{\mu} \tag{3.24}$$

where

$$\boldsymbol{\lambda} = [\lambda_1, \lambda_2, \ldots, \lambda_I]^{\mathrm{T}}, \tag{3.25}$$

$$\boldsymbol{\mu} = [\mu_1, \mu_2, \ldots, \mu_J]^{\mathrm{T}}, \tag{3.26}$$

are Lagrange multipliers, and

$$\mathbf{a}(\mathbf{x}) = [a_1(\mathbf{x}), a_2(\mathbf{x}), \ldots, a_I(\mathbf{x})]^{\mathrm{T}}, \tag{3.27}$$

$$\mathbf{c}(\mathbf{x}) = [c_1(\mathbf{x}), c_2(\mathbf{x}), \ldots, c_J(\mathbf{x})]^{\mathrm{T}}. \tag{3.28}$$

The SQP solves the problem in (3.23) by forming a sequence of quadratic problems. At the kth iteration, the Lagrangian is modeled by using quadratic approximation, as in

$$\mathcal{L}(\mathbf{u}_{k+1}) = \mathcal{L}(\mathbf{u}_k) + \nabla \mathcal{L}(\mathbf{u}_k)\boldsymbol{\delta}_k + \frac{1}{2}\boldsymbol{\delta}_k^{\mathrm{T}}\nabla^2 \mathcal{L}(\mathbf{u}_k)\boldsymbol{\delta}_k \tag{3.29}$$

where

$$\mathbf{u} = \begin{bmatrix} \mathbf{x} \\ \boldsymbol{\lambda} \\ \boldsymbol{\mu} \end{bmatrix}, \quad \boldsymbol{\delta} = \begin{bmatrix} \boldsymbol{\delta}_{\mathbf{x}} \\ \boldsymbol{\delta}_{\boldsymbol{\lambda}} \\ \boldsymbol{\delta}_{\boldsymbol{\mu}} \end{bmatrix}.$$

The increment $\boldsymbol{\delta}_k$ is found by solving the problem

$$\mathcal{L}(\mathbf{u}_k) + \nabla \mathcal{L}(\mathbf{u}_k)\boldsymbol{\delta}_k + \frac{1}{2}\boldsymbol{\delta}_k^{\mathrm{T}}\nabla^2 \mathcal{L}(\mathbf{u}_k)\boldsymbol{\delta}_k = 0 \tag{3.30}$$

If $\mathbf{u}_{k+1}$ is considered a local minimizer of (3.29) and consequently of (3.23), then the necessary optimality conditions, also known as the Karush-Kuhn-Tucker (KKT) conditions, must be satisfied. They are given by

$$\nabla_x \mathcal{L}(\mathbf{u}_{k+1}) = 0 \tag{3.31}$$

$$a_i(\mathbf{x}_{k+1}) = 0 \quad i = 1, 2, \dots, I \tag{3.32}$$

$$c_j(\mathbf{x}_{k+1}) \geq 0 \quad j = 1, 2, \dots, J \tag{3.33}$$

$$\boldsymbol{\mu}_{k+1} \geq \mathbf{0} \tag{3.34}$$

$$\mu_{j,k+1} c_j(\mathbf{x}_{k+1}) = 0 \quad j = 1, 2, \dots, J \tag{3.35}$$

For the considered problem, these conditions can be expressed as

$$\mathbf{Z}_k \boldsymbol{\delta}_{\mathbf{x}k} + \mathbf{g}_k - \mathbf{A}_k^{\mathrm{T}} \boldsymbol{\lambda}_{k+1} - \mathbf{C}_k^{\mathrm{T}} \boldsymbol{\mu}_{k+1} = 0 \tag{3.36}$$

$$\mathbf{A}_k \boldsymbol{\delta}_{\mathbf{x}k} = -\mathbf{a}_k(\mathbf{x}_k) \tag{3.37}$$

$$\mathbf{C}_k \boldsymbol{\delta}_{\mathbf{x}k} \geq -\mathbf{c}_k(\mathbf{x}_k) \tag{3.38}$$

$$\boldsymbol{\mu}_{k+1} \geq \mathbf{0} \tag{3.39}$$

$$(c_j(\mathbf{x}_k) + \mathbf{C}_{j,k} \boldsymbol{\delta}_{\mathbf{x}k}) \mu_{j,k+1} = 0 \quad j = 1, 2, \dots, J \tag{3.40}$$

where

$$\mathbf{Z}_k = \nabla_{\mathbf{xx}}^2 f(\mathbf{x}_k) - \nabla_{\mathbf{xx}}^2 \mathbf{a}^{\mathrm{T}}(\mathbf{x}_k) \boldsymbol{\lambda}_k - \nabla_{\mathbf{xx}}^2 \mathbf{c}^{\mathrm{T}} \boldsymbol{\mu}_k \tag{3.41}$$

$$\mathbf{g}_k = \nabla_{\mathbf{x}} f(\mathbf{x}_k) \tag{3.42}$$

$$\mathbf{A}_k = \begin{bmatrix} \nabla_{\mathbf{x}}^{\mathrm{T}} a_1(\mathbf{x}_k) \\ \nabla_{\mathbf{x}}^{\mathrm{T}} a_2(\mathbf{x}_k) \\ \vdots \\ \nabla_{\mathbf{x}}^{\mathrm{T}} a_I(\mathbf{x}_k) \end{bmatrix} \tag{3.43}$$

$$\mathbf{C}_k = \begin{bmatrix} \nabla_{\mathbf{x}}^{\mathrm{T}} c_1(\mathbf{x}_k) \\ \nabla_{\mathbf{x}}^{\mathrm{T}} c_2(\mathbf{x}_k) \\ \vdots \\ \nabla_{\mathbf{x}}^{\mathrm{T}} c_J(\mathbf{x}_k) \end{bmatrix} \tag{3.44}$$

$$\nabla_{\mathbf{x}} = \begin{bmatrix} \dfrac{\partial}{\partial x_1} & \dfrac{\partial}{\partial x_2} & \cdots & \dfrac{\partial}{\partial x_N} \end{bmatrix}^{\mathrm{T}} \tag{3.45}$$

The expressions in (3.36)-(3.40) can be recognized as the KKT conditions of the problem

$$\underset{\mathbf{s}_k}{\text{minimize}} \quad \frac{1}{2} \mathbf{s}_k^{\mathrm{T}} \mathbf{Z}_k \mathbf{s}_k + \mathbf{s}_k^{\mathrm{T}} \mathbf{g}_k \tag{3.46a}$$

$$\text{subject to} \quad \nabla_{\mathbf{x}} a_i(\mathbf{x}_k) \mathbf{s}_k = -a_i(\mathbf{x}_k), \quad i = 1, 2, \dots, I, \tag{3.46b}$$

$$\nabla_{\mathbf{x}} c_j(\mathbf{x}_k) \mathbf{s}_k \geq -c_j(\mathbf{x}_k), \quad j = 1, 2, \dots, J \tag{3.46c}$$

where $\mathbf{s}_k = \boldsymbol{\delta}_{\mathbf{x}k}$. The Lagrangian multipliers of this problem are equal to $\boldsymbol{\lambda}_{k+1}$ and $\boldsymbol{\mu}_{k+1}$ of the original problem. Clearly, the problem in (3.46) is convex and can be easily solved. The solution $\mathbf{s}_k$ is used to form a new iterate

$$\mathbf{x}_{k+1} = \mathbf{x}_k + \alpha_k \mathbf{s}_k. \tag{3.47}$$

where α_k determines the step length. It is obtained by using a line search method similar to the line search used in quasi-Newton algorithm. The iterative procedure is repeated until the step length or the gradient magnitude reaches specified tolerances ε_1 and ε_2, as in

$$\|\alpha_k \boldsymbol{\delta}_{\mathbf{x}k}\| \leq \varepsilon_1 \tag{3.48}$$

$$\|\mathbf{g}_k\| \leq \varepsilon_2. \tag{3.49}$$

To reduce the computational complexity of the SQP algorithm, the Hessian is usually approximated by using the BFGS formula [69].

3.6 Branch and Bound

Branch and bound (B&B) is a family of algorithms used for global solving of NP-hard problems [78]. NP-hard problems are nonconvex problems for which no deterministic polynomial-time algorithm can be found. Such problems can be solved in an acceptable time only for small number of variables [71].

Combinatorial problems are NP-hard. These problems can be solved by performing an exhaustive search over the whole solution space, which is computationally expensive. Instead of the exhaustive search, "smarter" strategies can be incorporated into the search procedure. One way is to employ B&B framework.

Outline of the generic B&B is given in Algorithm 1 [78]. Let $f(\mathbf{x})$ denote the objective function, X denote the whole search space, $\mathbf{x} \in X$, and $\mathbf{x}^*$ denote current (or predefined) optimum. The B&B framework is based on an iterative division of X into smaller search spaces $S_n \subseteq X$, $n = 1, 2, \ldots, N$. Such iterative division results in a tree structure, where each subproblem is stored in one node of the tree. The tree is explored in the following manner. First, a list T containing all subproblems to be explored is formed, i.e. $T = X$. At each node, a partial solution $\hat{\mathbf{x}}$, and a lower bound of the objective function value, $LB(f(\hat{\mathbf{x}}))$, over a particular local search space are obtained. If obtained $LB(f(\hat{\mathbf{x}}))$ is suboptimal compared to the current optimum lower bound, $LB(f(\hat{\mathbf{x}})) > LB(f(\mathbf{x}^*))$, or if a solution is infeasible, that node and all of its children nodes can be pruned, i.e. eliminated from further examination, that is $T = T \setminus S_n$. In this way, B&B eliminates the regions of search space that cannot lead to a better solution.

If $LB(f(\hat{\mathbf{x}})) \leq LB(f(\mathbf{x}^*))$, current optimum is updated, $\mathbf{x}^* = \hat{\mathbf{x}}$. The search is finished when all subproblems are explored and the best solution $\mathbf{x}_{\text{opt}} = \mathbf{x}^*$ is returned.

**Algorithm 1** Generic branch and bound algorithm [78]

 1: Initialize $T = X$ and $\mathbf{x}^*$
 2: **while** $\{T \neq \emptyset\}$ **do**
 3:     Choose a subproblem S_n from T
 4:     **if** a solution $\hat{\mathbf{x}} \in S_n$ is found such that $LB(f(\hat{\mathbf{x}})) \leq LB(f(\mathbf{x}^*))$ **then**
 5:         $\mathbf{x}^* = \hat{\mathbf{x}}$
 6:     **end if**
 7:     **if** S_n cannot be pruned **then**
 8:         Partition S_n into $S_1, S_2, ..., S_r$ {r can be different at each iteration}
 9:         Insert $S_1, S_2, ..., S_r$ into T
10:     **end if**
11:     Remove S_n from T
12: **end while**
13: Return optimum $\mathbf{x}_{\text{opt}} = \mathbf{x}^*$

There are several search strategies regarding the order of the tree exploration: depth-first, breadth-first, best-fit, and cyclic best-fit search [78]. These strategies are illustrated in Figure 3.3. Depth-first algorithm starts from the root and propagates through the tree by examing the first unexplored child node at each branching, i.e. in every iteration the algorithm goes deeper into the tree. In breadth-first search, the nodes that share the same "depth level" are examined first, before going into next tree level. Best-fit search does not explore specific branches exclusively in a depth of breadth first manner. As an addition to the objective function being minimized, it uses a heuristic merit function whose value indicates which problem to explore next. This enables the algorithm to converge to the optimum solution much faster. However, for best-fit search the whole unexplored tree must be stored beforehand, which can be memory consuming. Finally, cyclic best-fit search is a strategy which combines the best-fit and the depth-first search. The tree is divided into so called contours according to predifined rules. Then, it is explored by iteratively solving the best subproblem of the each contuor. The best subproblem is determined by the merit function introduced in best-fit search.

The choice of the search strategy depends on the problem at hand and it greatly influences the algorithm's efficiency, in terms of number of pruning performed, memory usage and overall computation time.

(a) Depth-first search.

(b) Breadth-first search.

(c) Best-fit search.

(d) Cyclic best-fit search.
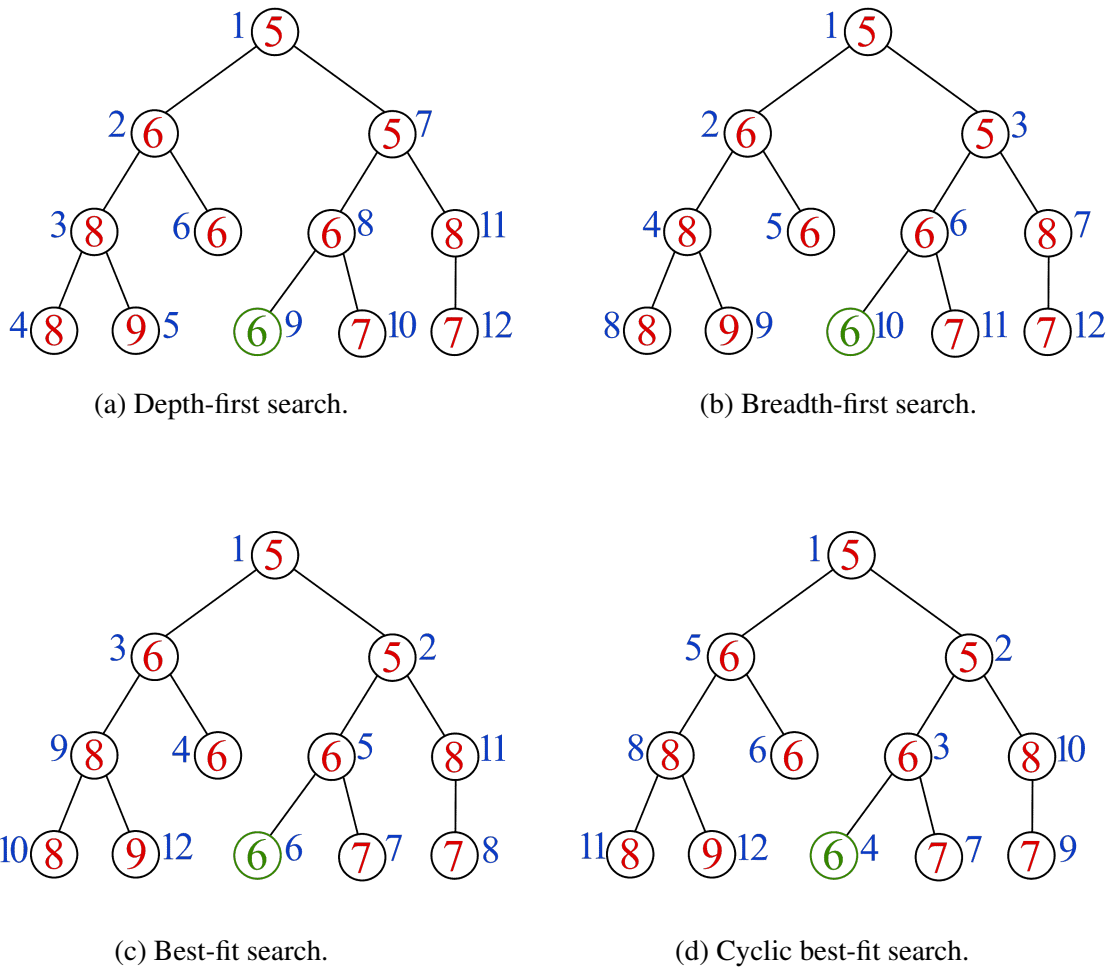
Figure 3.3: Examples of different tree-searching strategies for branch and bound. Blue numbers determine the node-searching order, whereas red numbers indicate the value of lower bound of objective function at a particular node. The optimum node is colored in green. In this example, the value of the merit functions in best-fit and cyclic best-fit search is shown equal to the value of lower bound of objective function. Furthermore, in cyclic best-fit strategy, the nodes with the same depth level are grouped into the same contours. Adapted from [78].

Chapter 4

L_1 Pencil Beams

In this chapter, sythesis of pencil-beam linear antenna arrays with minimum L_1-norm is presented. The proposed method is based on convex optimization [79]. The properties of the proposed L_1 pencil beams are analyzed and several design examples are provided.

4.1 Motivation

A general optimization problem describing the design of linear array forming pencil-beam is given by

$$
\begin{aligned}
\underset{\mathbf{a}}{\text{minimize}} \quad & \varepsilon(\mathbf{a}, \theta_s) \\
\text{subject to} \quad & \sum_{n=1}^{N} a_n = 1
\end{aligned}
\tag{4.1}
$$

where ε is a measure of the sidelobe error, $\mathbf{a} = [a_1,\ a_2,\ \ldots,\ a_N]^{\mathrm{T}}$ is the vector of excitation coefficients, and θ_s is the beginning of the sidelobe region in which the error is minimized. The measure of the sidelobe error ε is often expressed via L_p-norm

$$
\varepsilon_p(\mathbf{a}, \theta_s) = 4\pi \left(\int_{\theta_s}^{\frac{\pi}{2}} |f(\mathbf{a}, \theta)|^p \cos\theta \, d\theta \right)^{\frac{1}{p}}
\tag{4.2}
$$

where $f(\mathbf{a}, \theta)$ is the array factor of linear antenna array with elements placed at the x-axis of a coordinate system. Common choices for p are $p = 2$ and $p \to \infty$, for which the problem in (4.1) can be expressed in a convex form and readily solved. Moreover, for these values of p, optimum solutions of (4.1) can be obtained via analytic methods. However, the optimization approach offers more flexibility as it supports incorporating additional design requirements into the general problem (4.1).

Linear arrays with minimum L_2-norm are obtained analytically via discrete prolate spheroidal sequences (DPSS) [80]. These arrays radiate minimum energy in the sidelobe region, which is a consequence of monotonically decreasing side lobes. On the other hand, L_∞ arrays exhibit equiripple power density within the sidelobe region. These arrays are known as Dolph-Chebyshev arrays [21]. Convex optimization of such arrays is also considered [72]. An important property of such arrays is that they achieve the narrowest main lobe for specified sidelobe level. Dolph-Chebyshev arrays are a representative choice when the design of pencil beams is considered, since they offer a good tradeoff between the level of the side lobes and the width of the main lobe [1].

The L_2- and L_∞-based designs are also well known in FIR filter theory. The frequency responses of such filters have similar shapes as the array factors of the $\lambda/2$-spaced L_2 and L_∞ antenna arrays. Other norms have been rarely considered. In [81], the design of L_1 FIR filters was presented. In the paper referred to, it was shown that L_1 FIR filters exhibit higher stopband flatness than do the L_2 filters, which is paid with wider transition bands. It is expected that utilization of L_1-norm in the context of pencil-beam design will provide similar behavior, resulting in array factors suitable for many applications.

In this work, pencil-beam linear antenna arrays with minimum L_1-norm are proposed. A convex optimization method for their design is presented. In addition, a detailed analysis of the properties of such arrays is presented.

4.2 Convex Optimization of L_1 Pencil Beams

Using the general optimization problem given by (4.1) and assuming $p = 1$, the synthesis of linear pencil-beam antenna arrays with minimum L_1-norm is given by

$$
\begin{aligned}
&\underset{\mathbf{a}}{\text{minimize}} && \varepsilon_1(\mathbf{a}, \theta_s) \\
&\text{subject to} && \sum_{n=1}^{N} a_n = 1
\end{aligned}
\tag{4.3}
$$

where

$$
\varepsilon_1(\mathbf{a}, \theta_s) = 4\pi \int_{\theta_s}^{\frac{\pi}{2}} |f(\mathbf{a}, \theta)| \cos\theta \, d\theta
\tag{4.4}
$$

To solve the above optimization problem, error $\varepsilon_1(\mathbf{a}, \theta_s)$ can be rearranged in the following manner. First, the array factor from (2.10) is introduced into (4.4), resulting in

$$
\varepsilon_1(\mathbf{a}, \theta_s) = 4\pi \int_{\theta_s}^{\frac{\pi}{2}} \left| \sum_{n=1}^{N} a_n e^{j\frac{2\pi}{\lambda} x_n \sin\theta} \right| \cos\theta \, d\theta
\tag{4.5}
$$

Then, by introducing $\omega = \sin(\theta)$, the error function takes the form

$$\varepsilon_1(\mathbf{a}, \omega) = 4\pi \int\limits_{\omega_s}^{1} \left| \sum_{n=1}^{N} a_n e^{j\frac{2\pi}{\lambda}x_n\omega} \right| d\omega = 4\pi \int\limits_{\omega_s}^{1} |f(\mathbf{a}, \omega)| \, d\omega \tag{4.6}$$

where $\omega_s = \sin(\theta_s)$. The integration in (4.6) can be performed numerically. To prepare the problem for numerical integration, the integrand in (4.6) should be evaluated in a finite number of points. Here, it is evaluated in Q equidistant points, $\omega_q \in [\omega_s, 1]$, $q = 1, 2, \ldots, Q$. The integrand values at these points can be obtained in a matrix form, as in

$$t_q = |f(\mathbf{a}, \omega_q)| = \|\mathbf{A}_q \mathbf{a}\|, \quad q = 1, 2, \ldots, Q \tag{4.7}$$

where $\| \cdot \|$ denotes the L_2-norm and $\mathbf{A}_q$ is given by

$$\mathbf{A}_q = \begin{bmatrix} \cos(\frac{2\pi}{\lambda}\omega_q x_1) & \cos(\frac{2\pi}{\lambda}\omega_q x_2) & \cdots & \cos(\frac{2\pi}{\lambda}\omega_q x_N) \\ \sin(\frac{2\pi}{\lambda}\omega_q x_1) & \sin(\frac{2\pi}{\lambda}\omega_q x_2) & \cdots & \sin(\frac{2\pi}{\lambda}\omega_q x_N) \end{bmatrix} \tag{4.8}$$

Integral in (4.6) can be approximated via several methods, for example by utilizing rectangular rule, trapezoidal rule, or Simpson's rule. Here, it is approximated via Simspon's 1/3 rule in an odd number of points Q, resulting in

$$\varepsilon_a(\mathbf{t}, \omega_s) = 4\pi \frac{1-\omega_s}{3(Q-1)} \left(t_1 + 4 \sum_{m=1}^{(Q-1)/2} t_{2m} + 2 \sum_{m=1}^{(Q-3)/2} t_{2m+1} + t_Q \right) \tag{4.9}$$

where $\mathbf{t} = [t_1, t_2, \ldots, t_Q]^{\mathrm{T}}$. Finally, coefficients of pencil-beam antenna array with minimum L_1-norm are obtained by solving the optimization problem

$$\begin{aligned} \underset{\mathbf{a}, \mathbf{t}}{\text{minimize}} \quad & \varepsilon_a(\mathbf{t}, \omega_s) \\ \text{subject to} \quad & \|\mathbf{A}_q \cdot \mathbf{a}\| \leq t_q, \quad q = 1, 2, \ldots, Q, \\ & \sum_{n=1}^{N} a_n = 1 \end{aligned} \tag{4.10}$$

The problem in (4.10) is convex. Moreover, it is recognized as a second-order cone program with Q second-order cone constraints and one equality constraint. Therefore, it can be solved by using available solvers for convex optimization. Here, it is solved by using MOSEK optimization toolbox [74] running under Matlab environment.

4.3   Analysis of L_1 Pencil Beams

4.3.1   Practical Design Considerations

The starting angle of the sidelobe region, $\omega_s = \sin\theta_s$, should be carefully chosen. In experiments, designer might choose any angle. However, pencil-beam arrays radiate power only in a single direction, possibly with the narrowest main lobe. To achieve such behavior, the L_1 error is minimized throughout the region $\theta \in [0, \pi/2]$, that is, for $\omega \in [0, 1]$. It leads to $\theta_s = 0$ and, consequently, $\omega_s = 0$.

In practice, error (4.9) should be approximated in a sufficiently large number of points, Q. Throughout this chapter, $Q = 2001$ is used.

The following sections bring the analysis of the proposed L_1 pencil beams, as well as two design examples.

4.3.2   Features of L_1 Pencil Beams

To illustrate features of the proposed L_1 pencil beams, arrays having 10, 20, and 40 elements, with equal interelement spacing of 0.5λ are optimized. Figure 4.1 shows the obtained array factors and Figure 4.2 shows the corresponding excitation coefficients. As expected, array factors have monotonically decreasing side lobes. The optimum excitation coefficients are all positive, exhibit a bell-shaped magnitudes, and are symmetric around the array's center.

Figure 4.3 illustrates the properties of L_1 pencil beams with various numbers of antenna elements, N. As shown in Figure 4.3a, the mainlobe width decreases with an increase in N. The levels of the first, second, and third side lobe for the arrays with various number of elements are shown in Figure 4.3b. Clearly, the level of the first side lobe does not change significantly, remaining approximately at -21 dB for all N. Such property is very attractive since sidelobe level lower than -20 dB is rarely required [1].

As a consequence of the decreasing sidelobes, high beam efficiency is achieved. The obtained beam efficiency is greater than 98 % for all arrays, as illustrated in Figure 4.3c. The dynamic range ratio of excitation coefficients obtained for various N is shown in Figure 4.3d. It is clear that the DRR increases linearly with an increase in N. From the obtained data, the value of DRR can be estimated as

$$DRR = 0.26N + 0.49 \tag{4.11}$$
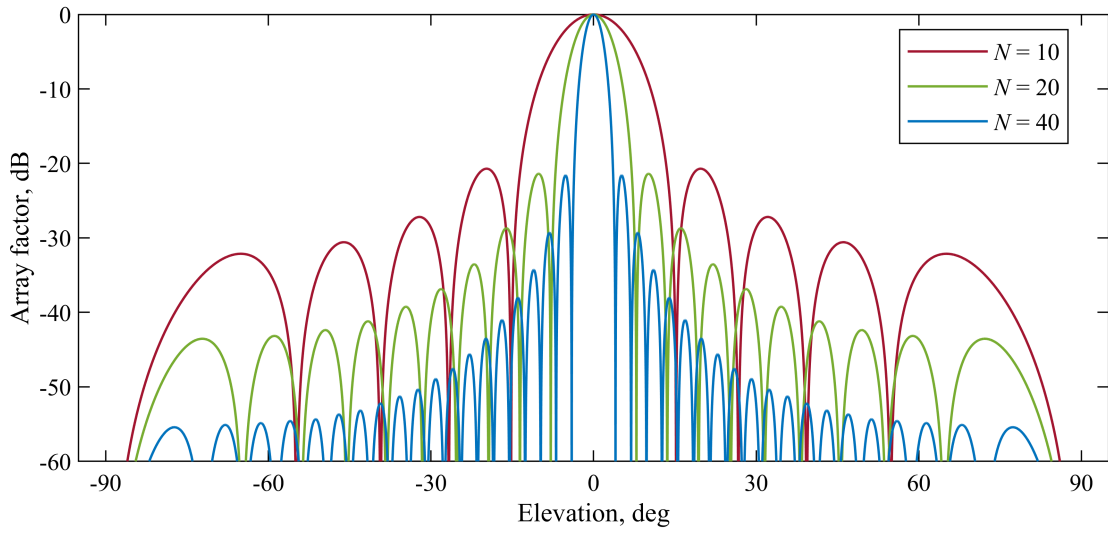
Figure 4.1: Array factors of L_1 pencil beams with 10, 20, and 40 array elements.

(a)

(b)

(c)
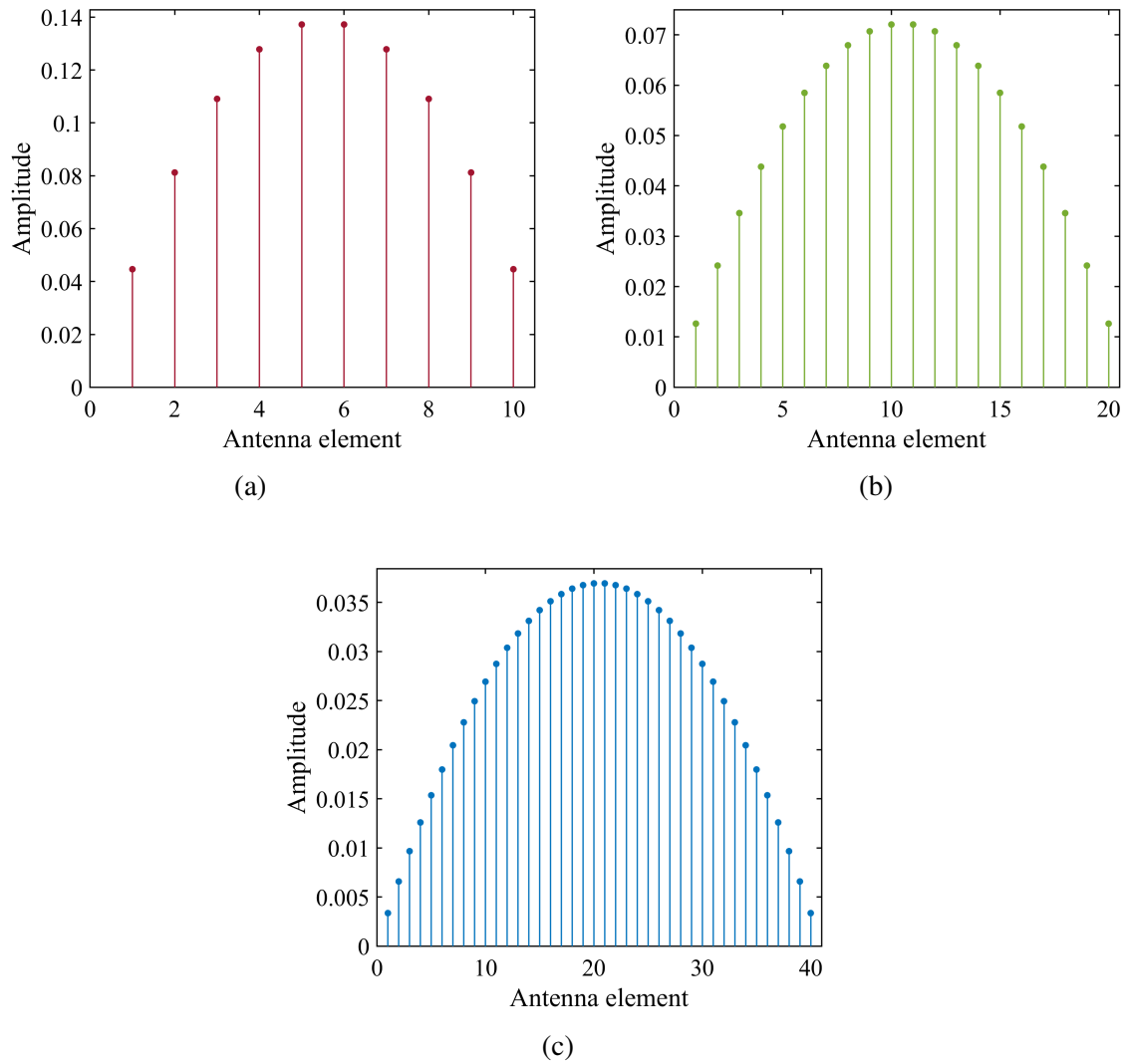
Figure 4.2: Coefficients of L_1 pencil beams with 10, 20, and 40 array elements.
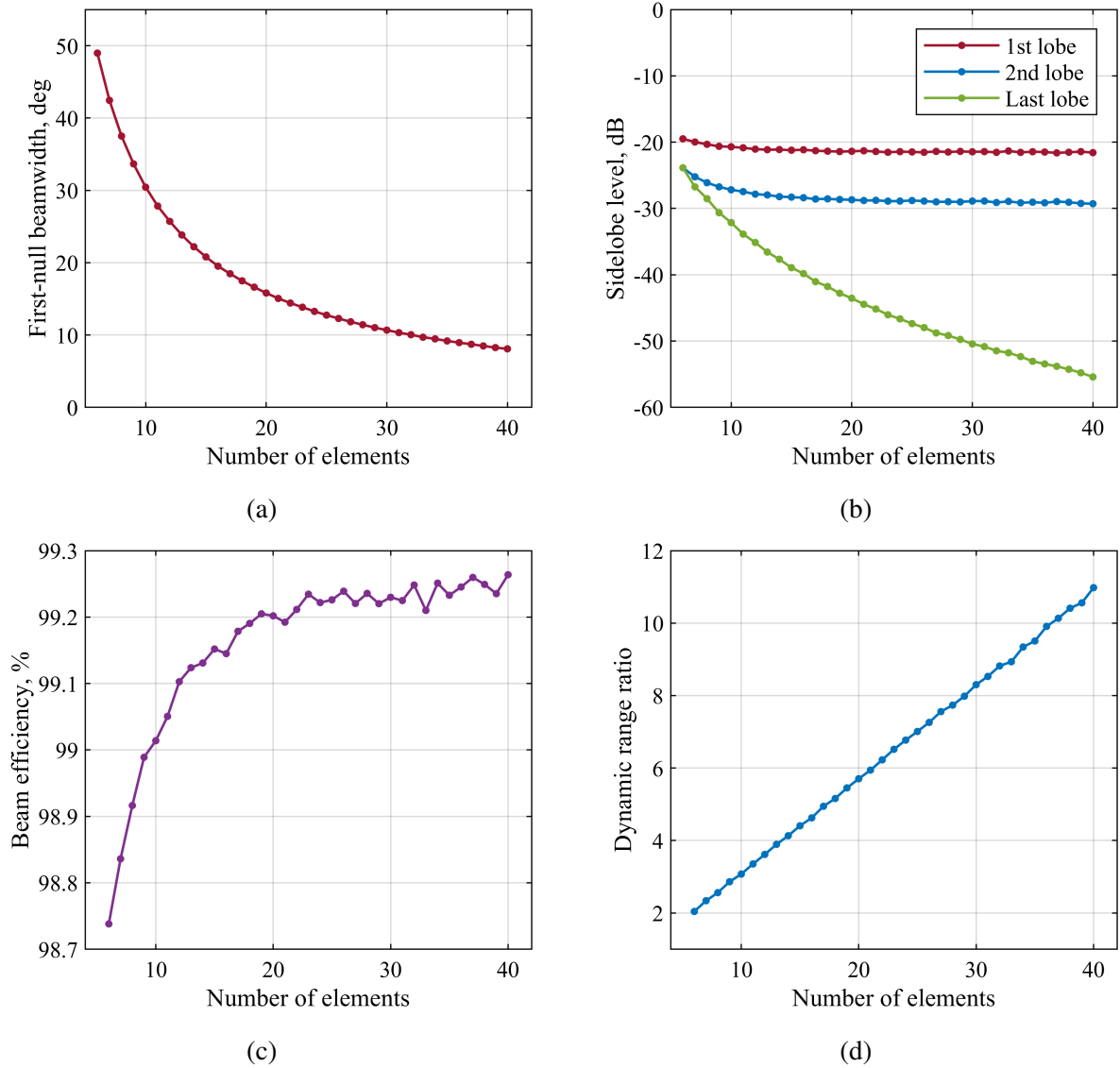
Figure 4.3: First-null beamwidth (a), sidelobe level (b), beam efficiency (c), and dynamic range ratio (d) of L_1 pencil beams with various number of elements.

4.3.3 Comparison with Other Pencil Beams

In this section, a comparison with other design methods is provided. First, L_1 pencil-beam arrays with 10 to 40 elements, equal interelement spacing of 0.5λ, and $\theta_s = 0$ are designed. Then, the Gaussian [22], Gegenbauer [24], and Kaiser-Hamming [27] arrays with the same number of elements are designed to achieve approximately the same sidelobe level as the L_1 arrays. Note that Gegenbauer arrays can be designed to exhibit either $-$ the minimum sidelobe power or minimum DRR for a specified SLL. Here, the arrays with minimum sidelobe power are used for comparison. In the case of Kaiser-Hamming and Gaussian arrays, minor differences in the obtained and the required SLL are expected, since SLL is not an input parameter of such designs.

Figure 4.4 shows the first-null beamwidth, directivity, beam efficiency, and dynamic range ratio of the obtained array factors for various numbers of antenna elements. Clearly, the Kaiser-Hamming and Gaussian arrays have the narrowest main lobes. They are followed by the L_1 and Gegenbauer arrays. As expected, the directivities exhibit the opposite behavior. However, due to decreasing sidelobes, the beam efficiency of the L_1 arrays is higher than the efficiency of the corresponding Gaussian and Kaiser-Hamming arrays. The L_1 arrays have only slightly lower efficiency than do the Gegenbauer arrays. However, they exhibit significantly lower DRR.

Figure 4.4: First-null beamwidth (a), directivity (b), beam efficiency (c), and dynamic range ratio (d) of L_1 pencil beams compared to Gaussian [22], Gegenbauer [24] and Kaiser-Hamming [27] pencil beams having 10 to 40 elements.

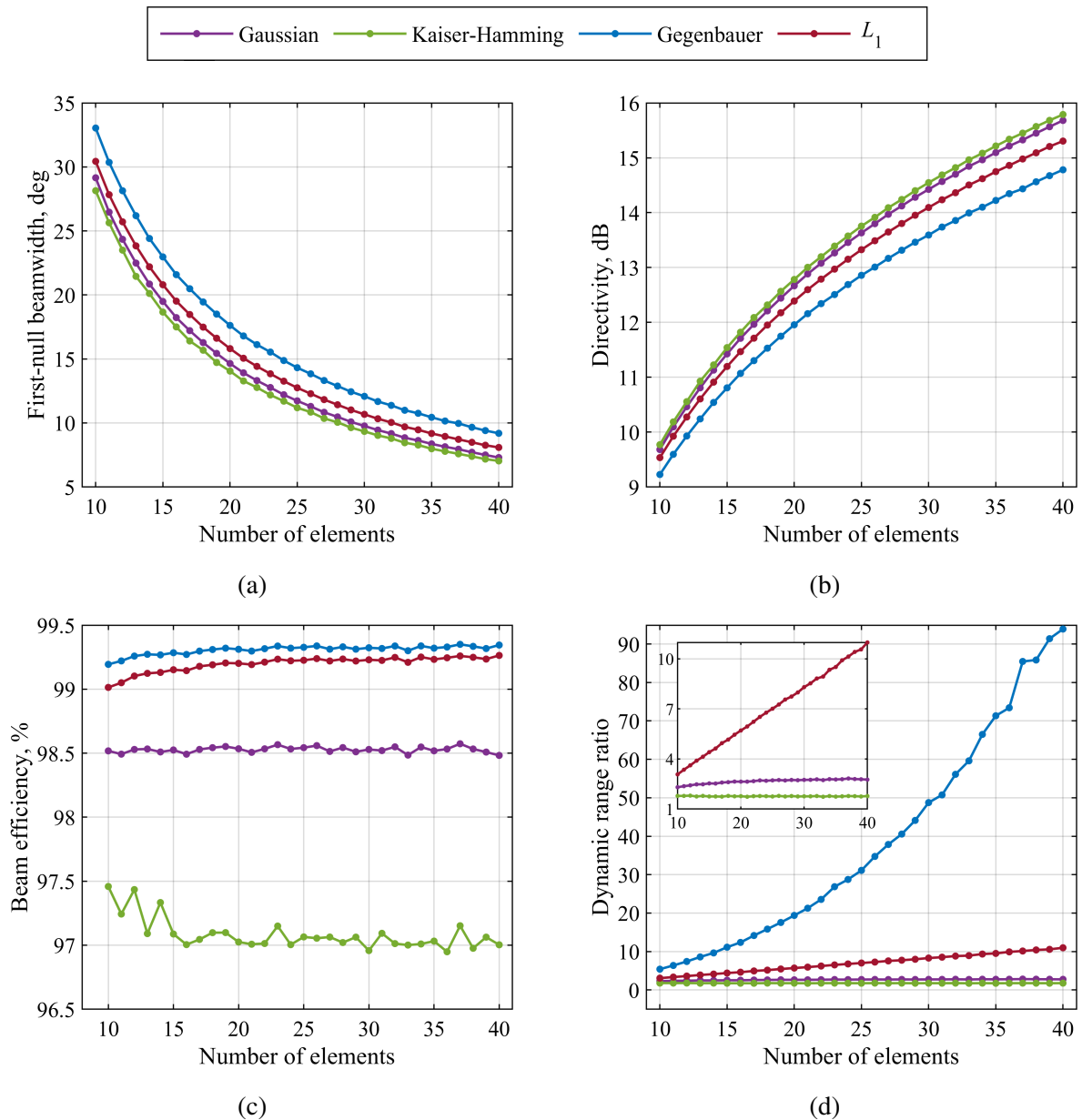Array factors of the arrays with 16 elements are shown in Figure 4.5, for convenience. Their comparison in a numeric form is provided in Table 4.1.

To conclude, L_1 pencil beams simultaneously offer a high beam efficiency and a low dynamic range ratio of excitation coefficients. In addition, they exhibit a convenient level of the first side lobe of -21 dB. The coefficients of L_1 arrays are obtained in a convex form, which offers design time and robustness similar to those obtained by analytic expressions.
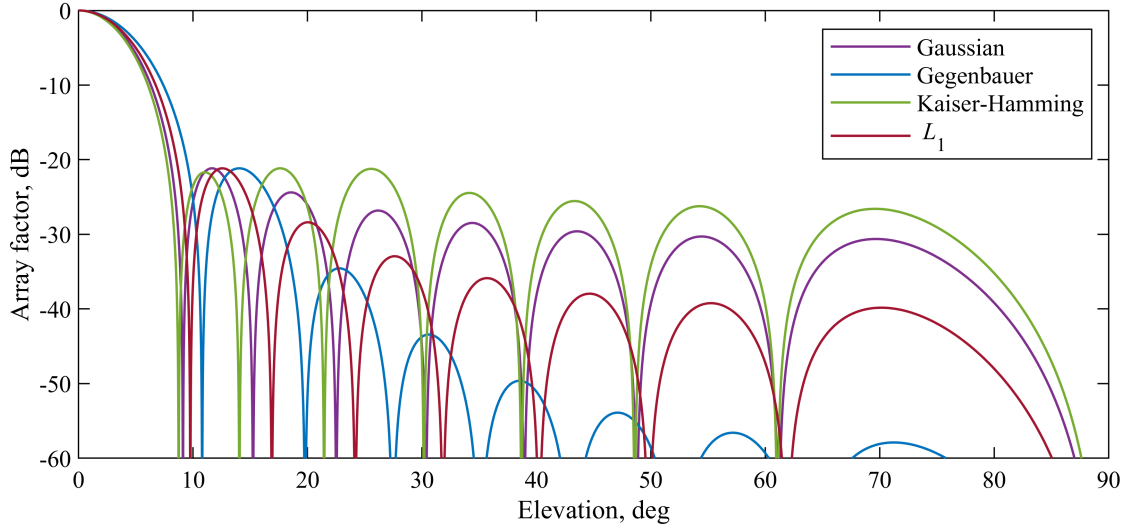
Figure 4.5: Array factors of L_1, Gaussian [22], Gegenbauer [24], and Kaiser-Hamming [27] arrays with 16 elements.

Table 4.1: Sidelobe level, SLL, first-null beamwidth, FNBW, 3dB-beamwidth, BW3, beam efficiency, BE, directivity, DIR, and dynamic range ratio, DRR, of proposed L_1, Gaussian, Gegenbauer and Kaiser-Hamming arrays with 16 elements.

Array type	SLL, dB	FNBW, deg	BW3, deg	BE, %	DIR, dB	DRR
Proposed L_1	-21.1	19.5	7.87	99.15	11.5	4.63
Gaussian	-21.1	18.2	7.40	98.49	11.7	2.53
Gegenbauer	-21.1	21.6	8.63	99.27	11.1	12.4
Kaiser-Hamming	-21.1	17.5	7.10	96.98	11.8	1.75

4.3.4   Design of Unequally Spaced L_1 Pencil Beams

Previous example considered arrays with equally spaced elements. In this example, L_1 pencil beams are designed for the arrays with unequally spaced elements. Clearly, optimum positioning of the antenna elements is a difficult task, which is not supported by the method described in this chapter. However, nonequally spaced design often utilizes fixed positions obtained by

other design methods. This approach is used in the following examples. The optimization of element positions is considered in Chapter 6.

Two arrays that consist of 35 elements are designed. Their positions are obtained by employing the method in [61]. The method referred to starts from the equidistant array with interelement spacing of 0.5λ. Positions of the first array are obtained by using 400 iterations and target main lobe width $\vartheta = 5°$. Positions of the second array are obtained also by using 400 iterations but with $\vartheta = 6°$. These positions are listed in Tables 4.2 and 4.3, respectively, and are shown in Figure 4.6, for convenience. The method in [61] assumes uniform element excitations.

Table 4.2: Positions of antenna elements obtained with the method from [61], for target main lobe width of $\vartheta = 5°$.

n	x_n, λ	n	x_n, λ	n	x_n, λ
1, 35	± 10.5757	7, 29	± 5.7750	13, 23	± 2.4251
2, 34	± 9.7693	8, 28	± 5.1497	14, 22	± 1.9326
3, 33	± 8.8973	9, 27	± 4.5548	15, 21	± 1.4391
4, 32	± 8.0264	10, 26	± 4.0004	16, 20	± 0.9588
5, 31	± 7.1855	11, 25	± 3.4544	17, 19	± 0.4771
6, 30	± 6.4265	12, 24	± 2.9388	18	0.0000

Table 4.3: Positions of antenna elements obtained with the method from [61], for target main lobe width of $\vartheta = 6°$.

n	x_n, λ	n	x_n, λ	n	x_n, λ
1, 35	± 9.4456	7, 29	± 4.9670	13, 23	± 2.0170
2, 34	± 8.6329	8, 28	± 4.4581	14, 22	± 1.7509
3, 33	± 7.7575	9, 27	± 3.9106	15, 21	± 1.1663
4, 32	± 6.9050	10, 26	± 3.4844	16, 20	± 0.8926
5, 31	± 6.1714	11, 25	± 2.9360	17, 19	± 0.3814
6, 30	± 5.5650	12, 24	± 2.5963	18	0.0000
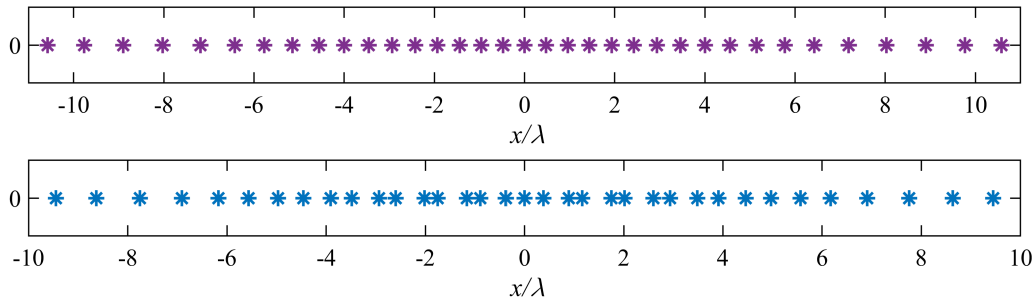
Figure 4.6: Positions of antenna elements from Table 4.2 (top) and Table 4.3 (bottom).

After the positions are found, coefficients of L_1 pencil beams are found by solving the problem (4.10). Coefficients of the obtained L_1 pencil beams are shown in Figures 4.7a and 4.7b, whereas their numerical values are given in Tables 4.4 and 4.5. Note that the array with positions from Table 4.2 contains only positive coefficients, whereas the array with positions from Table 4.3 contains coefficients that take both, positive and negative values. Both arrays have coefficients that exhibit even symmetry around arrays' center. The corresponding array factors are shown in Figures 4.8b and 4.8b, from which it is clear that the sidelobes no longer exhibit monotonically decreasing behaviour.

(a) (b)
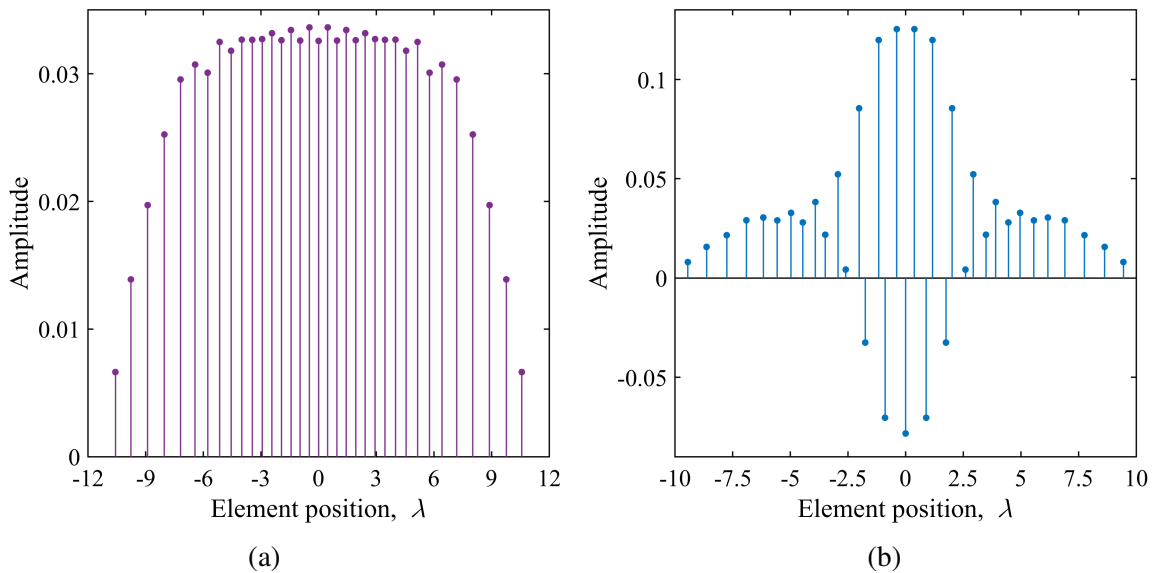
Figure 4.7: Coefficients of L_1 pencil beams with 35 unequally spaced elements with positions from Table 4.2 (a) and Table 4.3 (b).

Table 4.4: Optimum coefficients of proposed L_1 pencil beam with 35 unequally spaced elements placed at positions listed in Table 4.2.

n	a_n	n	a_n	n	a_n
1, 35	0.0066	7, 29	0.0301	13, 23	0.0332
2, 34	0.0139	8, 28	0.0325	14, 22	0.0326
3, 33	0.0197	9, 27	0.0318	15, 21	0.0334
4, 32	0.0252	10, 26	0.0327	16, 20	0.0326
5, 31	0.0296	11, 25	0.0327	17, 19	0.0336
6, 30	0.0307	12, 24	0.0327	18	0.0326

Table 4.5: Optimum coefficients of proposed L_1 pencil beam with 35 unequally spaced elements placed at positions listed in Table 4.3.

n	a_n	n	a_n	n	a_n
1, 35	0.0081	7, 29	0.0328	13, 23	0.0855
2, 34	0.0157	8, 28	0.0280	14, 22	-0.0325
3, 33	0.0216	9, 27	0.0383	15, 21	0.1199
4, 32	0.0291	10, 26	0.0218	16, 20	-0.0704
5, 31	0.0305	11, 25	0.0522	17, 19	0.1254
6, 30	0.0290	12, 24	0.0043	18	-0.0783
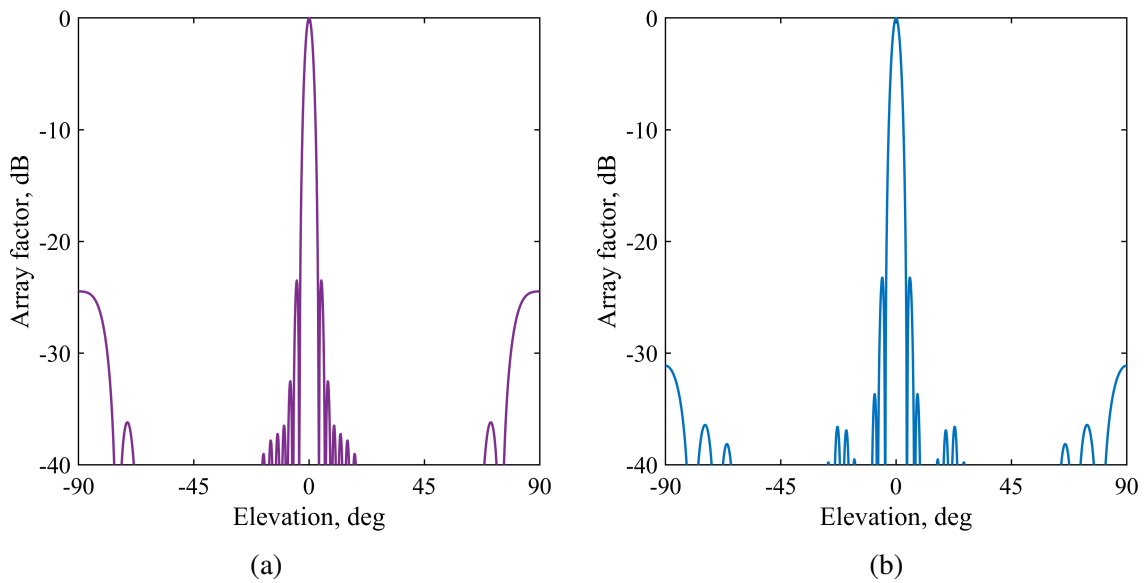
Figure 4.8: Array factors of L_1 pencil beams with 35 unequally spaced elements with positions from Table 4.2 (a) and Table 4.3 (b).

The beam parameters of unequally spaced L_1 arrays are given in Table 4.6 together with the parameters of the array with equal element spacing of 0.5λ. Clearly, in this case, unequally spaced arrays offered a lower sidelobe level, narrower main beam as well as a higher beam efficiency and directivity. In addition, a lower DRR is obtained for the first array. The results obtained in these examples suggest that the proposed method can be applied to arrays with nonequally spaced geometry as well, which is an advantage over some analytical methods. The result can be obtained in a few seconds, which enables fast experimenting.

Table 4.6: Sidelobe level, SLL, first-null beamwidth, FNBW, 3dB-beamwidth, BW3, beam efficiency, BE, directivity, DIR, and dynamic range ratio, DRR, of proposed L_1 pencil beams with 35 unequally and equally spaced elements.

Spacing	SLL, dB	FNBW, deg	BW3, deg	BE, %	DIR, dB	DRR
Unequal, Table 4.2	−23.50	7.63	3.00	99.32	15.65	5.07
Unequal, Table 4.3	−23.22	8.54	3.37	99.46	15.15	29.44
Equal, $\lambda/2$	−21.44	9.18	3.70	99.23	14.75	9.51

Chapter 5

Global Optimization of L_1 Pencil Beams with Multiple Constraints

In previous chapter, unconstrained optimization of L_1 pencil beams was introduced and the obtained arrays were analyzed. It was shown that their excitation dynamic range ratio was relatively low. However, an application at hand might require even lower DRR. The simplest way to accomplish this is incorporating additional DRR constraints in the design. Unfortunately, DRR constraints are not convex and the corresponding problem is hard to solve globally.

In this chapter, a method for global optimization of pencil-beam linear antenna arrays optimum in L_1 sense is presented. The proposed optimization is based on branch and bound search, which can globally solve the design problem containing constraints for the dynamic rage ratio of excitation coefficients and the maximum sidelobe level [82]. Design examples are provided to illustrate the features of the proposed approach.

5.1 L_1 Pencil Beams with Constrained DRR

The convex optimization of L_1 linear pencil-beam antenna arrays is described by problem (4.10). Here, this problem is equipped with the constraints that bound the dynamic range ratio of excitation coefficients to a value D. The DRR constraints are given by

$$\frac{\max\{|a_n|\}}{\min\{|a_n|\}} \leq D, \quad n = 1, 2, \ldots, N \tag{5.1}$$

where N is the number of array elements and a_n, $n = 1, 2, \ldots, N$, are the excitations. When these constraints are added to (4.10), the optimization problem becomes

$$\begin{aligned}
\underset{\mathbf{a},\mathbf{t},w}{\text{minimize}} \quad & \varepsilon_a(\mathbf{t},\omega_s) \\
\text{subject to} \quad & \sum_{n=1}^{N} a_n = 1, \\
& \|\mathbf{A}_q \cdot \mathbf{a}\| \le t_q, \quad q = 1,2,\ldots,Q, \\
& |a_n| \le Dw, \quad n = 1,2,\ldots,N, \\
& |a_n| \ge w, \quad n = 1,2,\ldots,N, \\
& w \ge 0
\end{aligned}$$

(5.2)

where the error $\varepsilon_a(\mathbf{t},\omega_s)$ is defined in (4.9) and w is an auxiliary variable. The constraints $|a_n| \ge w$, $n = 1,2,\ldots,N$, are not convex, which makes the problem difficult to solve globally. Here, it is solved by adapting the branch and bound method from [37], [38]. The method referred to is based on the observation that if the coefficient signs are known in advance, the optimization problem becomes convex. However, specifying the coefficient signs requires solving a large number of optimization problems. Apparently global solution can be obtained by the exhaustive search of the whole sign space. Nevertheless, to reduce the computational complexity, a branch and bound is utilized to cut out the combinations of signs that cannot improve the result [38].

5.1.1 Global Solving of Optimization Problem

Here, the optimization of L_1 pencil beams with constrained DRR in (5.2) is solved with the branch and bound algorithm from [37], which is briefly explained hereafter. Assuming the signs of coefficients are known, the problem (5.2) is reformulated as

$$\begin{aligned}
\underset{\mathbf{a},\mathbf{t},w}{\text{minimize}} \quad & \varepsilon_a(\mathbf{t},\omega_s) \\
\text{subject to} \quad & \sum_{n=1}^{N} a_n = 1, \\
& \|\mathbf{A}_q \cdot \mathbf{a}\| \le t_q, \quad q = 1,2,\ldots,Q, \\
& a_n \le Dw, \quad n \in \mathbb{S}^+, \\
& a_n \ge w, \quad n \in \mathbb{S}^+, \\
& -a_n \le Dw, \quad n \in \mathbb{S}^-, \\
& -a_n \ge w, \quad n \in \mathbb{S}^-, \\
& w \ge 0
\end{aligned}$$

(5.3)

where $\mathbb{S}^+ \subseteq \{1,2,\ldots,N\}$ and $\mathbb{S}^- \subseteq \{1,2,\ldots,N\}$ are the sets of indexes for which the coefficients are positive and negative, respectively.

To find the optimum solution of (5.2), the tree [37] containing all combinations of signs is formed. At the root, all coefficients have positive values. The first branching is implemented by assigning negative values to each coefficient a_s, $s = 1, 2, \ldots, N$. In all further branching, negative values are assigned to the subsequent coefficients a_s, $s = p+1, p+2, \ldots, N$, where p is the position of the previously assigned negative value. At the root, $p = 0$ is assumed. The corresponding tree for the antenna array having four elements is shown in Figure 5.1. The algorithm utilizes a depth-first search strategy. At each node of the tree, the optimization problem (5.3) is solved. Depending on its result, the pruning or further branching is performed. The details about pruning can be found in [37].
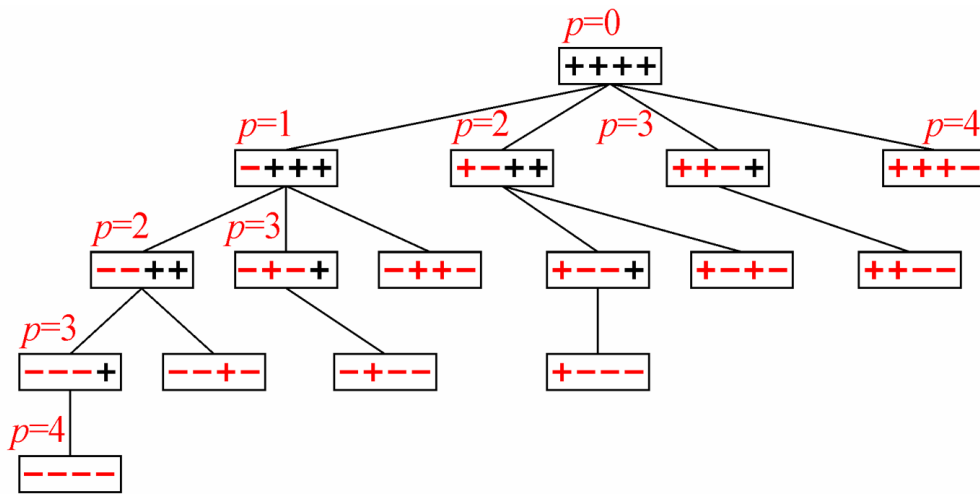
Figure 5.1: The tree containing all combinations of coefficient signs. Signs that are marked in red are specified in the corresponding node of the tree. Figure is taken from [37].

5.1.2 Properties of L_1 Pencil Beams with Constrained DRR

This section considers the influence of constraining the DRR on array factors of pencil beams optimum in L_1 sense. In that context, pencil-beam arrays with 20 elements and DRR constrained to $D = 2$, 3 and 4 are compared with DRR unconstrained arrays. The array elements are placed at the x-axis with equal interelement spacing of 0.5λ. Parameters $Q = 1001$ and $\theta_s = 0$ are used.

The obtained array factors are shown in Figure 5.2. In addition, the parameters of the obtained arrays are given in Table 5.1. It is clear that for smaller values of D obtained main lobes become narrower. However, constraining the DRR deteriorates the array factor in the sidelobe region. Although the relative deterioration increases with an increase of the elevation

angle, the first side lobe dominates. In particular, the level of -20 dB is exceeded for $D < 3.8$. The fact that the adjacent side lobes are significantly lower than the first side lobe suggests that there is still freedom for further improvement. Such an improvement may be achieved by constraining the SLL, which is considered in Section 5.2.

Optimum coefficients of the arrays with DRR constrained to $D = 2$, 3 and 4, as well of the arrays with unconstrained DRR are shown in Figure 5.3. Interestingly, all optimum coefficients are positive and symmetric.
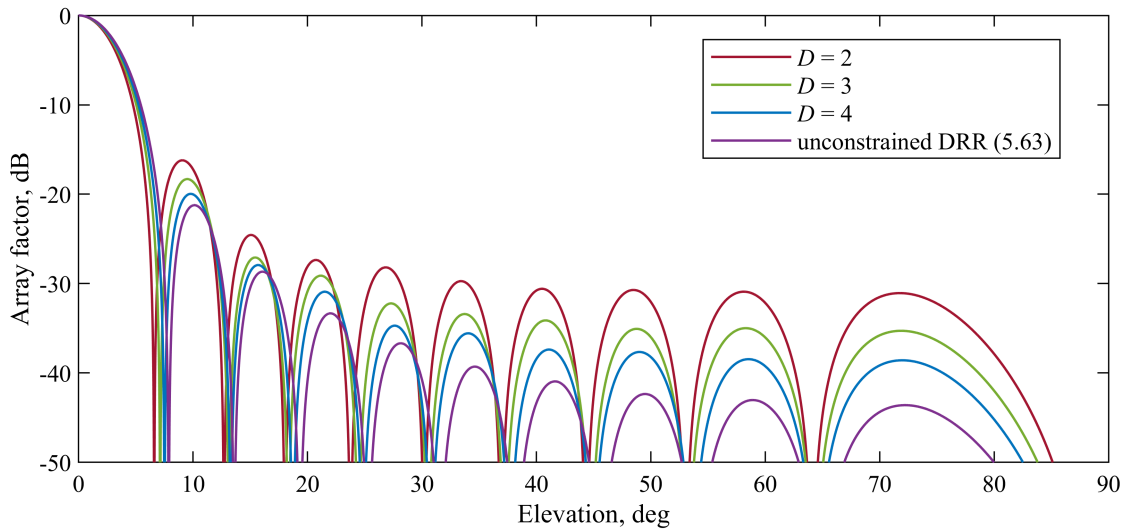
Figure 5.2: Array factors of L_1 pencil-beam arrays having 20 elements, with DRR constrained to $D = 2$, 3 and 4, as well as with unconstrained DRR.

Table 5.1: Dynamic range ratio, DRR, sidelobe level, SLL, first-null beamwidth, FNBW, 3dB-beamwidth, BW3, beam efficiency, BE, and directivity, DIR, of proposed pencil beams having 20 elements, with DRR constrained to $D = 2$, 3 and 4, as well as with unconstrained DRR.

D	DRR	SLL, dB	FNBW, deg	BW3, deg	BE, %	DIR, dB
2	2.00	-16.21	13.21	5.64	96.61	12.38
3	3.00	-18.30	14.25	5.94	98.15	12.66
4	4.00	-19.96	15.01	6.14	98.81	12.53
Unconstrained	5.63	-21.23	15.75	6.35	99.17	12.40
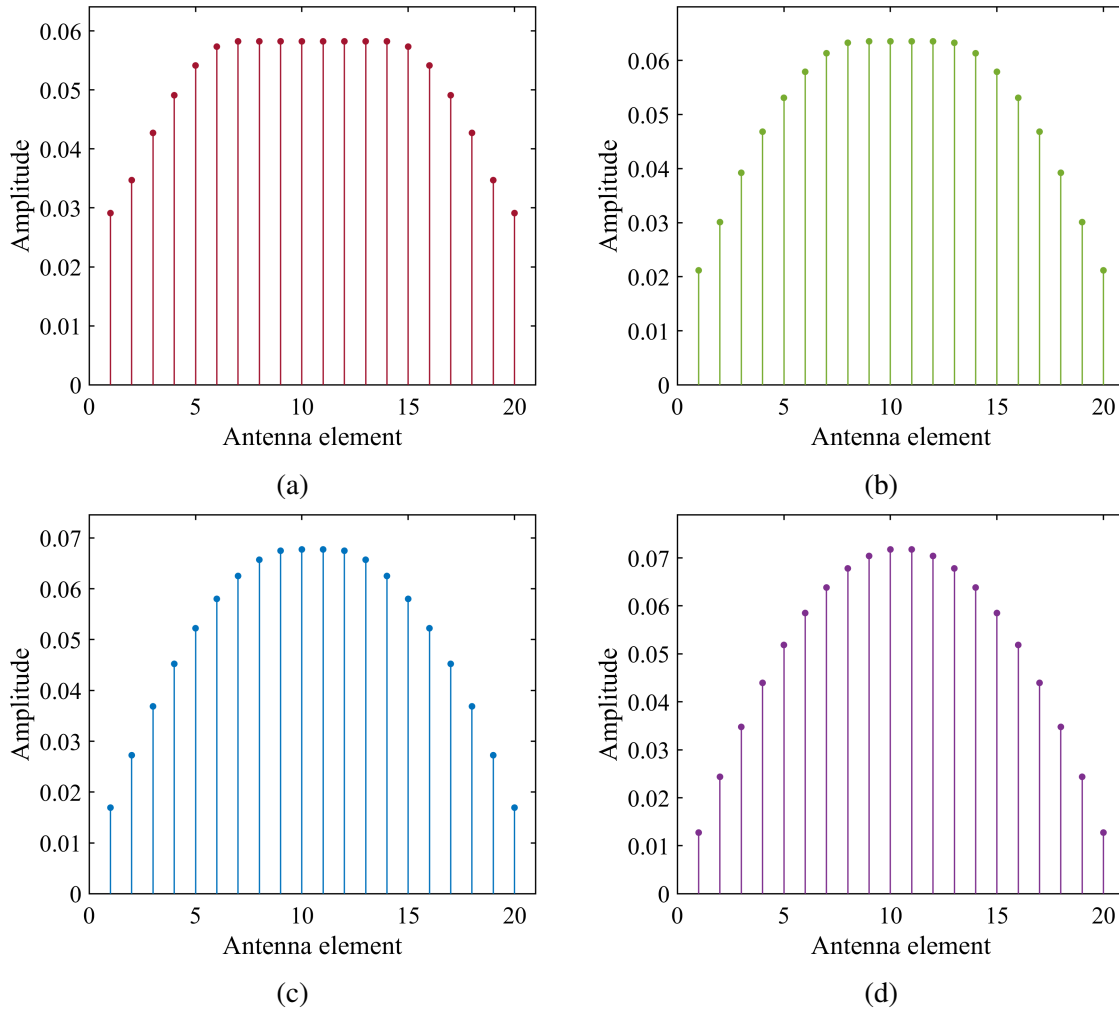
Figure 5.3: Coefficients of L_1 pencil beams having 20 elements, with DRR constrained to $D = 2$ (a), $D = 3$ (b), $D = 4$ (c), as well as with unconstrained DRR (d).

5.1.3   Unequally Spaced L_1 Pencil Beams with Constrained DRR

This section considers the design of L_1 pencil-beam arrays with unequally spaced elements and with constrained dynamic range ratio. In section 4.3.4 the design of two 35-element arrays were presented. It was shown that for the same number of elements with different positioning, the value of excitations' DRR can vary significantly. Here, the DRR constraints are incorporated into the design and their influence on the array factor of unequally spaced arrays is investigated.

The arrays with element positions from Table 4.3 are considered. The excitations' DRR is constrained to $D = 2$, 7, 8 and 10. Parameters $Q = 1001$ and $\theta_s = 0$ are used. The designed arrays are compared to the L_1 array with unconstrained DRR. Figure 5.4 shows the obtained elements' coefficients. It is clear that in all cases, obtained coefficients exhibit even symmetry. The corresponding array factors are shown in Figure 5.5 together with the array factor of DRR-

unconstrained design. The influence of DRR constraint on unequally spaced arrays is different than the influence on equally spaced arrays. In equally spaced arrays, the deterioration has regular behaviour along the sidelobe region, i.e. the lower the value of DRR, the detorioration is higher. Here, there is no such consistency. The first side lobe does not increase significantly, whereas the last side lobe arises with a significant level. However, for D being considered, the side lobes do not exceed the level of -20dB.

Parameters of the proposed beams with both $-$ constrained and unconstrained DRR $-$ are given in Table 5.2. It is clear that constraining the DRR of excitation coefficients pays off because it improves the DRR significantly and causes relatively low degradation of other parameters.
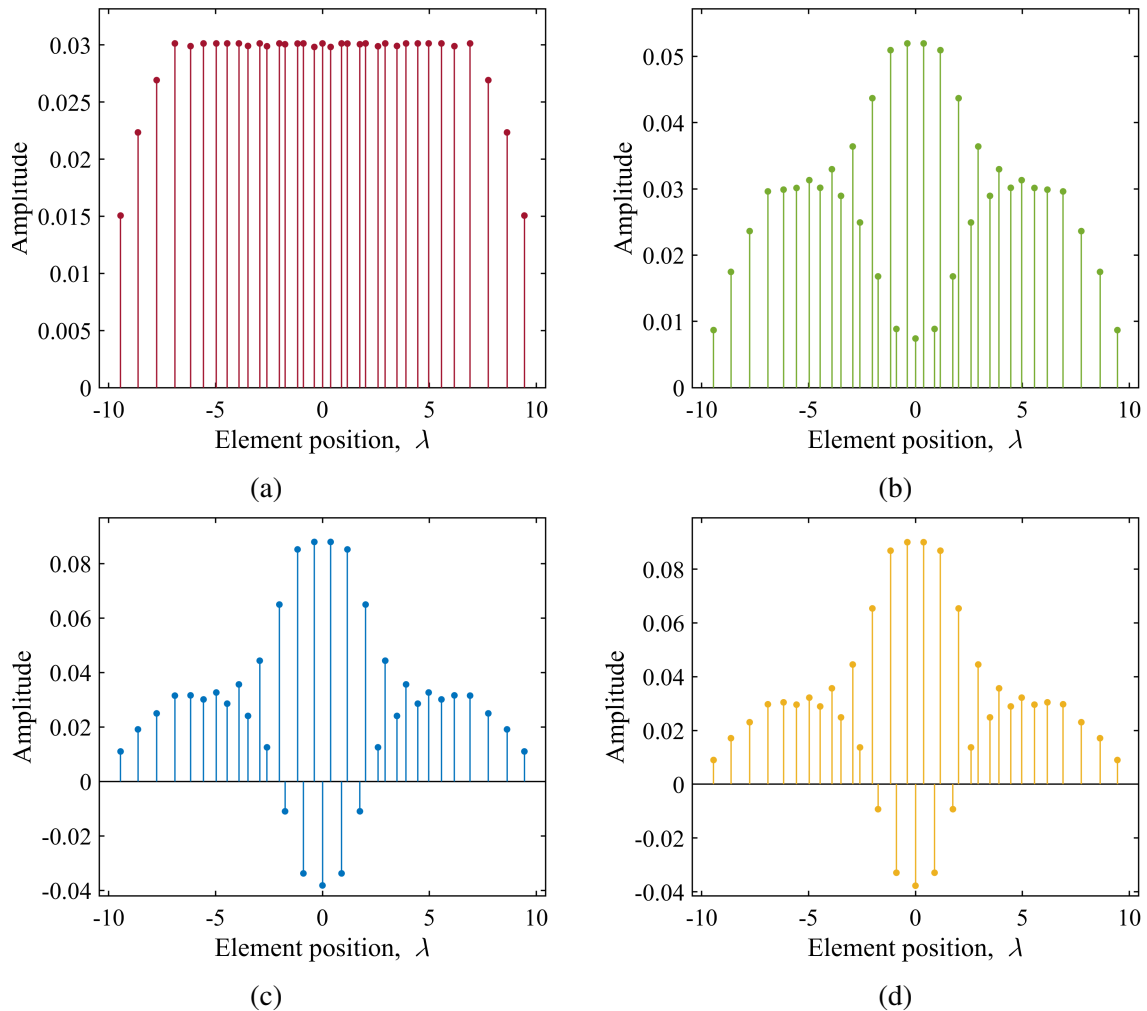
Figure 5.4: Coefficients of L_1 pencil beams having 35 unequally spaced elements with positions from Table 4.3 and DRR constrained to $D = 2$ (a), $D = 7$ (b), $D = 8$ (c), and $D = 10$ (d).
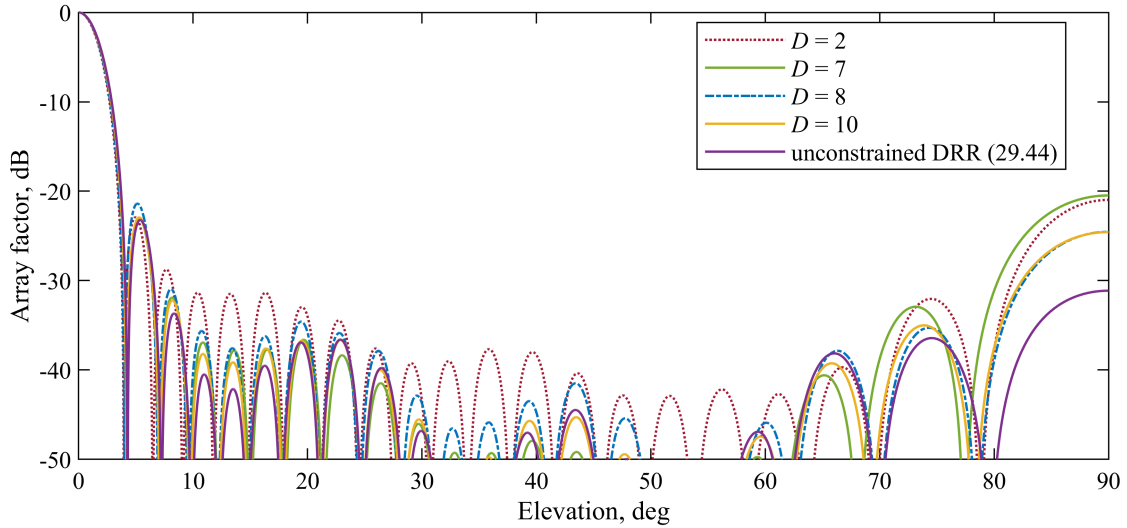
Figure 5.5: Array factors of L_1 pencil beams having 35 unequally spaced elements with positions from Table 4.3, with DRR constrained to $D = 2, 7, 8,$ and 10, as well as with unconstrained DRR.

Table 5.2: Dynamic range ratio, DRR, sidelobe level, SLL, first-null beamwidth, FNBW, 3dB-beamwidth, BW3, beam efficiency, BE, and directivity, DIR, of proposed pencil beams having 35 elements with positions from Table 4.3, with DRR constrained to $D = 2, 7, 8,$ and 10, as well as of pencil beam with unconstrained DRR.

D	DRR	SLL, dB	FNBW, deg	BW3, deg	BE, %	DIR, dB
2	2.00	-20.97	7.91	3.15	98.94	15.42
7	7.00	-20.48	8.37	3.31	99.21	15.21
8	8.00	-21.38	8.00	3.22	99.06	15.34
10	10.00	-22.91	8.37	3.32	99.34	15.22
Unconstrained	29.44	-23.22	8.54	3.37	99.46	15.15

5.2 L_1 Pencil Beams with Constrained DRR and SLL

As shown in the previous section, constraining the DRR of L_1 pencil-beam arrays results in deterioration of the array factor. In $\lambda/2$ spaced arrays, the rise of the first side lobe is significant. Similar behavior is encountered in unequally spaced arrays with predefined element positions. However, in the latter, excessive lobes may also occur at high elevation angles, which is dependent on elements' positions. To prevent an excessive rise in the sidelobe region, the maximum sidelobe level should be constrained to some specified value δ. This constraint can be easily added to the problem in (5.2).

The design of L_1 pencil beams with constrained DRR and SLL is given by the problem

$$
\begin{aligned}
& \underset{\mathbf{a}, \mathbf{t}, w}{\text{minimize}} && \varepsilon_a(\mathbf{t}, \omega_s) \\
& \text{subject to} && \sum_{n=1}^{N} a_n = 1, \\
& && |f(\mathbf{a}, \theta)| \leq \delta \qquad \theta \in \left[\theta_{sl}, \frac{\pi}{2}\right], \\
& && \|\mathbf{A}_q \cdot \mathbf{a}\| \leq t_q, \qquad q = 1, 2, \ldots, Q, \\
& && |a_n| \leq Dw, \quad n = 1, 2, \ldots, N, \\
& && |a_n| \geq w, \qquad n = 1, 2, \ldots, N, \\
& && w \geq 0
\end{aligned}
\tag{5.4}
$$

where $f(\mathbf{a}, \theta)$ is array factor defined in (2.10) and θ_{sl} is the beginning of the region in which excessive side lobes are expected. A good choice of θ_{sl} is the position of the first null in the array factor obtained by the SLL-unconstrained design.

The SLL constraint in (5.4) is approximated by using finite grid $\omega_r \in [\sin \theta_{sl}, 1]$, $r = 1, 2, \ldots, R$, as in

$$
\|\mathbf{A}_r \mathbf{a}\| \leq \delta, \quad r = 1, 2, \ldots, R \tag{5.5}
$$

where

$$
\mathbf{A}_r = \begin{bmatrix} \cos(\frac{2\pi}{\lambda} \omega_r x_1) & \cos(\frac{2\pi}{\lambda} \omega_r x_2) & \cdots & \cos(\frac{2\pi}{\lambda} \omega_r x_N) \\ \sin(\frac{2\pi}{\lambda} \omega_r x_1) & \sin(\frac{2\pi}{\lambda} \omega_r x_2) & \cdots & \sin(\frac{2\pi}{\lambda} \omega_r x_N) \end{bmatrix} \tag{5.6}
$$

By incorporating (5.5) into (5.4), the problem takes the form

$$
\begin{aligned}
& \underset{\mathbf{a}, \mathbf{t}, w}{\text{minimize}} && \varepsilon_a(\mathbf{t}, \omega_s) \\
& \text{subject to} && \sum_{n=1}^{N} a_n = 1, \\
& && \|\mathbf{A}_r \cdot \mathbf{a}\| \leq \delta, \qquad r = 1, 2, \ldots, R, \\
& && \|\mathbf{A}_q \cdot \mathbf{a}\| \leq t_q, \qquad q = 1, 2, \ldots, Q, \\
& && |a_n| \leq Dw, \quad n = 1, 2, \ldots, N, \\
& && |a_n| \geq w, \qquad n = 1, 2, \ldots, N, \\
& && w \geq 0
\end{aligned}
\tag{5.7}
$$

The objective function and all constraints in (5.7) are convex, except the constraints $|a_n| \geq w$, $n = 1, 2, \ldots, N$. However, as used in Section 5.1.1, these constraints become convex provided the signs of coefficients are known. For known coefficients' signs, the optimization problem takes the form

$$
\begin{aligned}
\underset{\mathbf{a}, \mathbf{t}, w}{\text{minimize}} \quad & \varepsilon_a(\mathbf{t}, \omega_s) \\
\text{subject to} \quad & \sum_{n=1}^{N} a_n = 1, \\
& \|\mathbf{A}_r \cdot \mathbf{a}\| \leq \delta, \quad r = 1, 2, \ldots, R, \\
& \|\mathbf{A}_q \cdot \mathbf{a}\| \leq t_q, \quad q = 1, 2, \ldots, Q, \\
& a_n \leq Dw, \quad n \in \mathbb{S}^{+}, \\
& a_n \geq w, \quad n \in \mathbb{S}^{+}, \\
& -a_n \leq Dw, \quad n \in \mathbb{S}^{-}, \\
& -a_n \geq w, \quad n \in \mathbb{S}^{-}, \\
& w \geq 0
\end{aligned}
\tag{5.8}
$$

The branch and bound method presented in [37], which was used to solve the problem (5.3), cannot be applied to solve the problem in (5.8) because for certain combinations of signs some of the constraints $\|\mathbf{A}_r \mathbf{a}\| \leq \delta$, $r = 1, 2, \ldots, R$, might be infeasible. In order to intercept such cases and to solve the problem globally, a branch and bound method is used that implements pruning based on feasibility test. The feasibility test was successfully applied in the design of sparse FIR filters [83]. Here, it is developed for examining the feasibility of DRR-constrained problems.

5.2.1 Branch and Bound Based on Feasibility Test

To solve the problem in (5.8), a tree that contains all combinations of coefficients' signs is formed. The tree for antenna array having four elements is shown in Figure 5.6. The level of branching is denoted by p. At the root, $p = 0$ and all signs are unspecified and marked with 'X'. At the pth level, the signs of the first p coefficients are specified ($+$ and $-$), whereas the remaining $N - p$ coefficients can take arbitrary signs. At the leaves, $p = N$ and, consequently, all signs are specified. Since the equality constraint in (5.8) forces a positive sum of the coefficients, it is expected that the majority of optimum coefficients will have positive values. Therefore, the branching should start with positive rather than with negative signs. In this way, optimization time can be greatly reduced since this type of branching ensures reaching the leaves at the early stages of the optimization procedure. Reaching the leaves at early stages is beneficial because at each leaf the problem (5.8) is solved to update upper bound of the objective function.
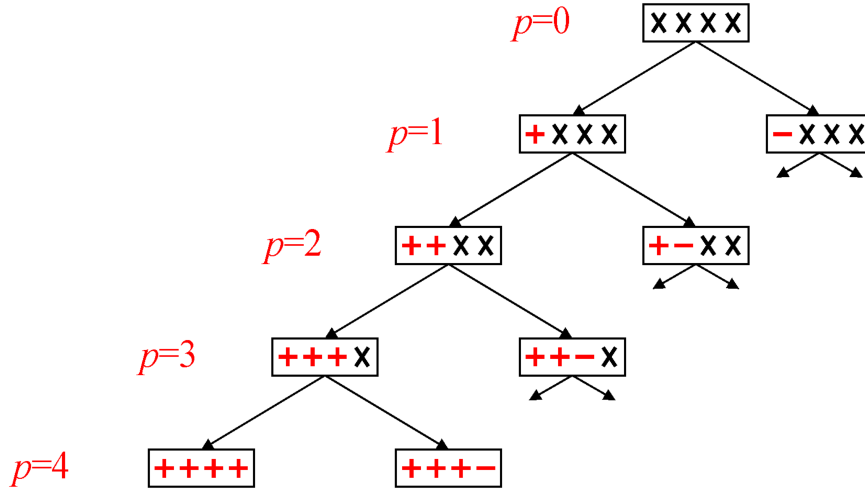
Figure 5.6: The tree containing all combinations of coefficient signs. At the pth level, exactly p coefficient signs are specified and they are marked in red. Unspecified signs are marked with 'X'. Figure is taken from [82].

Let ε_{opt} denote the value of the objective function at the optimum. Assuming p coefficient signs are specified and $N - p$ signs are arbitrary, ε_{opt} can be reached if and only if the constraints

$$
\begin{aligned}
\varepsilon_a(\mathbf{t}) &\leq \varepsilon_{opt} \\
\sum_{n=1}^{N} a_n &= 1 \\
\|\mathbf{A}_r \cdot \mathbf{a}\| &\leq \delta, \quad r = 1, 2, \ldots, R \\
\|\mathbf{A}_q \cdot \mathbf{a}\| &\leq t_q, \quad q = 1, 2, \ldots, Q \\
a_n &\leq Dw, \quad n \in \mathbb{S}^+, \quad n \leq p \\
a_n &\geq w, \quad n \in \mathbb{S}^+, \quad n \leq p \\
-a_n &\leq Dw, \quad n \in \mathbb{S}^-, \quad n \leq p \\
-a_n &\geq w, \quad n \in \mathbb{S}^-, \quad n \leq p \\
a_n &\leq Dw, \quad n > p \\
-a_n &\leq Dw, \quad n > p \\
w &\geq 0
\end{aligned}
\tag{5.9}
$$

form a nonempty set. If the set is empty, this particular node and all its children do not contain combinations of signs that satisfy the constraints. Therefore, the entire subtree coming from this node can be pruned.

The set of constraints in (5.9) is examined by solving the problem

$$\underset{\mathbf{a},\mathbf{t},w,\sigma}{\text{minimize}} \quad \sigma \tag{5.10a}$$

$$\text{subject to} \quad \varepsilon_a(\mathbf{t}) \leq \varepsilon_{opt} + \sigma, \tag{5.10b}$$

$$\sum_{n=1}^{N} a_n = 1, \tag{5.10c}$$

$$\|\mathbf{A}_r \cdot \mathbf{a}\| \leq \delta + \sigma, \quad r = 1,2,\ldots,R, \tag{5.10d}$$

$$\|\mathbf{A}_q \cdot \mathbf{a}\| \leq t_q + \sigma, \quad q = 1,2,\ldots,Q, \tag{5.10e}$$

$$a_n - Dw \leq \sigma, \quad n \in \mathbb{S}^+, \quad n \leq p, \tag{5.10f}$$

$$-a_n + w \leq \sigma, \quad n \in \mathbb{S}^+, \quad n \leq p, \tag{5.10g}$$

$$-a_n - Dw \leq \sigma, \quad n \in \mathbb{S}^-, \quad n \leq p, \tag{5.10h}$$

$$a_n + w \leq \sigma, \quad n \in \mathbb{S}^-, \quad n \leq p, \tag{5.10i}$$

$$a_n - Dw \leq \sigma, \quad n > p, \tag{5.10j}$$

$$-a_n - Dw \leq \sigma, \quad n > p, \tag{5.10k}$$

$$-w \leq \sigma \tag{5.10l}$$

The variable σ relaxes the constraints in (5.9) and ensures that the problem in (5.10) is always feasible [72]. If the optimum $\sigma_{opt} > 0$ is obtained, the set (5.9) is empty, whereas $\sigma_{opt} \leq 0$ indicates the set is not empty.

The above technique is often utilized in the first phase of interior point methods for convex optimization [72], where it is used for the search for a feasible point. Here, it is used only for the feasibility test. It is important to note that σ is incorporated only into the inequality constraints. Therefore, the problem in (5.10) is valid only for $D > 1$. Namely, for $D = 1$, the inequality constraint pairs (5.10f) and (5.10g), as well as (5.10h) and (5.10i) represent equality constraints.

At the root, ε_{opt} is assigned a large positive value, for example, $\varepsilon_{opt} = 4\pi$, which is a loose upper bound of the L_1 error function in (4.9). The tree is then explored by using depth-first algorithm. At each node, fesibility test is performed by solving the optimization problem in (5.10). If the problem is feasible, the search goes deeper into the tree, otherwise the branch is pruned. If a leaf is reached, the problem in (5.8) is solved as well. If the optimum $\varepsilon^* < \varepsilon_{opt}$ is obtained in (5.8), an update is made $\varepsilon_{opt} = \varepsilon^*$.

5.2.2 Influence of DRR and SLL Constraints

In this example, the influence of DRR and SLL constraints on the array factors is investigated. Arrays having 20 elements with interelement spacing of 0.5λ are optimized. The optimizations

are run for $\delta = 0.1$ (SLL ≤ -20 dB) and for D in the range $[1.6, 5.6]$ in steps of 0.1. The value of $D = 5.6$ corresponds to the DRR of the unconstrained L_1 beam pattern. The values of D less than 1.6 are not considered because, for these values, an SLL lower than -20 dB cannot be achieved. The constraints on SLL are applied in the region $\theta \in [7.87°, 90°]$. The value of $\theta = 7.87°$ matches the angle of the first null in L_1 pencil beam obtained by solving the unconstrained optimization problem in (4.10) for $\omega_s = 0$. Parameters $Q = 1001$ and $R = 10N$ are used.

The obtained array factors for all values of D are shown in Figure 5.7. In addition, Table 5.3 brings the parameters of the obtained beams for selected values of D. Similarly to the example analyzed in 5.1.2, the decrease of D causes the rise of the sidelobes. For $D > 4.3$, the SLL is lower than -20 dB, which indicates that the SLL constraints are not active, as in the array factors marked in orange. $D \leq 4.3$ activates the SLL constraints and keeps the maximum value of SLL exactly at -20 dB, as in the array factors marked in blue. In the sidelobe region, a monotonic decrease of the side lobes is maintained if $D \geq 2.46$.
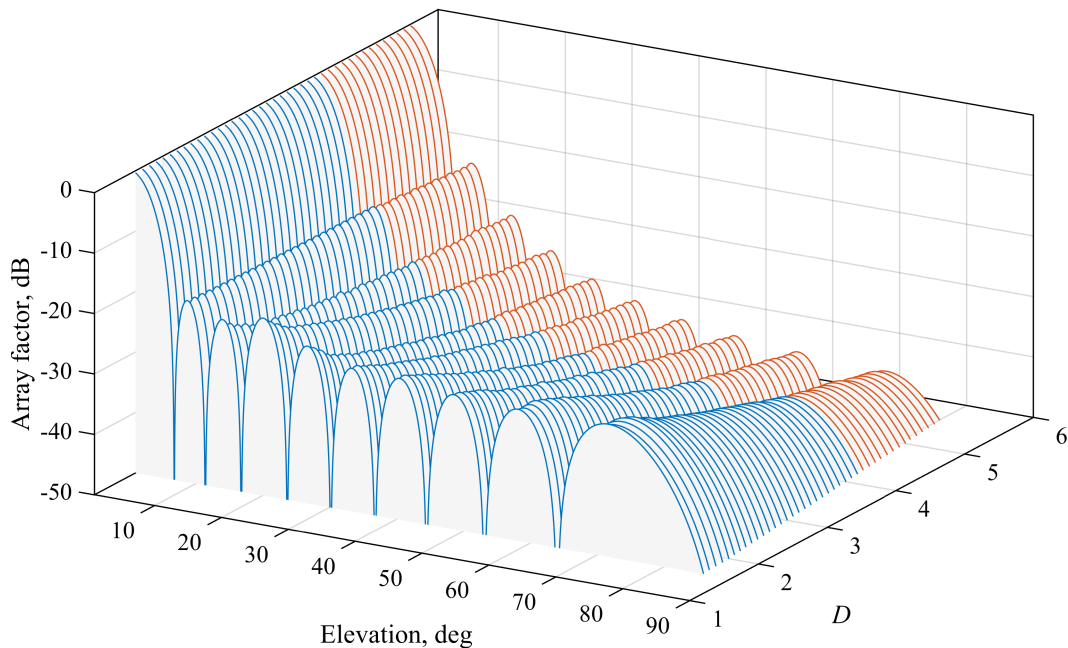
Figure 5.7: Array factors of L_1 pencil beams with 20 elements, SLL constrained to -20 dB, and DRR constrained to various values between $D = 1.6$ and $D = 5.6$. Blue and orange colors indicate patterns in which SLL constraints are active and inactive, respectively.

Table 5.3: Sidelobe level, SLL, first-null beamwidth, FNBW, 3dB-beamwidth, BW3, beam efficiency, BE, and directivity, DIR of proposed pencil beams with 20 elements and DRR constrained to value D.

D	SLL, dB	FNBW, deg	BW3, deg	BE, %	DIR, dB	Coefficients
1.6	−20.0	13.6	5.60	96.48	12.8	positive
2.0	−20.0	14.1	5.78	97.81	12.8	positive
2.5	−20.0	14.4	5.90	98.34	12.7	positive
3.0	−20.0	14.6	6.00	98.59	12.6	positive
3.5	−20.0	14.8	6.08	98.73	12.6	positive
4.0	−20.0	15.0	6.15	98.82	12.5	positive
4.5	−20.5	15.3	6.22	98.97	12.5	positive
5.0	−20.9	15.5	6.29	99.08	12.4	positive
5.5	−21.3	15.7	6.35	99.18	12.4	positive

5.2.3 Array Factors with Very Low DRR and Constrained SLL

The proposed method supports coefficients with positive and negative signs. However, in the previous example, all arrays were obtained with positive coefficients. Generally, such behavior has been encountered in arrays with DRRs constrained to medium or high values. However, constraining the DRR to low values, especially when the number of elements is large, might cause the appearence of negative coefficients. Generally, the arrays with low SLL require some coefficients to take low values. On the other hand, the DRR constraints push the coefficients to higher values. Therefore if both of these requirements are strong, a small number of negative coefficients could appear in the optimum solution, trying to compensate large poisitve coefficients in their neighbourhoods. Apparently, negative coefficients offer more degrees of freedom during the optimization process, thus providing better results.

Here, the arrays having 41 elements with the spacing of 0.5λ are considered. DRR is constrained to $D = 1.3$, 1.4, and 1.5, and SLL is constrained to $\delta = 0.1$. The values $D < 1.3$ are not considered because DRR < 1.3 cannot be obtained for SLL ≤ -20 dB. For $D > 1.5$, all coefficients take positive values and they are omitted from this analysis. The constraint on SLL is applied in the region $\theta \in [3.96°, 90°]$. The value of $\theta = 3.96°$ matches the angle of the first null in L_1 pencil beam obtained by solving the unconstrained optimization problem in (4.10) for $\omega_s = 0$. Parameters $Q = 1001$ and $R = 10N$ are used.

The obtained array factors are given in Figure 5.8. It is clear that the proposed arrays no longer exhibit monotonic decrease of the sidelobes. Figure 5.9 shows the corresponding excitation coefficients. The coefficients are not symmetric and 1 or 2 negative coefficients appear at the optimum. Numerical values of the coefficients obtained for $D = 1.3$ are given in Table 5.4, for convenience. In addition, the parameters of the proposed beams are listed in Table 5.5.

Figure 5.8: Array factors of L_1 pencil-beam arrays with 41 elements, DRR constrained to $D = 1.3, 1.4$, and 1.5, and SLL constrained to -20 dB.

(a)

(b)

(c)
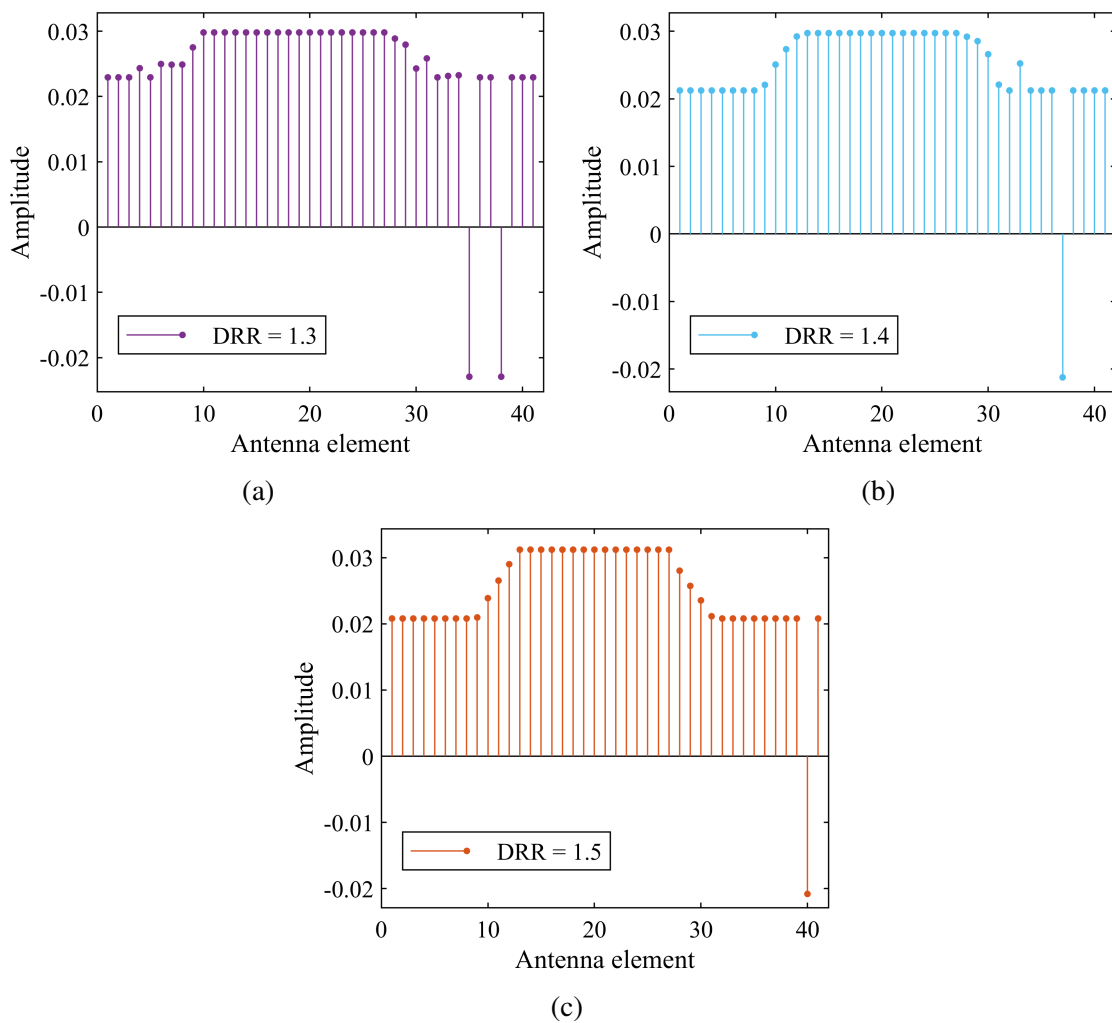
Figure 5.9: Coefficients of L_1 pencil beams with 41 elements, DRR constrained to $D = 1.3$ (a), $D = 1.4$ (b), and $D = 1.5$ (c), and SLL constrained to -20 dB.

Table 5.4: Optimum coefficients of proposed array with 41 elements, DRR constrained to $D = 1.3$, and SLL constrained to -20 dB.

n	a_n	n	a_n	n	a_n	n	a_n
1	0.0229	12	0.0298	22	0.0298	32	0.0229
2	0.0229	13	0.0298	23	0.0298	33	0.0231
3	0.0229	14	0.0298	24	0.0298	34	0.0233
4	0.0243	15	0.0298	25	0.0298	35	-0.0229
5	0.0229	16	0.0298	26	0.0298	36	0.0229
6	0.0250	17	0.0298	27	0.0298	37	0.0229
7	0.0249	18	0.0298	28	0.0289	38	-0.0229
8	0.0249	19	0.0298	29	0.0279	39	0.0229
9	0.0275	20	0.0298	30	0.0243	40	0.0229
10	0.0298	21	0.0298	31	0.0258	41	0.0229
11	0.0298						

Table 5.5: Dynamic range ratio, DRR, sidelobe level, SLL, first-null beamwidth, FNBW, 3dB-beamwidth, BW3, beam efficiency, BE, and directivity, DIR of proposed L_1 pencil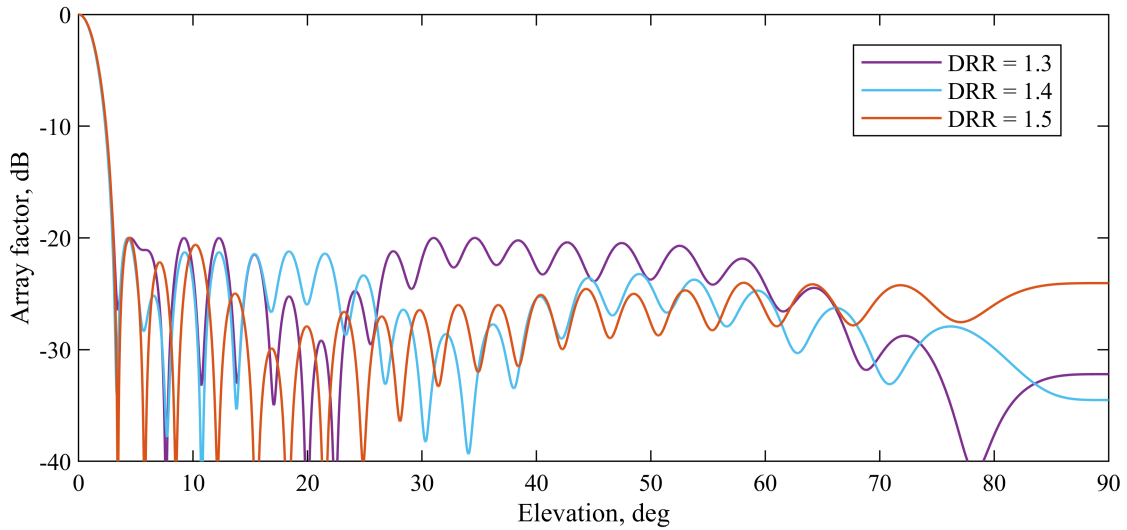 beams having 41 elements with DRR constrained to $D = 1.3, 1.4,$ and 1.5, and SLL constrained to -20 dB, as well as of pencil beam with unconstrained DRR and SLL.

D	DRR	SLL, dB	FNBW, deg	BW3, deg	BE, %	DIR, dB
1.3	1.30	-20.00	6.88	2.78	84.87	15.31
1.4	1.40	-20.00	6.65	2.73	90.40	15.66
1.5	1.50	-20.00	6.85	2.83	92.50	15.62
Unconstrained	10.54	-20.78	7.74	3.14	99.11	15.45

5.2.4 Unequally Spaced L_1 Pencil Beams with Constrained DRR and SLL

Previous examples brought the designs of the arrays with equally spaced antenna elements. However, the method supports placing the elements at arbitrary positions. In this example, L_1 pencil beams with constrained DRR and SLL are designed assuming the elements are spaced unequally.

In [59], the pencil beam arrays having 24 elements have been obtained by optimizing elements' coefficients as well as their positions. Here, the positions from [59] are utilized. These positions are given in Table 5.6, for convenience. In the proposed arrays, sidelobe level is constrained to SLL $= -28.8$, which corresponds to the value in [59]. The SLL constraints are

applied in the region $\theta \in [4.12°, \ 90°]$, where $\theta = 4.12°$ matches the angle of the first null in L_1 pencil beam obtained by solving the unconstrained optimization problem in (4.10) for given element positions and $\omega_s = 0$. Regarding the bounds for DRR used in this design, two values are chosen: the original DRR obtained in [59] which corresponds to $D = 4.69$, and somewhat lower value of $D = 3.69$. Parameters $Q = 1001$ and $R = 10N$ are used.

The array factors obtained with the proposed method are shown in Figure 5.10, together with the array factor of the array from [59]. The corresponding coefficients are given in Figure 5.11. Clearly, all coefficients take positive values. The proposed method can provide arrays with the same or lower DRR than the array from [59], while maintaining similar overall performances. This is illustrated in Table 5.7, which brings the parameters of the examined arrays. Optimum coefficients of the proposed array having 24 elements, DRR constrained to $D = 3.69$, and SLL constrained to -28.8 dB are provided in Table 5.8, for convenience.

Table 5.6: Positions of antenna elements taken from [59].

n	x_n, λ	n	x_n, λ	n	x_n, λ
1, 24	± 9.500	5, 20	± 6.195	9, 16	± 2.893
2, 23	± 8.723	6, 19	± 5.361	10, 15	± 2.070
3, 22	± 7.884	7, 18	± 4.535	11, 14	± 1.244
4, 21	± 7.037	8, 17	± 3.713	12, 13	± 0.415
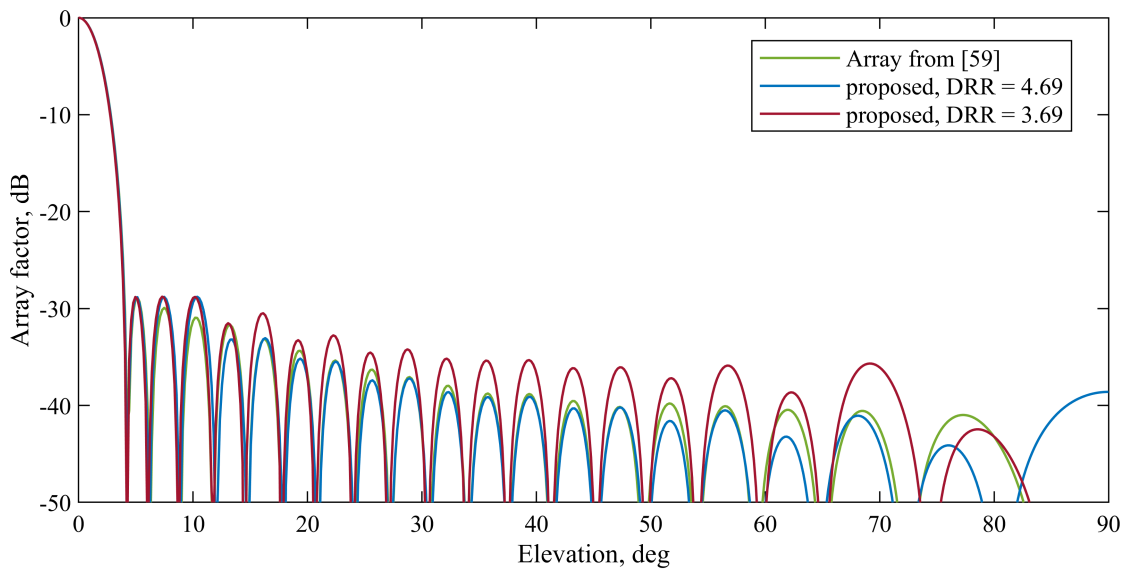
Figure 5.10: Array factors of L_1 pencil-beam arrays having 24 elements with positions from Table 5.6, DRR constrained to $D = 4.69$ and 3.69, and SLL constrained to -28.8 dB, together with array factor of array from [59].
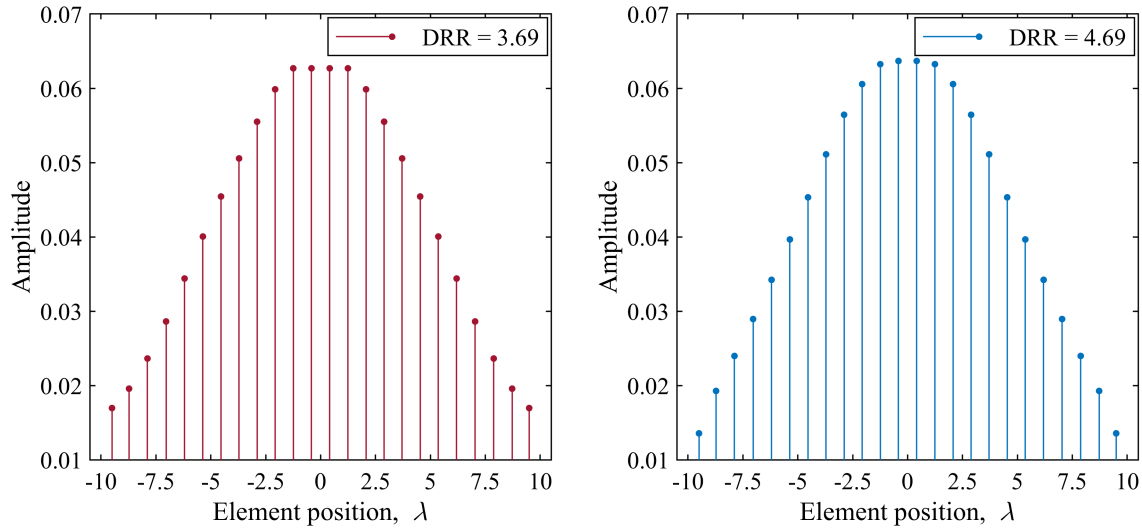
Figure 5.11: Coefficients of L_1 pencil beams having 24 elements with positions from Table 5.6, DRR constrained to $D = 3.69$ and 4.69, and SLL constrained to -28.8 dB.

Table 5.7: Sidelobe level, SLL, first-null beamwidth, FNBW, 3dB-beamwidth, BW3, beam efficiency, BE, and directivity, DIR, of proposed pencil beams having 24 elements with positions from Table 5.6, DRR constrained to $D = 4.69$ and 3.69, and SLL constrained to -28.8 dB, as well as of pencil beam from [59].

Method	DRR	SLL, dB	FNBW, deg	BW3, deg	BE, %	DIR, dB
Proposed, $D = 3.69$	3.69	-28.8	8.43	3.19	99.21	15.37
Proposed, $D = 4.69$	4.69	-28.8	8.56	3.24	99.46	15.32
[59]	4.69	-28.8	8.62	3.25	99.49	15.37

Table 5.8: Optimum coefficients of proposed array having 24 elements with positions from Table 5.6, DRR constrained to $D = 3.69$, and SLL constrained to -28.8 dB.

n	a_n	n	a_n	n	a_n	n	a_n
1	0.0170	7	0.0454	13	0.0627	19	0.0400
2	0.0196	8	0.0506	14	0.0627	20	0.0344
3	0.0236	9	0.0555	15	0.0599	21	0.0286
4	0.0286	10	0.0599	16	0.0555	22	0.0236
5	0.0344	11	0.0627	17	0.0506	23	0.0196
6	0.0400	12	0.0627	18	0.0454	24	0.0170

Chapter 6

Design of Unequally Spaced Arrays by Using General-Purpose Optimization Methods

In this chapter, the design of unequally spaced linear and planar antenna arrays with uniformly excited elements is considered. Optimization of the positions of antenna elements generally leads to nonlinear and nonconvex problems. For solving these problems, the application of general-purpose methods for nonlinear optimization is proposed. Both − unconstrained and constrained − optimization is utilized. In particular, the quasi-Newton method is used for solving unconstrained optimization problems [64], whereas the constraints are handled by using sequential quadratic programming [65]. Arrays are optimized to achieve either, the maximum directivity or maximum beam efficiency.

6.1 Preliminaries

6.1.1 Problem Formulation

The optimization of unequally spaced arrays with arbitrary element positions and uniform excitation is given by the problem

$$\underset{\mathbf{w}}{\text{minimize}} \quad \varepsilon(\mathbf{w}) \tag{6.1}$$

where $\varepsilon(\mathbf{w})$ is error function describing design specifications and $\mathbf{w}$ is row vector containing element positions, i.e., $\mathbf{w} = [x_1, \, x_2, \, ...,x_N]$ for linear arrays and $\mathbf{w} = [x_1, \, x_2,..., \, x_N, \, y_1, \, y_2, \, ..., \, y_N]$ for planar arrays. Special case of the problem in (6.1) occurs when the array is symmetric about x and y axes. In that case, the positions of all antenna elements can be obtained as

$$\mathbf{x} = [\mathbf{x}_0, -\mathbf{x}_1, \mathbf{x}_1, \mathbf{0}_2, \mathbf{0}_2, \mathbf{x}_3, -\mathbf{x}_3, -\mathbf{x}_3, \mathbf{x}_3] \tag{6.2}$$

$$\mathbf{y} = [\mathbf{y}_0, \mathbf{0}_1, \mathbf{0}_1, -\mathbf{y}_2, \mathbf{y}_2, \mathbf{y}_3, \mathbf{y}_3, -\mathbf{y}_3, -\mathbf{y}_3] \tag{6.3}$$

where $\mathbf{x}_i$, $\mathbf{y}_i$, $i = 0, 1, 2, 3$ are row vectors that contain coordinates of N_0 elements at the origin, N_1 elements at the positive x-axis, N_2 elements at the positive y-axis, and N_3 elements in the interior of the first quadrant. The vectors $\mathbf{0}_1$ and $\mathbf{0}_2$ contain N_1 and N_2 zeros, respectively. Such a geometry is illustrated in Figure 6.1 for planar arrays. Apparently, the optimization problem in (6.1) for the symmetric array can be expressed as

$$\underset{\mathbf{w_s}}{\text{minimize}} \quad \varepsilon(\mathbf{w}) \tag{6.4}$$

where $\mathbf{w_s} = \mathbf{x}_1$ for linear and $\mathbf{w_s} = [\mathbf{x}_1, \mathbf{x}_3, \mathbf{y}_2, \mathbf{y}_3]$ for planar arrays.

The problems (6.1) and (6.4) are unconstrained optimization problems. However, the constraints can also be added to (6.1) and (6.4) to include specific requirements. In further text, these problems will be tailored separately for unconstrained and for constrained optimizations assuming various objective functions. Since the problems include powers radiated in certain spatial regions, the relationship between the radiated power and the vectors of variables and coefficients is considered first.
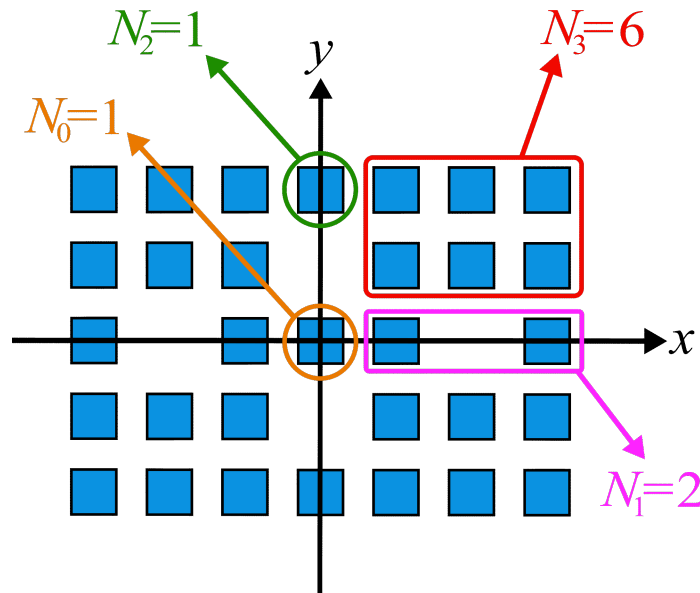
Figure 6.1: Geometry of symmetric planar array with one element placed at the origin ($N_0 = 1$), two elements at the positive x-axis ($N_1 = 2$), one element at the positive y-axis ($N_2 = 1$), and six elements in the interior of the first quadrant ($N_3 = 6$).

6.1.2 Radiated Power in Linear Antenna Arrays

If antenna elements are placed at the *x*-axis of a coordinate system, the power radiated in the mainlobe region $\Psi = \{(\theta : \theta \in [-\theta_s, \theta_s]\}$ is given by

$$P(\mathbf{a}, \mathbf{w}, \Psi) = 2\pi \int\limits_{-\theta_s}^{\theta_s} |f(\mathbf{a}, \mathbf{w}, \theta)|^2 \cos(\theta) \, d\theta \qquad (6.5)$$

where θ_s is the start of the sidelobe region, $\mathbf{w}$ is the vector of elements positions, and $\mathbf{a}$ is the vector of excitation coefficients. The integral in (6.5) can be obtained in analytic form, as in

$$P(\mathbf{a}, \mathbf{w}, \Psi) = \mathbf{a}^{\mathrm{T}} \mathbf{A_L} \mathbf{a}, \qquad (6.6)$$

where entries of matrix $\mathbf{A_L}$ are obtained as

$$(A_L)_{pq} = 4\pi \sin(\theta_s) \mathrm{sinc}\left[\frac{2\pi}{\lambda}(x_p - x_q)\sin(\theta_s)\right] \qquad (6.7)$$

where $p = 1, 2, ..., N$, $q = 1, 2, ..., N$, and $\mathrm{sinc}(\cdot)$ denotes the unnormalized sinc function.

The total radiated power $P(\mathbf{w}, \Omega)$ can be easily obtained by setting the region of interest to $\Omega = \{(\theta : \theta \in [-\pi/2, \pi/2]\}$, as in

$$P(\mathbf{a}, \mathbf{w}, \Omega) = \mathbf{a}^{\mathrm{T}} \mathbf{B_L} \mathbf{a}, \qquad (6.8)$$

where elements of matrix $\mathbf{B_L}$ are obtained as

$$(B_L)_{pq} = 4\pi \, \mathrm{sinc}\left[\frac{2\pi}{\lambda}(x_q - x_p)\right]. \qquad (6.9)$$

6.1.3 Radiated Power in Planar Antenna Arrays

Generally, the power radiated by an antenna array in the region $\Psi = \{(\theta, \varphi) : \theta \in [\theta_1, \theta_2], \varphi \in [\varphi_1, \varphi_2]\}$ can be expressed as

$$P(\mathbf{a}, \mathbf{w}, \Psi) = \int\limits_{\varphi_1}^{\varphi_2} \int\limits_{\theta_1}^{\theta_2} |f(\mathbf{a}, \mathbf{w}, \theta, \varphi)|^2 \sin(\theta) \, d\theta \, d\varphi \qquad (6.10)$$

The integral in (6.10) can be evaluated numerically. However, for certain array geometries and shapes of the region Ψ, it can be evaluated analytically. Such is the case in calculation of the power radiated (or collected) in the rectangular region of interest, as well as in calculation of the total radiated power.

6.1.3.1 Power Radiated in Rectangular Region of Interest

Here, the power radiated by planar antenna array within a rectangular region of interest is considered. Such a case is illustrated in Figure 6.2. The region is defined as $\Psi = \{(u,v) : |u| \leq u_0, \ |v| \leq v_0\}$, where $u = \sin(\theta)\cos(\varphi)$ and $v = \sin(\theta)\sin(\varphi)$. The power is obtained as [84]

$$P(\mathbf{a}, \mathbf{w}, \Psi) = \mathbf{a}^{\mathsf{T}} \mathbf{A_P} \mathbf{a} \tag{6.11}$$

where entries of matrix $\mathbf{A_P}$ are obtained as

$$(A_P)_{pq} = 4\, u_0 v_0 \, \mathrm{sinc}\left[\frac{2\pi}{\lambda} u_0 (x_q - x_p)\right] \mathrm{sinc}\left[\frac{2\pi}{\lambda} v_0 (y_q - y_p)\right], \tag{6.12}$$

where $p = 1, 2, ..., N$, and $q = 1, 2, ..., N$.
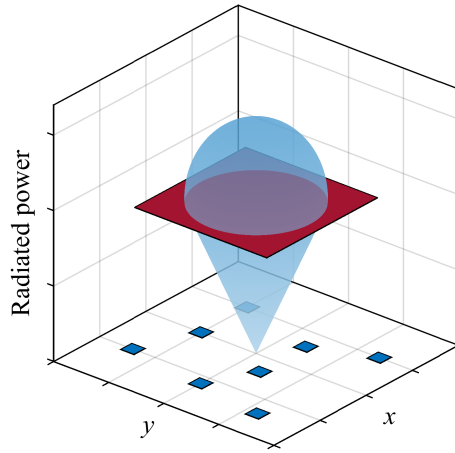
Figure 6.2: Illustration of planar antenna array with mainlobe pointing at the broadside direction and rectangular region of interest, colored in red, in which radiated power is calculated.

6.1.3.2 Power Radiated in Circular Region of Interest

As shown in the previous section, for planar arrays, the power radiated in a rectangular region of interest can be obtained analytically. Unfortunately, such is not the case if the region is circular. However, in that case the integral (6.10) must be evaluated numerically, which can be a computationally expensive task. Therefore, to reduce the number of variables, only in this case symmetric arrays will be considered, assuming the elements are not placed on the x- and y-axis, that is $N_0 = 0$, $N_1 = 0$, $N_2 = 0$. Circular region of interest and symmetric array are illustrated in Figure 6.3. For such arrays, the array factors can be expressed by using only the positions of elements in the first quadrant, $\mathbf{w_s} = [\mathbf{x}_3, \mathbf{y}_3]$, as in

$$f_{\mathrm{sym}}(\mathbf{w_s}, u, v) = 4 \sum_{n=1}^{N_3} \frac{1}{N} \cos\left(\frac{2\pi}{\lambda}(x_3)_n \cdot u\right) \cos\left(\frac{2\pi}{\lambda}(y_3)_n \cdot v\right) \tag{6.13}$$

The power radiated in region $\Psi = \{(u,v) : 0 \leq u^2 + v^2 \leq \sin^2(\theta_s)\}$ can be evaluated as [60]

$$P(\mathbf{a}, \mathbf{w_s}, \Psi) = \int_\Psi \left[4 \sum_{n=1}^{N_3} \frac{1}{N} \cos(\frac{2\pi}{\lambda}(x_3)_n \cdot u) \cos(\frac{2\pi}{\lambda}(y_3)_n \cdot v) \right]^2 du\, dv \qquad (6.14)$$

The integral in (6.14) can be evaluated by using rectangle rule above a finite grid $\theta_d \in [0, \theta_s]$, $d = 1, 2, \ldots, D$, and $\varphi_f \in [0, 2\pi)$, $f = 1, 2, \ldots, F$, as in

$$P(\mathbf{a}, \mathbf{w_s}, \Psi) \approx \frac{\theta_s}{D-1} \cdot \frac{2\pi}{F-1} \sum_{d=1}^{D-1} \sum_{f=1}^{F-1} \left[f_{\text{sym}}(\mathbf{w_s}, u_{df}, v_{df}) \right]^2 \sin(\theta_d) \qquad (6.15)$$

where $u_{df} = \sin(\theta_d)\cos(\varphi_f)$ and $v_{df} = \sin(\theta_d)\sin(\varphi_f)$.
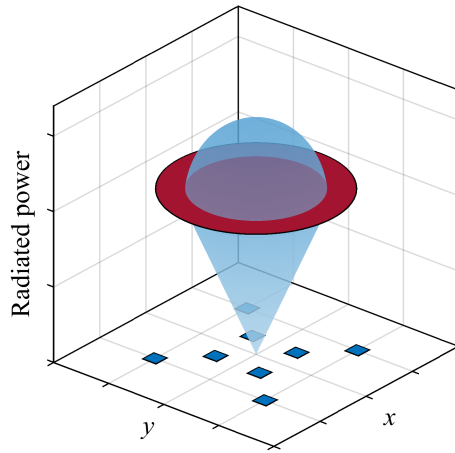
Figure 6.3: Illustration of symmetric planar antenna array with mainlobe pointing at the broadside direction and circular region of interest, colored in red, in which radiated power is calculated.

6.1.3.3   Total Radiated Power

For the case of planar arrays, $P(\Omega)$ usually denotes the total power radiated in the half-space above the array, that is $\Omega = \{(u,v) : u^2 + v^2 \leq 1\}$. Its value can be obtained analytically as in [84]

$$P(\mathbf{a}, \mathbf{w}, \Omega) = \mathbf{a}^{\mathrm{T}} \mathbf{B_P} \mathbf{a}, \qquad (6.16)$$

where entries of matrix $\mathbf{B_P}$ are calculated by using

$$(B_P)_{pq} = 2\pi \, \text{sinc}\left[\frac{2\pi}{\lambda} \sqrt{(x_q - x_p)^2 + (y_q - y_p)^2} \right], \qquad (6.17)$$

where $p = 1, 2, ..., N$, and $q = 1, 2, ..., N$.

The expressions provided in sections 6.1.2 and 6.1.3 are valid for arbitrary coefficient values. However, since in uniformly excited arrays the only optimization variables are element positions, the excitation coefficients have predefined values. In all optimizations considered in further text, the vector **a** takes the form

$$\mathbf{a} = [1/N, 1/N, ..., 1/N]^{\mathrm{T}} \tag{6.18}$$

Consequently, the expressions for array factor and radiated power take the forms $f(\mathbf{w}, \theta)$, $f(\mathbf{w}, \theta, \varphi)$, $f_{\mathrm{sym}}(\mathbf{w_s}, u, v)$, $P(\mathbf{w}, \Psi)$, $P(\mathbf{w_s}, \Psi)$, and $P(\mathbf{w}, \Omega)$.

6.2 Design Based on Unconstrained Optimization

6.2.1 Maximization of Beam Efficiency

Maximizing the beam efficiency of antenna arrays is important in applications such as satellite communications and microwave power transfer systems. The problem of maximization of beam efficiency of linear and planar arrays is given by the optimization problem

$$\underset{\mathbf{w}}{\text{minimize}} \quad -\frac{P(\mathbf{w}, \Psi)}{P(\mathbf{w}, \Omega)} \tag{6.19}$$

for the arrays with arbitrary element positions and

$$\underset{\mathbf{w_s}}{\text{minimize}} \quad -\frac{P(\mathbf{w}, \Psi)}{P(\mathbf{w}, \Omega)} \tag{6.20}$$

for symmetric arrays. Depending on the arrays' geometry and shape of the region of interest, the powers $P(\mathbf{w}, \Psi)$ and $P(\mathbf{w}, \Omega)$ are calculated by using expressions (6.6)-(6.9) for linear arrays and (6.11), (6.12), (6.16), and (6.17) for planar arrays.

6.2.2 Maximization of Directivity

The unconstrained optimization of unequally spaced planar arrays with maximum directivity is given by the problem

$$\underset{\mathbf{w}}{\text{minimize}} \quad -\frac{|f(\mathbf{w}, \theta_0, \varphi_0)|^2}{P(\mathbf{w}, \Omega)/4\pi} \tag{6.21}$$

for the arrays with arbitrary element positions and

$$\underset{\mathbf{w_s}}{\text{minimize}} \quad -\frac{|f(\mathbf{w}, \theta_0, \varphi_0)|^2}{P(\mathbf{w}, \Omega)/4\pi} \tag{6.22}$$

for symmetric arrays, where $\theta_0 = 0$ and $\varphi_0 = 0$ assuming the directivity is maximized at the broadside direction. The total radiated power in the half-space above the array, $P(\mathbf{w}, \Omega)$, is given in (6.16).

6.2.3 Solver for Unconstrained Optimization

The problems (6.19)-(6.22) are not convex. In this research, the quasi-Newton method is utilized for their solving. The solver implementing this method is available in various optimization tools. Here, function *fminunc* from Matlab Optimization Toolbox [85] is employed. This function supports BFGS and DFP formula for Hessian matrix update. In the following examples, the BFGS formula is utilized since it ensures faster convergence in most practical problems.

6.2.4 Design Examples

In this section, examples are provided which illustrate the performances of the proposed optimization approach. The examples are worked out in Matlab 2023a running on a personal computer with Intel i9 processor operating at the clock of 3.6 GHz. Function *fminunc* is employed as the solver, with the options set according to Table 6.1. Clearly, these options select quasi-Newton method which utilizes BFGS formula for Hessian matrix update. For algorithm's terminating criteria, *StepTolerance* and *OptimalityTolerance*, default values are used. Since the algorithm must converge in all cases, the parameters *MaxIterations* and *MaxFunctionEvaluations* are set to high values.

Table 6.1: Options for function *fminunc*.

Option	Value
Algorithm	*quasi-newton*
HessianApproximation	*bfgs*
StepTolerance	10^{-6}
OptimalityTolerance	10^{-6}
MaxIterations	2000
MaxFunctionEvaluations	4000N

6.2.4.1 Linear Arrays with Maximum Beam Efficiency

In this example, the design of linear antenna arrays with 32 elements and maximum beam efficiency is considered. One array with arbitrary as well as one array with symmetric element positions are optimized by solving the problems in (6.19) and (6.20). In both cases, the start of the sidelobe region is set to $\theta_s = 3°$. The optimizations start from the array obtained with the method from [51], whose element positions are given in Table 6.2. The optima are reached in

56 iterations for the array with arbitrary, and 57 iterations for the array with symmetric element positions, requiring the computational time of 0.43 s and 0.64 s. Figure 6.4 shows convergence rates for both cases.

Table 6.2: Positions of antenna elements from [51] that are used as optimizations' starting point.

n	x_n, λ	n	x_n, λ	n	x_n, λ	n	x_n, λ
1, 32	± 10.4200	5, 28	± 6.4900	9, 24	± 3.7500	13, 20	± 1.7500
2, 31	± 9.1100	6, 27	± 5.7900	10, 23	± 3.2500	14, 19	± 1.2500
3, 30	± 8.1900	7, 26	± 5.1100	11, 22	± 2.7500	15, 18	± 0.7500
4, 29	± 7.3100	8, 25	± 4.3700	12, 21	± 2.2500	16, 17	± 0.2500
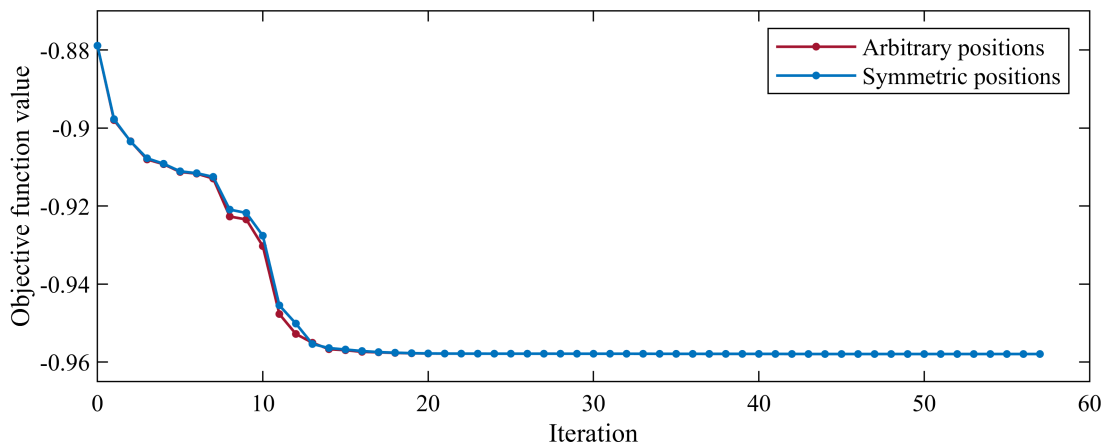
Figure 6.4: Convergence rate of optimization of linear arrays with maximum beam efficiency for arbitrary and symmetric elements' positions.

Both optimizations − the one with arbitrary and the other with symmetric elements positions − finished at the same optimum, which is listed in Table 6.3 and shown in Figure 6.5. The obtained array factor is shown in Figure 6.6, in comparison with the array factor from [61]. In addition, Table 6.4 shows their parameters. Clearly, both methods are able to find positions that ensure high beam efficiency, offering very similar arrays.

It is interesting to note that the optimum arrays contain no overlapping elements, nor the elements that are too close one to another. The minimum interelement spacing equals to 0.4510λ.

Table 6.3: Optimum positions of antenna elements obtained with proposed design.

n	x_n, λ	n	x_n, λ	n	x_n, λ	n	x_n, λ
1, 32	± 9.9251	5, 28	± 6.4660	9, 24	± 3.7659	13, 20	± 1.6754
2, 31	± 9.1141	6, 27	± 5.6530	10, 23	± 3.2327	14, 19	± 1.2108
3, 30	± 8.2313	7, 26	± 4.9789	11, 22	± 2.6859	15, 18	± 0.7032
4, 29	± 7.3412	8, 25	± 4.3671	12, 21	± 2.1948	16, 17	± 0.2522
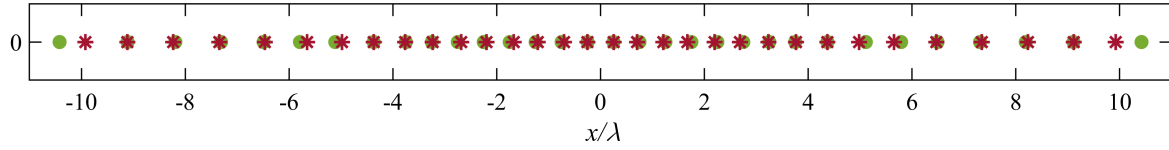
Figure 6.5: Element positions of optimum array (red), together with element positions of initial array from Table 6.2 (green).
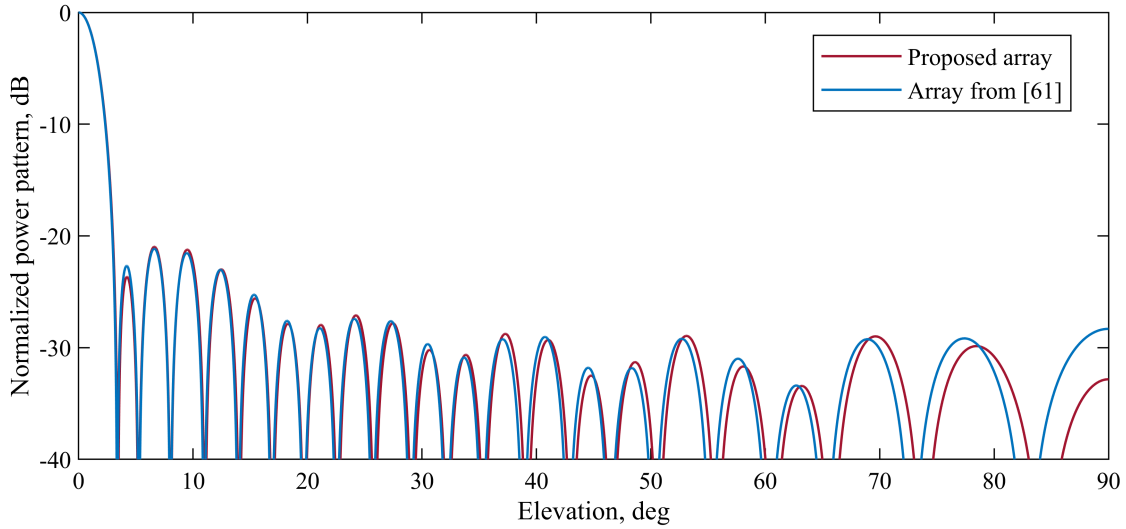
Figure 6.6: Normalized array factors of uniformly excited arrays with 32 unequally spaced elements obtained with proposed approach and with method from [61].

Table 6.4: Beam efficiency, BE, first-null beamwidth, FNBW, 3dB-beamwidth, BW3, sidelobe level, SLL, and directivity, DIR, of proposed unequally spaced arrays with 32 elements, and of array from [61].

Design method	BE, %	BW3, deg	FNBW, deg	SLL, dB	DIR, dB
Proposed	95.80	2.75	6.87	-20.21	15.88
Array from [61]	95.78	2.73	6.75	-21.14	15.92

6.2.4.2 Planar Arrays with Maximum Beam Efficiency in Rectangular Region of Interest

The second example illustrates an application of quasi-Newton method in the design of planar arrays that maximize beam efficiency within a specified rectangular region. An array with 100 antenna elements and square region of interest with $u_0 = v_0 = 0.2$ is considered.

Here, the optimization problem contains significantly larger number of design variables than does the problem in Section 6.2.4.1. However, if a symmetry is utilized, the number of variables decreases by a factor of four. Such a decrease also decreases the method's sensitivity

to optimization starting point, thus increasing the robustness and the probability of finding the global solution. In Section 6.2.4.1 it was illustrated that the design of a linear array results in the same symmetric array, regardless of whether the symmetry was forced or not. Such a behavior was also encountered in unconstrained optimization presented in [61], where the obtained linear arrays are symmetric even though the symmetry was not enforced. Expecting that planar arrays generating pencil beams act similarly to linear arrays, the unconstrained optimization is here performed assuming symmetrically placed elements.

The design is performed by solving the problem (6.20). As an optimization starting point, equidistant array with $\lambda/2$ spacing is used. The optimum solution is reached in 198 iterations, requiring the computational time of 2.91 s. Figure 6.7 shows optimization's convergence rate.
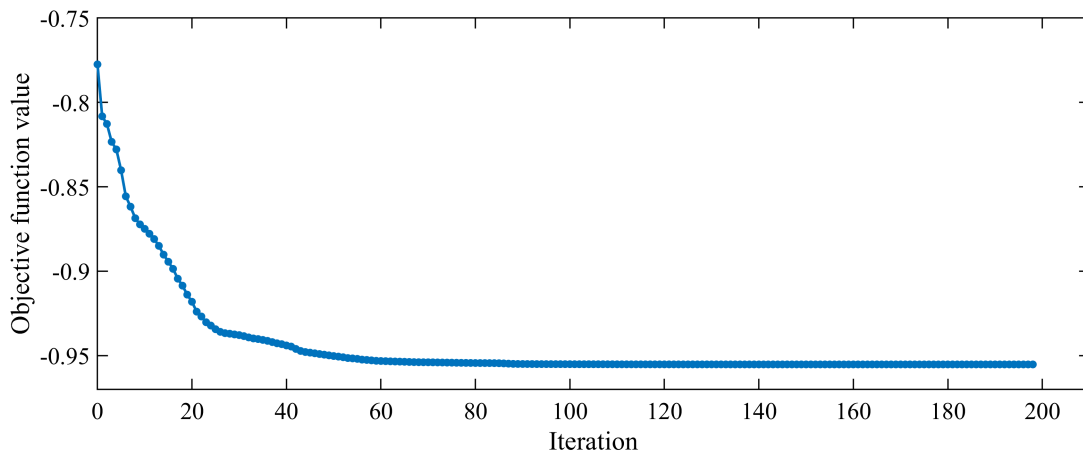
Figure 6.7: Convergence rate of optimization of planar array with symmetric element positions and maximum beam efficiency.

Obtained element positions and corresponding array factor are shown in Figure 6.8. Numerical values of elements' positions are given in Table 6.5, for convenience. Parameters of the proposed array are given in Table 6.6, together with parameters of the array obtained with particle swarm optimization in [60]. It is clear that the proposed approach provides an array with higher beam efficiency. However, the performed optimization resulted in several closely spaced elements, with some of them even overlapping. These elements are located on the *x*- and *y*-axes, or in their vicinity. On the other hand, the array in [60] is obtained by utilizing constrained optimization, which prevents overlapping. It gives the idea that introducing constraints in the proposed method might also be beneficial. Such an approach is described in Section 6.3.4.2.
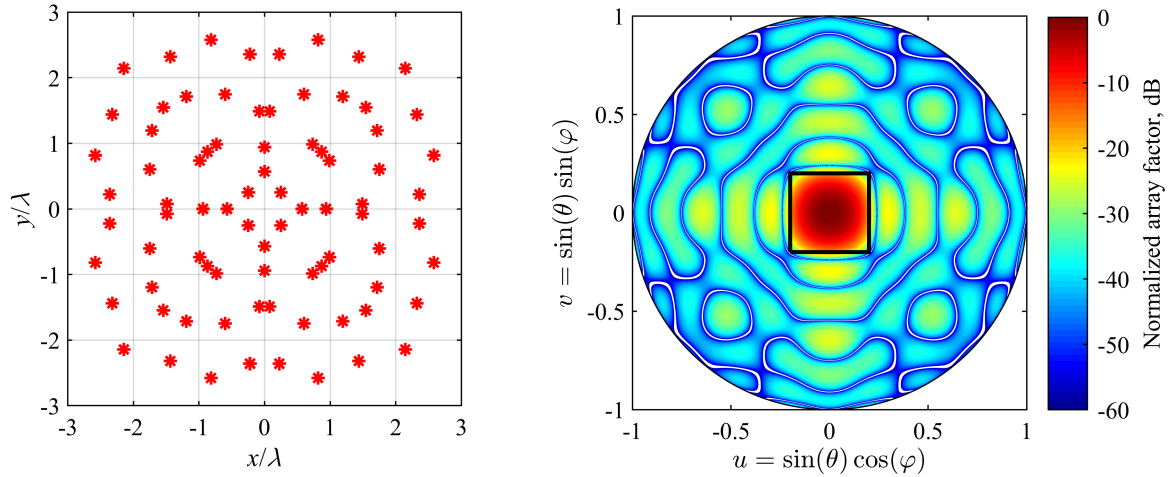
Figure 6.8: Element positions of optimum symmetric array with 100 elements (left) and corresponding normalized array factor (right). Region of interest is drawn in black.

Table 6.5: Element positions of symmetric array with maximum beam efficiency and 100 elements. Only elements in first quadrant are listed.

n	x_n, λ	y_n, λ	n	x_n, λ	y_n, λ	n	x_n, λ	y_n, λ
1	0.2492	0.2492	10	0.6032	1.7480	19	1.5460	1.5460
2	0.0000	0.5713	11	0.9395	0.0000	20	1.4368	2.3206
3	0.0000	0.9395	12	0.7333	0.9856	21	2.3597	0.2235
4	0.0758	1.4901	13	0.8702	0.8702	22	1.7480	0.6032
5	0.2235	2.3597	14	1.1929	1.7128	23	2.5794	0.8164
6	0.5713	0.0000	15	0.8164	2.5794	24	2.3206	1.4369
7	0.8703	0.8703	16	1.4901	0.0757	25	2.1428	2.1428
8	0.9856	0.7333	17	1.7480	0.6032			
9	0.6032	1.7480	18	1.7128	1.1929			

Table 6.6: Beam efficiency, BE, first-null beamwidth, FNBW, 3dB-beamwidth, BW3, sidelobe level, SLL, and directivity, DIR, of proposed symmetric array with 100 elements, as well as of array from [60].

Design method	BE, %	BW3, deg	FNBW, deg	SLL, dB	DIR, dB
Proposed	95.52	11.04	13.88	−17.17	24.92
Particle swarm [60]	91.06	11.60	27.60	−16.00	24.2

6.2.4.3 Planar Arrays with Maximum Directivity

In this example, directivity maximization described by the problem in (6.22) is performed. Directivity is maximized for the symmetric planar arrays with 9, 16, 25, 36, 49, 64, 81, and 100 elements. It is important to note that since the problem in (6.22) is unconstrained, the optimization starting point is always feasible regardless of which element positions are chosen. However, a good guess about the initial positions might significantly reduce the design time. Before choosing the initial positions, it will be considered how interelement spacing influences the directivity. The analysis of directivity in equally spaced arrays was performed in [86] and [68]. The former paper referred to analyzes the square array with 25 elements, whereas the latter considers several rectangular (nonsquare) geometries. Here, systematic analysis of various equidistant arrays is carried out.

First, the directivities of planar square arrays with 9, 16, 25, 36, 49, 64, 81, and 100 elements with different interelement spacings, starting from $d = 0.40\lambda$ to $d = 1.20\lambda$ in steps of 0.01λ are calculated. The results are shown in Figure 6.9. Apparently, for each array, an interelement spacing which provides maximum directivity can be encountered. Such array is a good candidate for optimization starting point. Table 6.7 lists the values of maximum directivities, corresponding interelement spacings, total arrays' length along x and y axis, and the increase of array size expressed relatively to the size of equally spaced array with interelement spacing of 0.5λ, calculated for the arrays with aforementioned number of elements. The parameter d from this table is used to form equidistant array for optimization starting point for a given N.
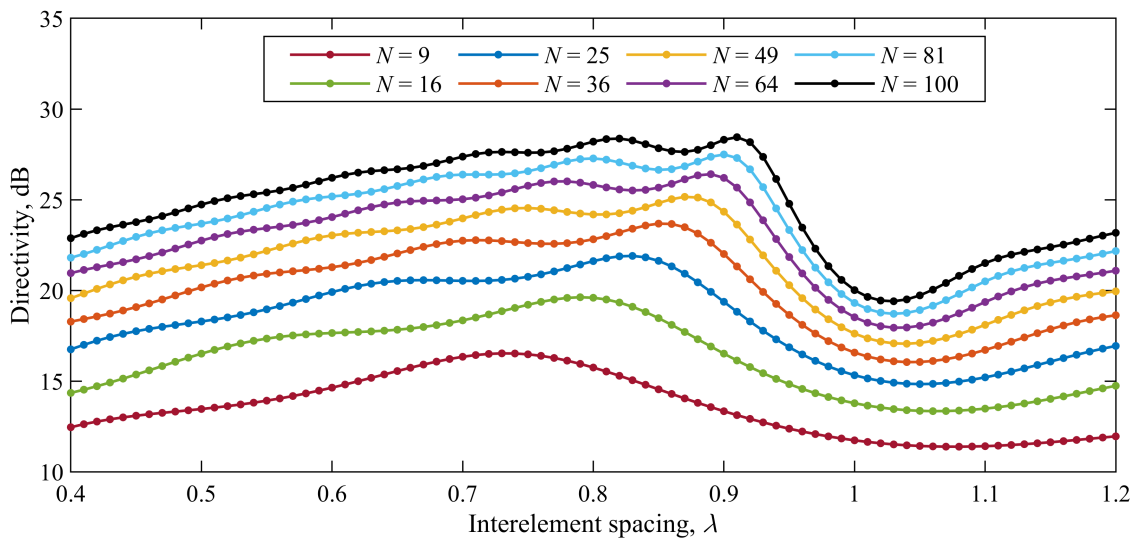
Figure 6.9: Directivities of equally-spaced planar square arrays calculated for various interelement spacings and various number of elements, N.

Table 6.7: Maximum directivity, D, corresponding interelement spacing, d, total arrays' length along x and y axis, L_x and L_y, and increase of array size expressed relatively to size of equally spaced array with interelement spacing of 0.5λ, Δ_s, calculated for equally spaced planar square arrays with various numbers of elements, N,

N	D, dB	d, λ	$L_x = L_y$, λ	Δ_s, %
9	16.5	0.73	1.46	+46
16	19.6	0.79	2.37	+58
25	21.9	0.83	3.32	+66
36	23.7	0.85	4.25	+70
49	25.2	0.87	5.22	+74
64	26.4	0.89	6.23	+78
81	27.5	0.90	7.20	+80
100	28.4	0.91	8.19	+82

The optimization is carried out for symmetric arrays with 9, 16, 25, 36, 49, 64, 81, and 100 elements. The number of iterations required to obtain the optimum array together with the computational time for each optimization run is given in Table 6.8. It is clear that in all cases the method exhibits fast convergence.

Table 6.8: Number of iterations and computational time for unconstrained optimizations of arrays with maximum directivity and various number of elements, N.

N	Number of iterations	Computational time, s
9	7	0.03
16	9	0.01
25	18	0.02
36	19	0.03
49	28	0.09
64	28	0.12
81	44	0.29
100	40	0.49

Figures 6.10 and 6.11 show the optimum positions of antenna elements and the corresponding array factors. Interestingly, the distributions of the optimum antenna elements exhibit similar shapes for all of the proposed arrays, i.e. the shapes change only the scale depending on the number of array elements. The minimum distances between elements and the sizes of all proposed arrays are given in Table 6.9. Clearly, the total array sizes are very close to those of the initial arrays, which are shown in Table 6.7. In all arrays, the obtained interelement spacing is larger than 0.5λ.
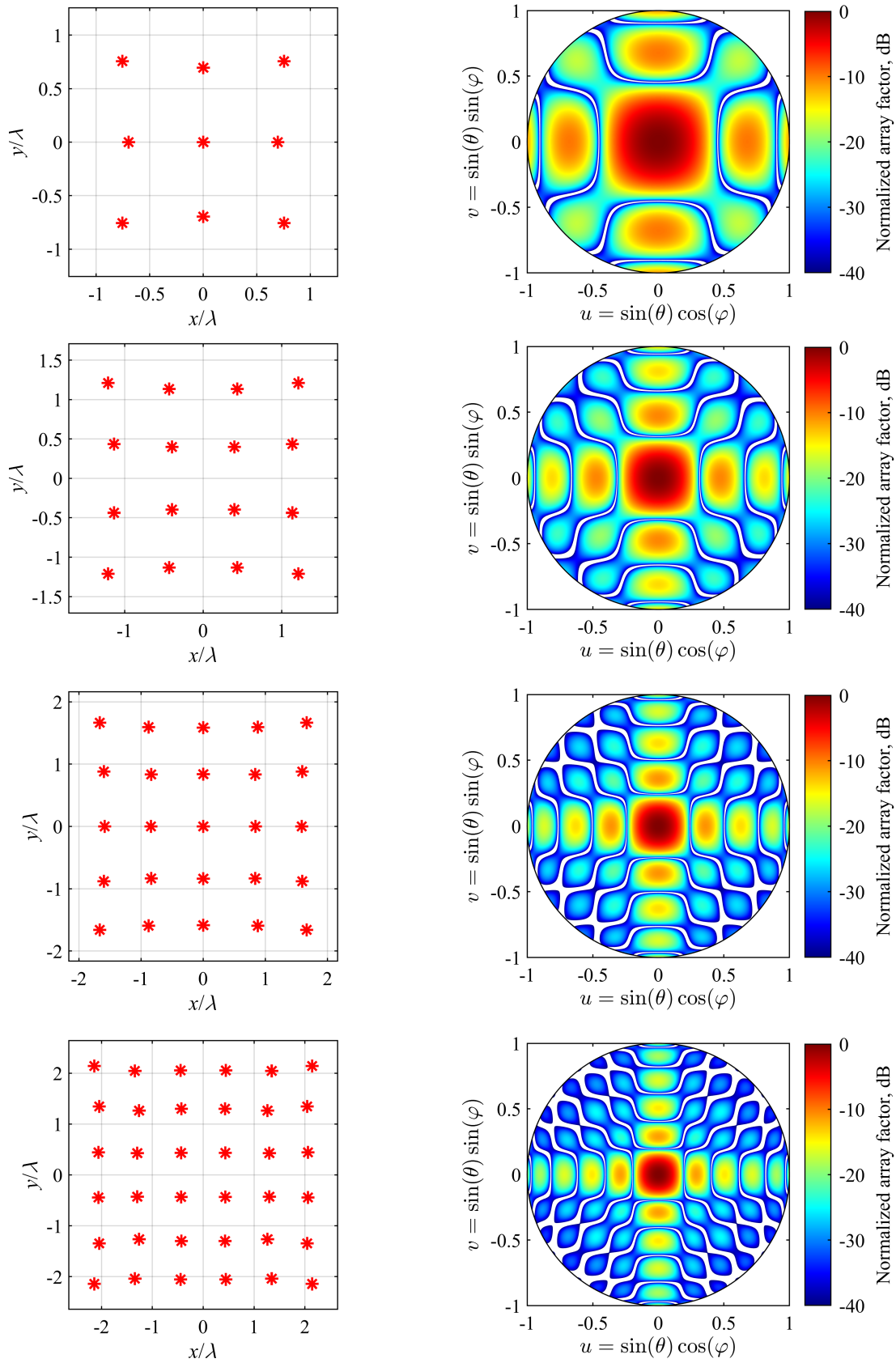
Figure 6.10: Optimum element positions of antenna arrays with 9, 16, 25, and 36 (left) and corresponding normalized array factors (right).
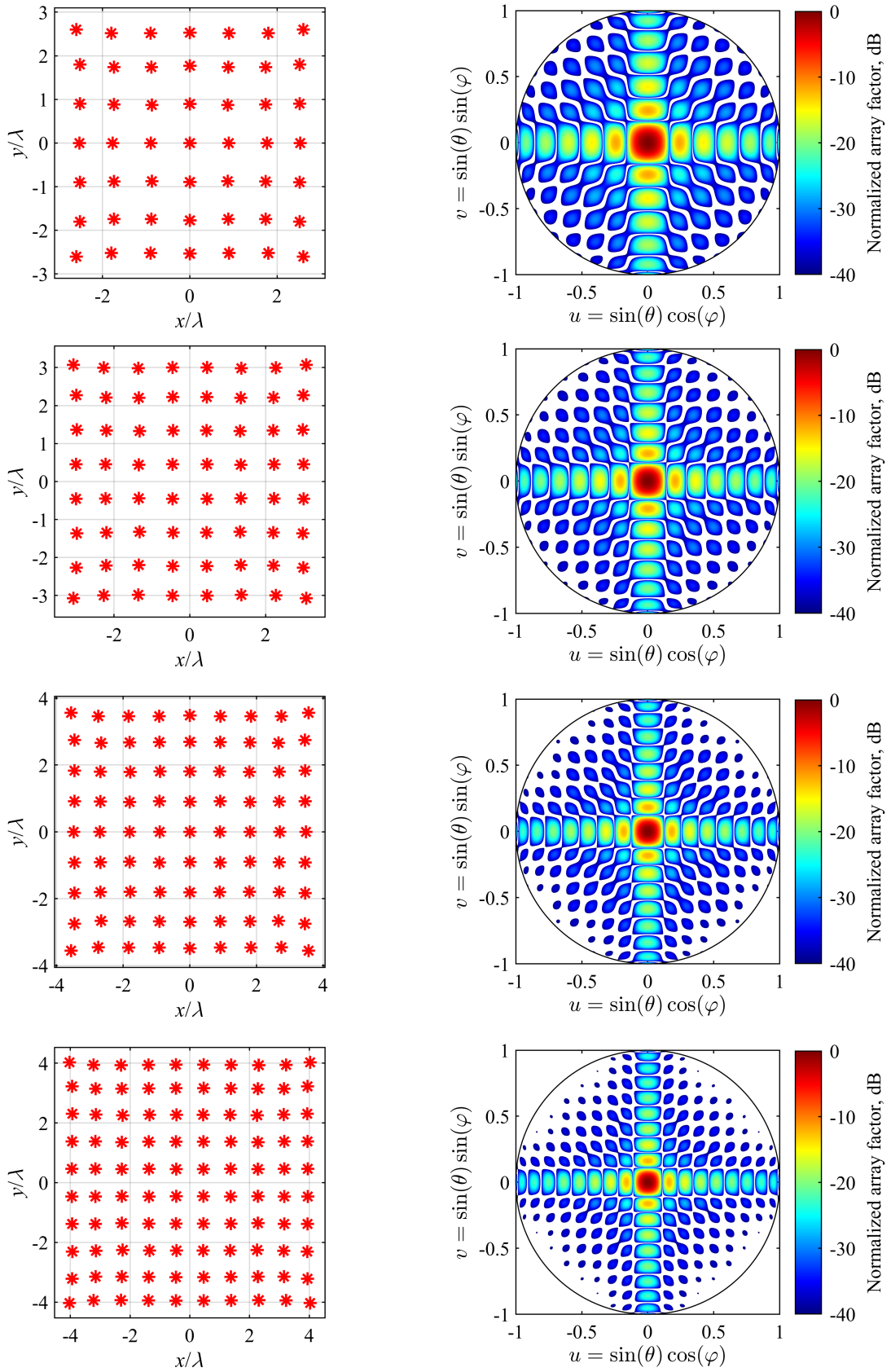
Figure 6.11: Optimum element positions of antenna arrays with 49, 64, 81, and 100 elements (left) and corresponding normalized array factors (right).

Table 6.9: Minimum interelement spacing, d_{min}, and array sizes calculated along x and y axis, L_x, L_y, of proposed arrays.

N	d_{min}, λ	L_x, λ	L_y, λ
9	0.6966	1.5128	1.5128
16	0.7367	2.4208	2.4208
25	0.7470	3.3257	3.3257
36	0.7573	4.2857	4.2857
49	0.7637	5.2024	5.2024
64	0.7759	6.1414	6.1414
81	0.7802	7.1176	7.1176
100	0.7812	8.0587	8.0587

Table 6.10 shows the parameters of equally spaced arrays with interelement spacing of $\lambda/2$, of equally spaced arrays with maximum directivity, and of optimum nonequally spaced arrays with maximum directivity. Clearly, the proposed arrays provide higher directivities than do both equally spaced arrays. The gain in directivity increases with an increase in number of elements. The main beams of the proposed arrays are narrower than the beams of the arrays with interelement spacing of $\lambda/2$ and similar to those obtained by equally spaced arrays with maximum directivity. The maximum sidelobe level of the proposed arrays is slightly lower.

Numerical values of elements' positions for the proposed arrays with 8, 49, and 100 elements are given in Tables 6.11, 6.12, and 6.13, for convenience.

Table 6.10: Directivity, D, 3 dB cutoff, θ_{3dB}, position of first zero, θ_z, and sidelobe level, SLL, of equally spaced arrays with spacing of $\lambda/2$, equally spaced arrays with maximum directivity, and of proposed nonequally spaced arrays.

N	Equally spaced arrays with spacing of $\lambda/2$				Equally spaced arrays with maximum directivity				Nonequally spaced arrays with maximum directivity			
	D, dB	θ_{3dB}, deg	θ_z, deg	SLL, dB	D, dB	θ_{3dB}, deg	θ_z, deg	SLL, dB	D, dB	θ_{3dB}, deg	θ_z, deg	SLL, dB
9	13.5	18.1	41.8	−9.5	16.5	12.3	27.2	−9.5	16.6	12.2	26.9	−9.7
16	16.5	13.2	30.0	−11.3	19.6	8.3	18.4	−11.3	19.8	8.3	18.4	−10.3
25	18.3	10.4	23.6	−12.0	21.9	6.2	13.9	−12.0	22.2	6.3	14.0	−10.9
36	20.2	8.6	19.5	−12.4	23.7	5.0	11.3	−12.4	24.1	5.1	11.3	−11.4
49	21.4	7.3	16.6	−12.7	25.2	4.2	9.5	−12.7	25.7	4.3	9.4	−11.6
64	22.7	6.4	14.5	−12.8	26.4	3.6	8.1	−12.8	27.1	3.7	8.1	−11.8
81	23.7	5.7	12.8	−12.9	27.5	3.2	7.1	−12.9	28.2	3.2	7.1	−12.0
100	24.7	5.1	11.5	−13.0	28.4	2.8	6.3	−13.0	29.3	2.8	6.4	−12.1

Table 6.11: Element positions of symmetric array with maximum directivity and 9 elements. Only elements in first quadrant and on positive x and y axes are listed.

n	x_n, λ	y_n, λ
1	0.3976	0.3976
2	0.4344	1.1333
3	1.1333	0.4344
4	1.2104	1.2104

Table 6.12: Element positions of symmetric array with maximum directivity and 49 elements. Only elements in first quadrant and on positive x and y axes are listed.

n	x_n, λ	y_n, λ	n	x_n, λ	y_n, λ	n	x_n, λ	y_n, λ
1	0.0000	0.0000	7	0.0000	2.5321	13	1.8012	2.5163
2	0.8945	0.0000	8	0.8712	0.8712	14	2.5175	0.9000
3	1.7684	0.0000	9	0.8827	1.7396	15	2.5163	1.8012
4	2.5321	0.0000	10	0.9000	2.5175	16	2.6012	2.6012
5	0.0000	0.8945	11	1.7396	0.8827			
6	0.0000	1.7684	12	1.7399	1.7399			

Table 6.13: Element positions of symmetric array with maximum directivity and 100 elements. Only elements in first quadrant are listed.

n	x_n, λ	y_n, λ	n	x_n, λ	y_n, λ	n	x_n, λ	y_n, λ
1	0.4565	0.4565	10	1.3842	3.9387	19	3.1486	3.1486
2	0.4597	1.3692	11	2.2730	0.4506	20	3.2192	3.9402
3	0.4506	2.2730	12	2.2737	1.3516	21	3.9511	0.4611
4	0.4617	3.1619	13	2.2542	2.2542	22	3.9387	1.3842
5	0.4611	3.9511	14	2.2776	3.1453	23	3.9343	2.3035
6	1.3692	0.4597	15	2.3035	3.9343	24	3.9402	3.2192
7	1.3748	1.3748	16	3.1619	0.4617	25	4.0293	4.0293
8	1.3516	2.2737	17	3.1575	1.3779			
9	1.3779	3.1575	18	3.1453	2.2776			

6.2.5   Concluding Remarks

The presented examples prove that the quasi-Newton method can be a valuable tool for the optimization of equally-excited unequally-spaced arrays. In linear arrays, this method ensures fast convergence, offering the results similar to those obtained by other gradient-based methods. However, its significant advantage is found in the ability of very simple formulation of the design problem.

In the case of planar arrays with maximum beam efficiency the method also exhibits fast convergence and provides insightful results. The optimization problems can be formulated easily enabling rapid experimenting with various design criteria. Unfortunately, the obtained results might contain closely spaced or overlapping elements, which causes difficulties in arrays' implementations. However, in further sections, it will be shown that this problem can be mitigated by using constrained optimization.

The optimization of the directivity of unequally spaced planar arrays yields higher directivity compared to their equally spaced counterparts. The gain in directivity increases with an increase in number of elements. The appearance of closely spaced or overlapping elements has not been encountered in this case.

6.3   Design Based on Constrained Optimization

In this section, the unconstrained optimization problems for the design of linear and planar arrays, given in (6.19)−(6.22), are extended with the constraints for

- minimum interelement spacing, d_{min},
- maximum sidelobe level, δ_{max}, that is achieved outside the region of interest, and
- maximum array size, which is specified by the minimum and maximum positions of antenna elements, x_{min} and x_{max} for linear and x_{min}, x_{max}, y_{min}, and y_{max} for planar arrays.

6.3.1   Maximization of Beam Efficiency

Constrained optimization problem for the design of linear arrays with maximum beam efficiency can be expressed as

$$\underset{\mathbf{w}}{\text{minimize}} \quad -\frac{P(\mathbf{w}, \Psi)}{P(\mathbf{w}, \Omega)} \tag{6.23a}$$

$$\text{subject to} \quad x_k - x_{k-1} \geq d_{min}, \quad k = 2, 3, ..., N, \tag{6.23b}$$

$$\underset{\theta}{\max} |f(\mathbf{w}, \theta)| \leq \delta_{max}, \quad \theta \in [\theta_s, \pi/2], \tag{6.23c}$$

$$x_{min} \leq x_n \leq x_{max}, \quad n = 1, 2, ..., N \tag{6.23d}$$

where θ_s is start of the sidelobe region. The powers $P(\mathbf{w}, \Psi)$ and $P(\mathbf{w}, \Omega)$ are obtained by using (6.6)$-$(6.9). In practical optimization, the constraint in (6.23c) can be approximated by calculating the maximum value of $|f(\mathbf{w}, \theta)|$ above a finite grid θ_g, $g = 1, 2, ..., G$, where $\theta_g \geq \theta_s$.

Constrained optimization problem for maximizing the beam efficiency of planar arrays within a rectangular region of interest $\Psi = \{(u, v) : |u| \leq u_0, |v| \leq v_0\}$ is given by

$$\underset{\mathbf{w}}{\text{minimize}} \quad -\frac{P(\mathbf{w}, \Psi)}{P(\mathbf{w}, \Omega)} \tag{6.24a}$$

$$\text{subject to} \quad (x_k - x_l)^2 + (y_k - y_l)^2 \geq d_{min}^2, \quad k = 1, 2, ..., N, \ l = k+1, ..., N, \tag{6.24b}$$

$$\max_{u,v} |f(\mathbf{w}, u, v)| \leq \delta_{max}, \quad |u| \geq u_0, \ |v| \geq v_0, \ u^2 + v^2 \leq 1, \tag{6.24c}$$

$$x_{min} \leq x_n \leq x_{max}, \quad n = 1, 2, ..., N, \tag{6.24d}$$

$$y_{min} \leq y_n \leq y_{max}, \quad n = 1, 2, ..., N \tag{6.24e}$$

where the powers $P(\mathbf{w}, \Psi)$ and $P(\mathbf{w}, \Omega)$ are obtained by using (6.11) and (6.16). Similarly to the constraint (6.23c), the constraint (6.24c) can be approximated by calculating maximum value of $|f(\mathbf{w}, u, v)|$ above a finite grid u_g, $g = 1, 2, ..., G$, and v_h, $h = 1, 2, ..., H$, where $|u_g| \geq u_0$, $|v_h| \geq v_0$, and $u_g^2 + v_h^2 \leq 1$.

The problems in (6.23) and (6.24) can be easily adapted for the design of symmetric arrays. In such a case, the optimizations are performed with respect to vector $\mathbf{w_s}$, as elaborated in Section 6.1.1. A problem similar to symmetric version of the problem (6.24) was considered in [60] in the context of particle swarm optimization.

The problem in (6.24) can be reformulated for maximizing the beam efficiency within a circular region of interest. For symmetric arrays with no elements placed on the x- and y-axis, the problem takes the form

$$\underset{\mathbf{w_s}}{\text{minimize}} \quad -\frac{P(\mathbf{w_s}, \Psi)}{P(\mathbf{w}, \Omega)} \tag{6.25a}$$

$$\text{subject to} \quad (x_k - x_l)^2 + (y_k - y_l)^2 \geq d_{min}^2, \quad k = 1, 2, ..., N, \ l = k+1, ..., N, \tag{6.25b}$$

$$\max_{\theta, \varphi} |f_{\text{sym}}(\mathbf{w_s}, \theta, \varphi)| \leq \delta_{max}, \quad \theta \in [\theta_s, \pi/2], \ \varphi \in [0, 2\pi], \tag{6.25c}$$

$$x_{min} \leq x_n \leq x_{max}, \quad n = 1, 2, ..., N, \tag{6.25d}$$

$$y_{min} \leq y_n \leq y_{max}, \quad n = 1, 2, ..., N \tag{6.25e}$$

where $P(\mathbf{w_s}, \Psi)$ and $P(\mathbf{w}, \Omega)$ are given by (6.15) and (6.16). The constraint (6.25c) can be approximated by calculating the maximum value of $|f_{\text{sym}}(\mathbf{w_s}, \theta, \varphi)|$ above a finite grid θ_g, $g = 1, 2, ..., G$, and φ_h, $h = 1, 2, ..., H$, where $\theta_s \leq \theta_g \leq \pi/2$ and $0 \leq \varphi_h \leq 2\pi$.

Problems (6.24) and (6.25) assume the array elements are placed within a rectangular area. If a circular area is desired, then the constraints (6.24d) and (6.24e) as well as (6.25d) and (6.25e) should be replaced with

$$x_n^2 + y_n^2 \le R_a^2, \quad n = 1, 2, ..., N \tag{6.26}$$

where R_a is the largest distance of an antenna element from the origin by using (6.26). The optimization problems for the design of arrays whose elements are placed in circular areas take the forms

$$\underset{\mathbf{w}}{\text{minimize}} \quad -\frac{P(\mathbf{w}, \Psi)}{P(\mathbf{w}, \Omega)} \tag{6.27a}$$

$$\text{subject to} \quad (x_k - x_l)^2 + (y_k - y_l)^2 \ge d_{min}^2, \quad k = 1, 2, ..., N, \ \ l = k+1, ..., N, \tag{6.27b}$$

$$\underset{u,v}{\max} |f(\mathbf{w}, u, v)| \le \delta_{max}, \quad |u| \ge u_0, \ |v| \ge v_0, \ u^2 + v^2 \le 1, \tag{6.27c}$$

$$x_n^2 + y_n^2 \le R_a^2, \quad n = 1, 2, ..., N \tag{6.27d}$$

for rectangular region of interest and

$$\underset{\mathbf{w_s}}{\text{minimize}} \quad -\frac{P(\mathbf{w_s}, \Psi)}{P(\mathbf{w}, \Omega)} \tag{6.28a}$$

$$\text{subject to} \quad (x_k - x_l)^2 + (y_k - y_l)^2 \ge d_{min}^2, \quad k = 1, 2, ..., N, \ \ l = k+1, ..., N, \tag{6.28b}$$

$$\underset{\theta, \varphi}{\max} |f_{\text{sym}}(\mathbf{w_s}, \theta, \varphi)| \le \delta_{max}, \quad \theta \in [\theta_s, \pi/2], \ \varphi \in [0, 2\pi], \tag{6.28c}$$

$$x_n^2 + y_n^2 \le R_a^2, \quad n = 1, 2, ..., N \tag{6.28d}$$

for circular region of interest.

6.3.2 Maximization of Directivity

The optimization problem for the design of antenna arrays with maximum directivity can also be equipped with the aforementioned constraints. The resulting problem takes the form

$$\underset{\mathbf{w}}{\text{minimize}} \quad -\frac{|f(\mathbf{w}, \theta_0, \varphi_0)|^2}{P(\mathbf{w}, \Omega)/4\pi} \tag{6.29a}$$

$$\text{subject to} \quad (x_k - x_l)^2 + (y_k - y_l)^2 \ge d_{min}^2, \quad k = 1, 2, ..., N, \ \ l = k+1, ..., N, \tag{6.29b}$$

$$\underset{\theta, \varphi}{\max} |f(\mathbf{w}, \theta, \varphi)| \le \delta_{max}, \quad \theta \in [\theta_s, \pi/2], \ \varphi \in [0, 2\pi], \tag{6.29c}$$

$$x_{min} \le x_n \le x_{max}, \quad n = 1, 2, ..., N, \tag{6.29d}$$

$$y_{min} \le y_n \le y_{max}, \quad n = 1, 2, ..., N \tag{6.29e}$$

where $P(\mathbf{w}, \Omega)$ is given by (6.16) and $\theta_0 = 0$ and $\varphi_0 = 0$ are used for the directivity at the broadside direction. The constraint (6.29c) can be evaluated by using the approximation which has been applied in the evaluation of constraint (6.25c). In addition, by using the optimization with respect to vector $\mathbf{w_s}$, the optimization problem (6.29) can be easily adapted for the design of symmetric arrays.

6.3.3   Solver for Constrained Optimization

Solving the optimization problems in (6.23)−(6.29) requires solvers for nonlinear constrained optimization. Such solvers can be found in many tools and software libraries, such as Matlab [85] and SciPy [87]. In this research, function *fmincon* from Matlab Optimization Toolbox [85] is used. This function implements several algorithms such as the interior point, sequential quadratic programming, trust region reflective, and active set [70].

The implementation of trust region reflective algorithm in function *fmincon* supports only bounds or linear equality constraints (but not both) and requires an analytically supplied gradient of the objective function. However, the problems being considered contain various linear and nonlinear constraints. Furthermore, the gradient of the objective function was not used to maintain problem formulation as simple as possible. For these reasons the trust region algorithm is not considered.

The other three algorithms can be applied in solving the aforementioned problems. A set of experiments was conducted where each of these algorithms was employed to solve the problems (6.24) and (6.29), while selecting various combinations of their constraints. Results showed that the application of the interior point algorithm failed to converge to an acceptable local minimum in all problems with constrained interelement spacing. Consequently this algorithm was omitted from further analysis.

The sequential quadratic programming and the active set are similar algorithms. Their main differences lie in the procedures for handling infeasible iterations and in the procedures that are used to solve quadratic programming subproblems. Furthermore, the active set can take steps outside the problem's bounds, whereas the SQP takes steps that are inside or at the bounds. In addition, the active set can take larger steps. More details on this can be found in [88], [89]. The application of these algorithms in solving optimization problems (6.23), (6.24), and (6.25) showed faster convergence of the active set algorithm. However, the SQP provided solutions with somewhat lower values of the objective functions. Furthermore, in solving optimization problem (6.29), the active set failed to converge within an acceptable number of iterations. Such behavior can be attributed to its larger optimization steps. Namely, in a numerically challenging design, large steps can cause unacceptable numerical error (and even oscillatory behavior) in calculation of the first order optimality measure near the optimum. Apparently, smaller optimization steps, such as those used in the SQP are preferable.

Finally, the SQP showed supreme convergence properties, justifying its reputation as the most effective method for constrained nonlinear optimization [70]. It always found solutions with lower objective function values within a given maximum number of iterations and function evaluations, even when started from remote starting points. Therefore, the SQP algorithm has been chosen for solving the discussed problems.

6.3.4   Design Examples

In this section, the examples are provided to illustrate features of the proposed design. The examples are worked out in Matlab 2023a running on a personal computer with Intel i9 processor operating at the clock of 3.6 GHz. Function *fmincon* is employed as solver, with the options set according to Table 6.14.

Table 6.14: Options for function *fmincon*.

Option	Value
Algorithm	*sqp*
StepTolerance	10^{-6}
OptimalityTolerance	10^{-6}
ConstraintTolerance	10^{-6}
MaxIterations	2000
MaxFunctionEvaluations	4000N

6.3.4.1   Linear Arrays with Maximum Beam Efficiency and Constrained Size and Interelement Spacing

This section illustrates the application of constrained optimization in the design of linear arrays with maximum beam efficiency. The problem in (6.23) is solved by utilizing only the constraints on minimum interelement spacing (6.23b), and maximum array size (6.23d). Such a problem was considered in [63], in the context of brain storm optimization. In the paper referred to, a symmetric array having 10 elements was designed, with interelement spacing constrained to $d_{min} = 0.4\lambda$ and the array size constrained to 4.5λ, The latter was implemented via the minimum and maximum position of antenna elements placed in the first quadrant, $x_{min} = 0.2\lambda$ and $x_{max} = 2.25\lambda$. Region of interest was specified as $\theta_s = \arcsin(0.2)$. Here, the array with the same specifications is designed. Optimization starts from equidistant array with $\lambda/2$ spacing.

The obtained element positions are listed in Table 6.15, whereas the corresponding array factor is shown in Figure 6.12. In addition, Table 6.16 gives the parameters of the proposed array and of the array from [63]. It is clear from the table that these two arrays differ negligibly. Apparently, both methods converge to the same optimum in this case. However, from

design procedure point of view, the proposed approach has several benefits. First, the design time is short. In this example optimum is reached within 10 iterations and in 0.1 s, which is significantly faster than 30 s reported in [63]. This is especially important when there are more design variables, and consequently, more constraints. In addition, the proposed method utilizes a known and widely available solver, which allows simple and straightforward implementation of the objective function and the constraints, as well as performing the optimization itself. On the other hand, the brain storm optimization requires more designer interaction, especially in forming an optimization strategy suitable for the problem at hand.

Table 6.15: Optimum positions of antenna elements obtained with proposed design.

n	$x_n,\ \lambda$
1,10	± 2.2445
2,9	± 1.5745
3,8	± 1.0445
4,7	± 0.6066
5,6	± 0.2066
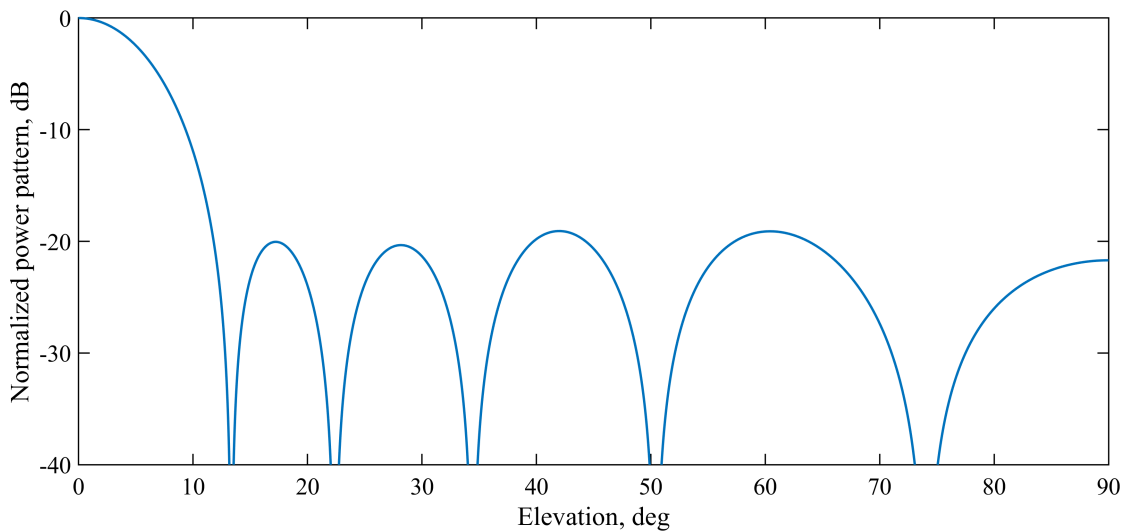
Figure 6.12: Normalized array factor of array obtained with proposed approach.

Table 6.16: Beam efficiency, BE, first-null beamwidth, FNBW, 3dB-beamwidth, BW3, sidelobe level, SLL, and directivity, DIR, of proposed unequally spaced arrays with 10 elements and of array obtained with method from [63].

Design method	BE, %	BW3, deg	FNBW, deg	SLL, dB	DIR, dB
Proposed	95.81	11.00	26.70	-18.42	9.89
Method from [63]	95.81	10.98	26.67	-18.53	9.90

6.3.4.2 Planar Arrays with Maximum Beam Efficiency in Rectangular Region of Interest and Various Constraints

This example considers the optimization of beam efficiency of planar arrays with constrained minimum interelement spacing, maximum SLL, and maximum size. Such a design is given by the problem in (6.24). Both array types − one with symmetric and the other with arbitrary elements' positions − are considered. The arrays are designed with $N = 100$ elements, square region of interest with $u_0 = v_0 = 0.2$, minimum interelement spacing of $d_{min} = 0.4\lambda$, array boundaries set to $x_{min} = y_{min} = -2.25\lambda$ and $x_{max} = y_{max} = 2.25\lambda$, and SLL constrained to $\delta_{max} = -15$ dB. The optimization of a symmetric array with the same specifications is performed in [60] by using particle swarm optimization.

In this example, both optimizations start from the array obtained in [60] (see Figure 6 therein). Figures 6.13 and 6.14 show the convergence rates of the SQP algorithm for both cases. Design with symmetric element positions contains four times less variables than the design with arbitrary positions. Consequently, a significantly lower number of iterations is required for the algorithm to converge in the former case, i.e. 101 iterations for symmetric array compared to 1917 iterations for the array with arbitrary element positions, requiring the computational time of 27.94 s and 794.40 s. It is interesting to note that even though the algorithm starts from a feasible point, before reaching the optimum, it passes through iterations containing infeasible points, which are in Figures 6.13 and 6.14 marked in red. This can be beneficial if the problem is highly nonlinear, which is the case in this example. Namely, staying exclusively inside the feasible region can be computationally expensive [70]. Extending the search area outside the feasible region improves the convergence.
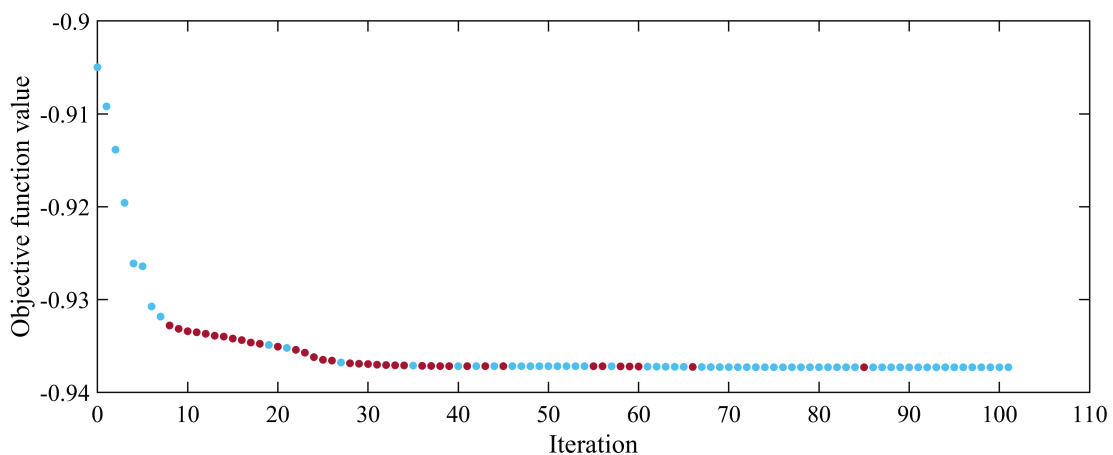
Figure 6.13: Convergence rate of optimization performed by sequential quadratic programming for planar array with symmetric elements' positions. Red color indicates infeasible, whereas cyan indicates feasible points.
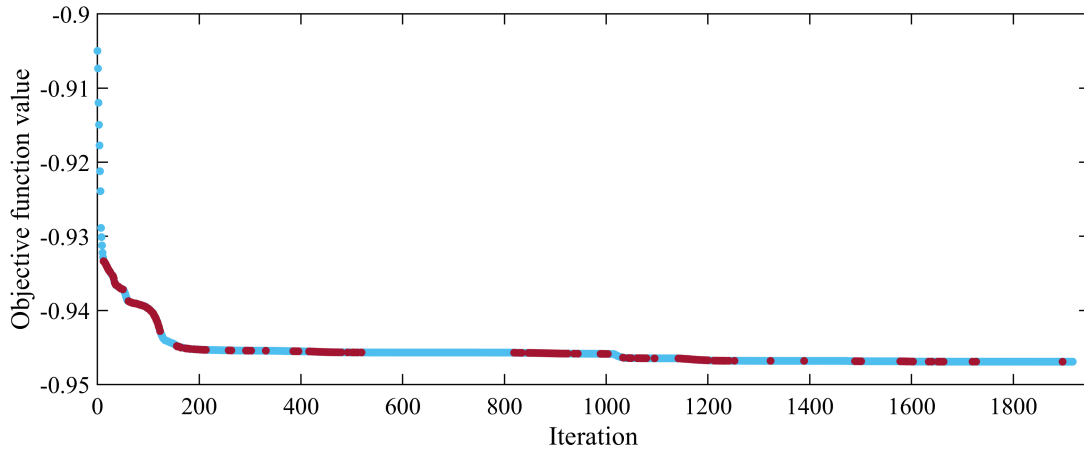
Figure 6.14: Convergence rate of optimization performed by sequential quadratic programming for planar array with arbitrary elements' positions. Red color indicates infeasible, whereas cyan indicates feasible points.

Comparison of the proposed arrays and the array in [60] is given in Table 6.17. Clearly, the proposed arrays provide higher beam efficiency, slightly higher directivity, and somewhat wider main beam. The beam efficiency of the proposed array with symmetric elements are 2.67 % higher than that obtained in [60]. An improvement of 3.63 % is obtained if all elements are allowed to take arbitrary positions. The sidelobe levels of all three arrays have been targeted to -15.0 dB. However, the array from [60] achieved -16 dB. Clearly, the proposed method is capable of exploiting more degrees of freedom, thus reaching a higher beam efficiency for specified design requirements. Figures 6.15 and 6.16 show elements' positions of the proposed arrays together with the corresponding array factors. Numerical values of the positions are provided in Tables 6.18 and 6.19, for convenience.

Table 6.17: Beam efficiency, BE, 3 dB cutoff, θ_{3dB}, position of first zero, θ_z, sidelobe level, SLL, and directivity, D, of proposed arrays with symmetric and arbitrary elements' positions and of array from [60].

Design method	BE, %	θ_{3dB}, deg	θ_z, deg	SLL, dB	D, dB
Proposed, symmetric positions	93.73	5.9	14.1	-15.0	24.3
Proposed, arbitrary positions	94.69	5.9	14.2	-15.0	24.3
Particle swarm [60]	91.06	5.8	13.8	-16.0	24.2
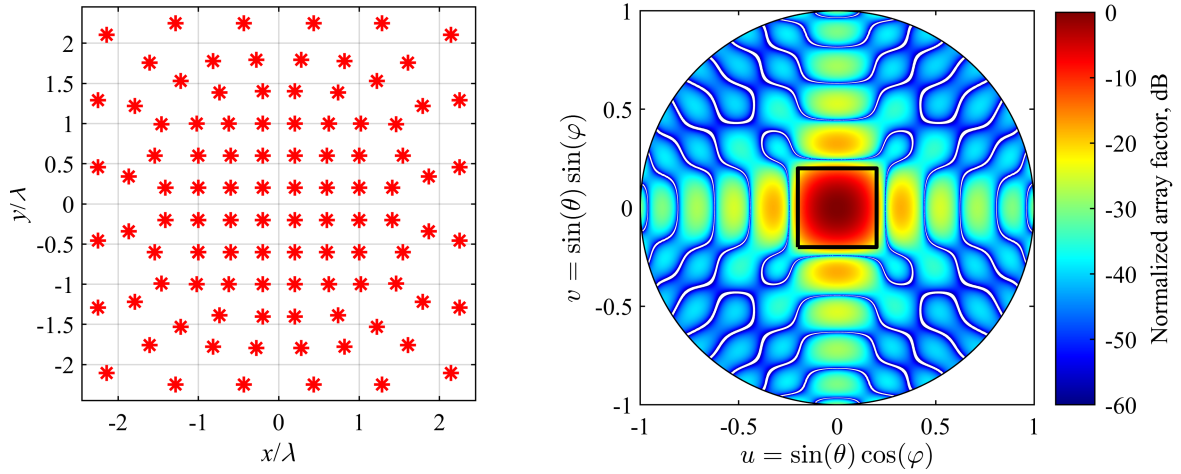
Figure 6.15: Element positions of optimum symmetric array with 100 elements (left) and corresponding normalized array factor (right). Region of interest is drawn in black.
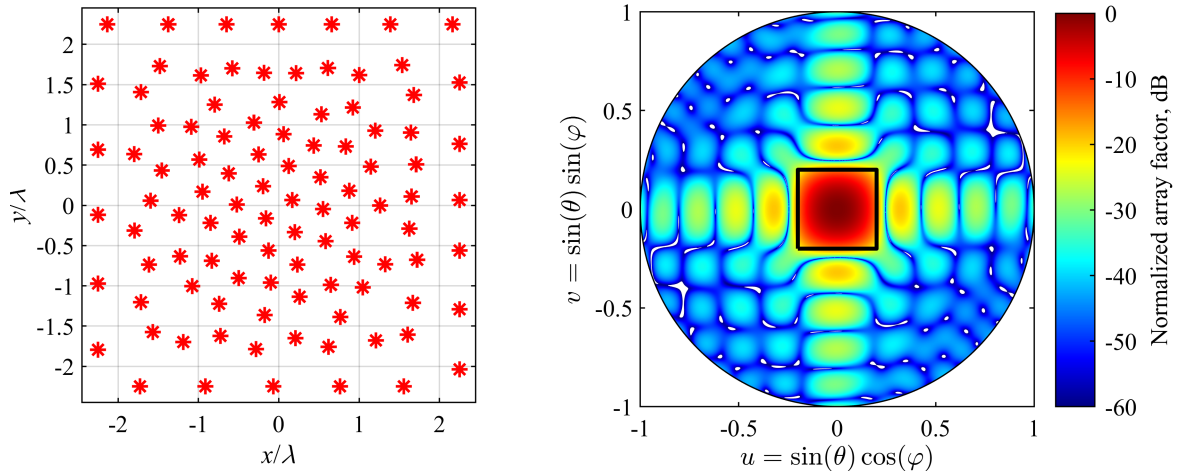
Figure 6.16: Element positions of optimum array with 100 elements and no symmetry requirement (left) and corresponding normalized array factor (right). Region of interest is drawn in black.

Table 6.18: Element positions of symmetric array with maximum beam efficiency and 100 elements. Only elements in first quadrant are listed.

n	x_n, λ	y_n, λ	n	x_n, λ	y_n, λ	n	x_n, λ	y_n, λ
1	0.2000	0.2000	10	2.2500	0.4573	19	1.2197	1.5284
2	0.6000	0.2000	11	0.2000	1.0000	20	2.2500	1.2896
3	1.0000	0.2000	12	0.6226	0.9994	21	0.4350	2.2500
4	1.4120	0.2000	13	1.0226	0.9994	22	0.2777	1.7942
5	1.8668	0.3425	14	1.4621	0.9912	23	1.2860	2.2500
6	0.2000	0.6000	15	1.7917	1.2178	24	1.6090	1.7580
7	0.6000	0.6000	16	0.2000	1.4018	25	2.1427	2.1065
8	1.0000	0.6000	17	0.7393	1.3874			
9	1.5459	0.6001	18	0.8185	1.7794			

Table 6.19: Element positions of array with maximum beam efficiency, 100 elements, and no symmetry requirement.

n	x_n, λ	y_n, λ	n	x_n, λ	y_n, λ	n	x_n, λ	y_n, λ
1	0.1677	0.0666	35	−2.2500	0.6934	69	1.6036	−1.6052
2	0.5177	0.3511	36	0.0090	1.2830	70	2.2500	−1.2911
3	0.8796	0.1806	37	−0.3127	1.0282	71	0.7624	−2.2500
4	1.1461	0.4789	38	−1.0890	0.9774	72	0.6197	−1.7574
5	1.6525	0.1106	39	−1.5000	0.9930	73	1.5563	−2.2500
6	0.1239	0.4902	40	−1.7991	0.6377	74	1.6699	−1.2107
7	0.4345	0.7423	41	−0.1827	1.6442	75	2.2500	−2.0365
8	0.8343	0.7318	42	−0.7973	1.2512	76	−0.1609	−0.1616
9	1.1993	0.9262	43	−0.9678	1.6130	77	−0.4894	−0.3898
10	2.2500	0.7650	44	−1.4798	1.7312	78	−0.8513	−0.2193
11	0.0609	0.8852	45	−2.2500	1.5107	79	−1.2283	−0.6322
12	1.0021	1.6191	46	−0.6508	2.2500	80	−1.5967	0.0574
13	0.9222	1.2147	47	−0.5783	1.7038	81	−0.1275	−0.5602
14	1.6452	0.9023	48	−1.3748	2.2500	82	−0.4969	−0.9052
15	1.7060	0.5070	49	−1.7157	1.4082	83	−0.8321	−0.6869
16	0.5312	1.1304	50	−2.1365	2.2500	84	−1.0775	−1.0027
17	0.6118	1.7067	51	0.2010	−0.3320	85	−2.2500	−0.1172
18	0.6566	2.2500	52	0.5510	−0.0475	86	−0.1005	−0.9593
19	1.5374	1.7433	53	0.9129	−0.2180	87	−1.1887	−1.6997
20	2.2500	1.5250	54	1.2597	−0.0023	88	−0.7420	−1.2212
21	−0.0008	2.2500	55	1.6232	−0.2884	89	−1.6147	−0.7357
22	0.2173	1.6409	56	0.2316	−0.7364	90	−1.7974	−0.3127
23	1.3883	2.2500	57	0.5844	−0.4462	91	−0.2835	−1.7854
24	1.6810	1.3700	58	0.9373	−0.6345	92	−0.7249	−1.6209
25	2.1634	2.2500	59	1.7213	−0.6761	93	−0.9141	−2.2500
26	−0.1942	0.2370	60	2.2500	0.0677	94	−1.5683	−1.5736
27	−0.5227	0.0088	61	0.2586	−1.1355	95	−2.2500	−0.9730
28	−0.9491	0.1685	62	0.6483	−0.9860	96	−0.0668	−2.2500
29	−1.2393	−0.1222	63	1.0469	−1.0192	97	0.2083	−1.6502
30	−1.4561	0.4319	64	1.3252	−0.7319	98	−1.7286	−2.2500
31	−0.2497	0.6332	65	2.2500	−0.5625	99	−1.7155	−1.2017
32	−0.6205	0.3967	66	−0.1765	−1.3632	100	−2.2500	−1.7917
33	−0.6768	0.8547	67	0.7670	−1.3854			
34	−0.9880	0.5666	68	1.2100	−1.6765			

6.3.4.3 Planar Arrays with Maximum Beam Efficiency in Circular Region of Interest and Various Constraints

Example 6.3.4.2 considered planar arrays radiating energy into a rectangular region. Here, circular region of interest with radius $r = \sin(\theta_s) = 0.2$ is considered. Arrays with two geometries are optimized − one in which elements are placed within a square area and the other in which they are placed within a circular area. In both cases, symmetric element positions are used.

Array with Elements Placed Within Square Area

An array with 100 elements is designed with minimum interelement spacing $d_{min} = 0.4\lambda$, SLL constrained to $\delta_{max} = -12$ dB, and the elements placed within a square area given by $x_{min} = y_{min} = -2.25\lambda$ and $x_{max} = y_{max} = 2.25\lambda$. The optimization of a symmetric array with the same specifications is performed in [60] by using particle swarm optimization.

The design is performed by solving the problem in (6.25). The optimization starts from the array obtained in [60] (see Figure 3 therein). Optimization's convergence rate is shown in Figure 6.17. The algorithm converges in 98 iterations, all of which are placed inside the feasible region. The required computational time equals 186.82 s.

Table 6.20 shows the comparison of the proposed array and the corresponding array from [60]. It is clear that the proposed array provides 2.96 % higher beam efficiency, slightly lower SLL, and wider main beam. Figure 6.18 shows elements' positions of the proposed array together with the corresponding array factor. The positions' numerical values are given in Table 6.21, for convenience.
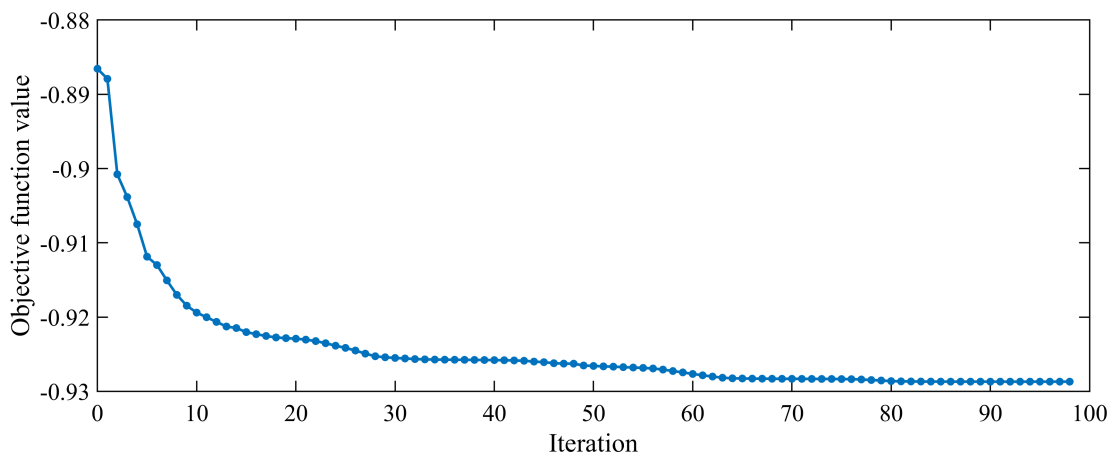

Figure 6.17: Convergence rate of optimization of array with 100 elements placed within square area. All iteration points are placed inside feasible region.

Table 6.20: Beam efficiency, BE, 3 dB cutoff, θ_{3dB}, position of first zero, θ_z, sidelobe level, SLL, and directivity, D, of proposed array with elements placed within square area and of corresponding array from [60].

Design method	BE, %	θ_{3dB}, deg	θ_z, deg	SLL, dB	D, dB
Proposed	92.92	5.92	14.28	-12.48	24.3
Particle swarm [60]	89.96	5.63	13.41	-12.30	24.3
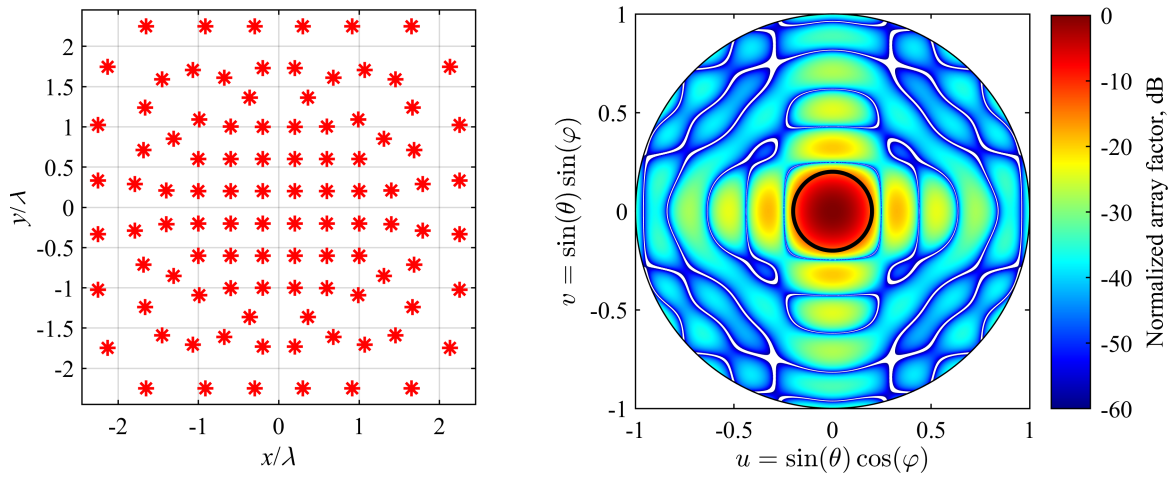
Figure 6.18: Element positions of optimum symmetric array with 100 elements placed within square area (left) and corresponding normalized array factor (right). Region of interest is drawn in black.

Table 6.21: Element positions of symmetric array with maximum beam efficiency and 100 elements placed within square area. Only elements in first quadrant are listed.

| n	x_n, λ	y_n, λ	n	x_n, λ	y_n, λ	n	x_n, λ	y_n, λ
1	0.2000	0.2000	10	2.2500	0.3319	19	1.6627	1.2393
2	0.6000	0.2000	11	0.2000	1.0000	20	2.1301	1.7444
3	1.0000	0.2000	12	0.6000	1.0024	21	0.2986	2.2500
4	1.3998	0.2111	13	0.9898	1.0921	22	0.2000	1.7288
5	1.7923	0.2883	14	1.3102	0.8526	23	0.9130	2.2500
6	0.2000	0.6000	15	2.2500	1.0220	24	1.4518	1.5889
7	0.6000	0.6000	16	0.3650	1.3644	25	1.6513	2.2500
8	1.0000	0.6000	17	0.6803	1.6106			
9	1.6849	0.7126	18	1.0690	1.7049			

Array with Elements Placed Within Circular Area

Taking into account that beam efficiency is maximized assuming circular region of interest, it is more appropriate to place the elements within a circular area. Therefore, in this example, such a design is considered. Array with 76 elements is optimized. Element positions are constrained to fit into a circle of radius $R_a = 2.25\lambda$. Moreover, interelement spacing is constrained to $d_{min} = 0.4\lambda$ and SLL is constrained to $\delta_{max} = -15$ dB. The design is performed by solving the problem in (6.28).

The optimization starting point is obtained from equidistant square array with 100 elements and the interelement spacing of $\lambda/2$. From this array, the elements that are distanced from the origin more than 2.4λ are removed, thus resulting in 76 elements which are used as a starting point. Clearly, such a starting point is infeasible. However, the used SQP solver handles infeasible points well. It is illustrated in Figure 6.19, which shows the convergence rate of the performed optimization. Clearly, a large number of iterations following the initial one are infeasible. However, the algorithm converged to a feasible solution in 376 iterations, requiring the computational time of 545.30 s.

Parameters of the proposed array are given in Table 6.22 together with the parameters of the array presented in Table IV in [84]. These two arrays have the same number of elements and the same radius of the region of interest. However, the array referred to is equidistant, with nonuniform coefficients. Clearly, these two arrays are not suitable for the comparison. Nevertheless, their analysis illustrates gain that can be achieved with unequally-spaced uniformly-excited arrays. Clearly, for the same beam efficiency, unequally spaced array can provide narrower beam and lower sidelobe level.

Figure 6.20 shows elements' positions of the proposed array together with the corresponding array factor. The positions' numerical values are given in Table 6.23, for convenience.
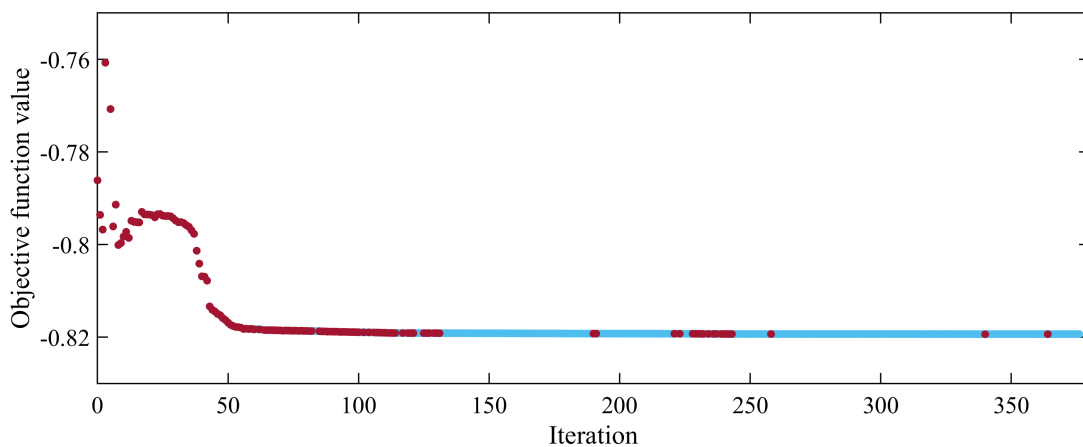
Figure 6.19: Convergence rate of optimization of array with 76 elements placed within circular area. Red color indicates infeasible, whereas cyan indicates feasible points.

Table 6.22: Beam efficiency, BE, position of first zero, θ_z, and sidelobe level, SLL, of proposed array with elements placed within circular area and of corresponding array from [84].

Design method	BE, %	θ_z, deg	SLL, dB
Proposed	81.94	13.95	-15.00
Method in [84]	81.54	24.65	-6.62
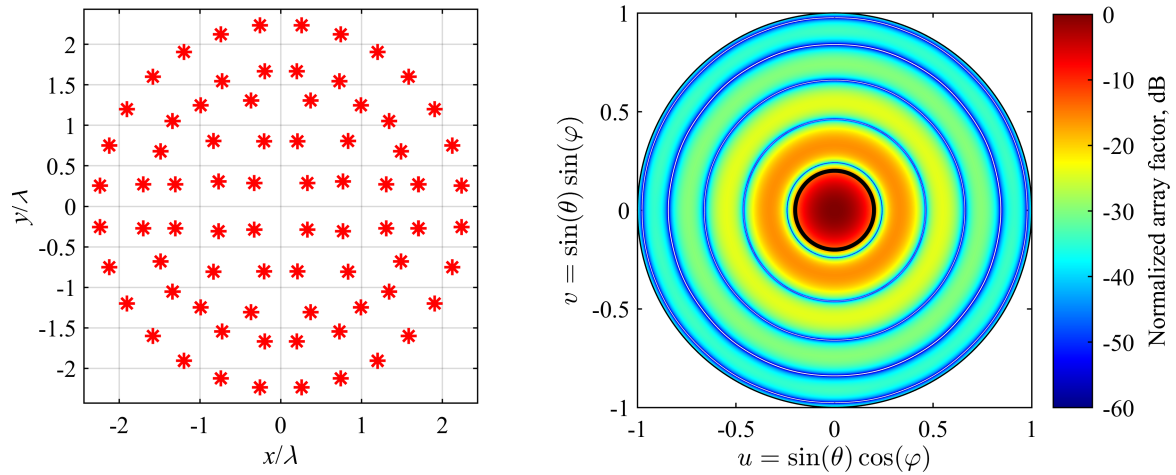
Figure 6.20: Element positions of optimum symmetric array with 76 elements placed in circular area (left) and corresponding normalized array factor (right). Region of interest is drawn in black.

Table 6.23: Element positions of symmetric array with maximum beam efficiency and 76 elements placed within circular area. Only elements in first quadrant are listed.

n	x_n, λ	y_n, λ	n	x_n, λ	y_n, λ	n	x_n, λ	y_n, λ
1	0.3310	0.2879	8	0.7244	1.5466	15	1.7031	0.2731
2	0.2054	0.8023	9	1.1971	1.9051	16	1.4863	0.6802
3	0.3689	1.3061	10	0.7401	2.1248	17	1.9042	1.1985
4	0.2000	1.6687	11	1.3031	0.2699	18	2.2354	0.2560
5	0.2563	2.2354	12	0.8312	0.8080	19	2.1202	0.7532
6	0.7707	0.3064	13	1.3393	1.0522			
7	0.9904	1.2479	14	1.5821	1.5998			

6.3.4.4 Planar Arrays with Maximum Directivity and Constrained Sidelobe Level

In this example, directivity maximization of symmetric arrays with constrained sidelobe level is illustrated. In [90], the maximization of directivity with constrained SLL was performed for sparse arrays with predefined element positions, assuming the excitations are design variables. In the paper referred to, authors considered arrays with 85 elements and SLL constrained to $\delta_{max} = -20$dB. They found that applying the SLL constraints in various sidelobe regions of

interest, $\theta_s = 14°, 15°, ..., 26°$, does not influence the obtained directivity (see Figure 6a in [90]). Normalized array factor obtained by the method from [90] for $\theta_s = 14°$ is shown in Figure 6.21.
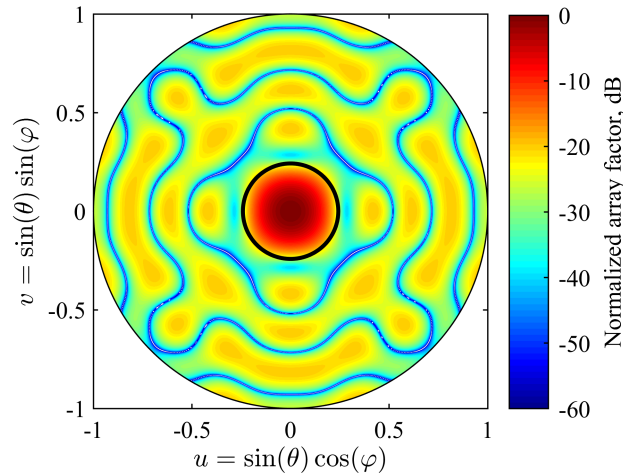
Figure 6.21: Normalized array factor obtained by method from [90] for $\theta_s = 14°$. Start of sidelobe region is drawn in black.

Here, the excitations are uniform whereas the element positions are optimized. The optimum arrays are obtained by solving the constrained optimization problem in (6.29), in which only the constraints set on SLL, (6.29c), are used. The optimizations are performed starting from the array in [90]. In addition, the optimizations are repeated starting from various randomly generated layouts. The layouts are obtained by changing the element positions of the array in [90] randomly in the range of $\pm 0.5\lambda$.

The SLL constraints are defined with the aforementioned values of θ_s and δ_{max}. However, the proposed approach allows lowering θ_s down to $8°$. Consequently, a narrower main beam can be obtained. In addition, the proposed arrays provide up to 5 dB higher directivity than do the arrays in [90]. Finally, the directivity exhibits low dependency on θ_s, which is similar behavior to that encountered in [90]. These observations are illustrated in Table 6.24, which shows the comparison of the proposed arrays and the arrays from [90], obtained for $\theta_s = 8°, 14°, 26°$.

Table 6.24: Directivity, D, 3 dB cutoffs and positions of first zeros calculated along x and y axis, $\theta_{3dB}^{(x)}$, $\theta_{3dB}^{(y)}$, $\theta_z^{(x)}$, and $\theta_z^{(y)}$, of proposed arrays and arrays in [90], obtained for various starts of sidelobe region, θ_s.

| θ_s, | | Arrays in [90] | | | | Proposed arrays | | | |
| | D, | $\theta_{3dB}^{(x)}$, | $\theta_{3dB}^{(y)}$, | $\theta_z^{(x)}$, | $\theta_z^{(y)}$, | D, | $\theta_{3dB}^{(x)}$, | $\theta_{3dB}^{(y)}$, | $\theta_z^{(x)}$, | $\theta_z^{(y)}$, |
deg	dB	deg	deg	deg	deg	dB	deg	deg	deg	deg
8	-	-	-	-	-	27.9	3.7	3.3	9.0	8.1
14	23.4	5.5	5.5	16.6	16.6	28.4	2.8	3.5	6.5	8.0
26	23.4	5.5	5.5	16.6	16.6	28.5	3.1	3.2	7.6	7.9

In the proposed arrays, higher directivities and narrower main beams are the consequences of increased arrays' sizes. For example, size of the array obtained for $\theta_s = 8°$ equals $8.29\lambda \times 8.57\lambda$, which is an increase of 71% compared to the array in [90]. However, it is important to note that the proposed arrays consist of uniformly excited elements, which reduces the design freedom that is here compensated with unequal spacing and by increasing the array size.

Changing the boundaries of the sidelobe region causes a redistribution of power in the power pattern. This may cause rising of the sidelobes in the region where SLL is not constrained, whereas directivity remains approximately the same. Therefore, in practice, it is best to employ SLL constraints in the region starting from the lowest possible θ_s. This is illustrated in Figure 6.22, which shows the optimum array factors together with corresponding elements' positions obtained for $\theta_s = 8°, 14°, 26°$. Clearly, for $\theta_s = 14°$ and $\theta_s = 26°$, unwanted lobes are obtained between the main lobe and the beginning of the sidelobe region.
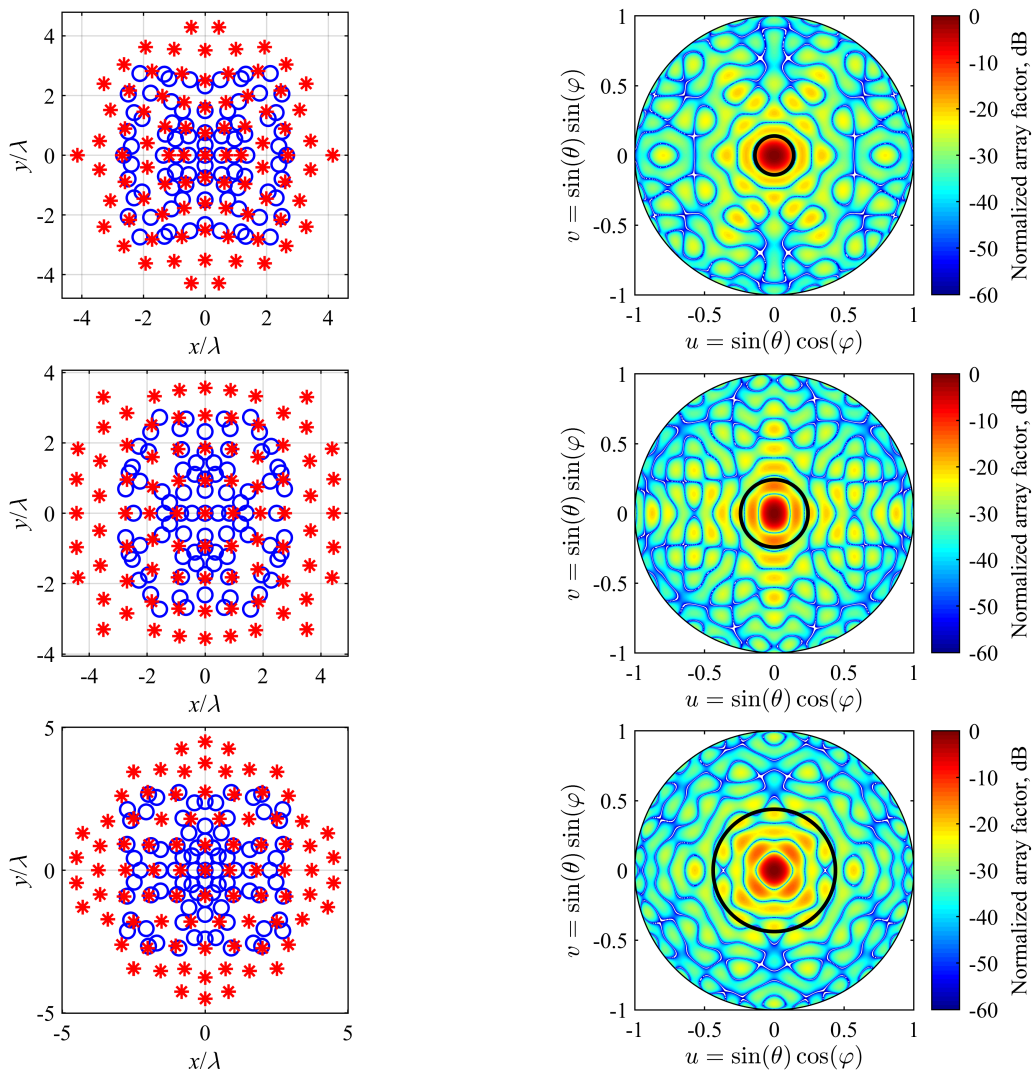
Figure 6.22: Starting (blue) and optimum (red) element positions of antenna arrays with 85 elements obtained for various starts of sidelobe region, $\theta_s = 8°$, $\theta_s = 14°$, and $\theta_s = 26°$ (left) and corresponding normalized array factors (right). Starts of sidelobe regions are drawn in black.

Numerical values of optimum positions obtained with $\theta_s = 8°$ are given in Table 6.25, for convenience.

Table 6.25: Element positions of symmetric array with maximum directivity, constrained sidelobe level, and 85 elements, obtained for $\theta_s = 8°$. Only elements in first quadrant and on positive x and y axes are listed.

n	x_n, λ	y_n, λ	n	x_n, λ	y_n, λ	n	x_n, λ	y_n, λ
1	0.0000	0.0000	10	0.4443	4.2864	19	0.6278	0.9101
2	2.6917	0.0000	11	0.9981	3.5547	20	0.6731	1.7688
3	0.6818	0.0000	12	2.6335	3.0353	21	1.9884	1.4576
4	1.1705	0.0000	13	2.4587	2.1706	22	3.4254	0.4805
5	4.1427	0.0000	14	0.7521	2.7315	23	1.8762	0.4059
6	0.0000	2.5019	15	1.9306	3.6192	24	1.3004	0.9572
7	0.0000	3.5111	16	3.2790	2.3927	25	2.5980	0.8893
8	0.0000	1.6137	17	1.3818	1.9821	26	1.7199	2.8171
9	0.0000	0.7386	18	3.0746	1.5196			

6.3.4.5 Planar Arrays with Maximum Directivity and Various Constraints

In the example considered in Section 6.3.4.4, directivity was optimized without constraints on array's size and interelement spacing. It was shown that a significantly higher directivity can be obtained at the expense of increased array size. Here, the example from Section 6.3.4.4 is extended with constraints on the array size and interlement spacing. Such a design is performed by solving the problem in (6.29).

Since in aforementioned example the array size was not constrained, the sidelobe region could start already at $\theta_s = 8°$. Here, the array size is constrained to $5\lambda \times 5\lambda$, which corresponds to the size of the array in [90], i.e. $x_{min} = y_{min} = -2.5\lambda$ and $x_{max} = y_{max} = 2.5\lambda$. Note that this is significantly smaller than the size of $8.29\lambda \times 8.57\lambda$ obtained for $\theta_s = 8°$ in 6.3.4.4. Consequently, with θ_s as low as $8°$, the proposed optimization cannot find a feasible solution. Therefore, in this example, the SLL-constraint region starts at $\theta_s = 14°$ and SLL is constrained to $\delta_{max} = -20$ dB. In addition, to prevent closely spaced elements, minimum interelement spacing is constrained to $d_{min} = 0.5\lambda$. One symmetric array and one array with arbitrary positions are considered. Optimizations start from the positions of elements in the array from [90].

Figure 6.23 shows the convergence rates of SQP algorithm for both − arbitrary and symmetric − array designs. The design with arbitrary positions contains 170, whereas the design with symmetric positions contains 42 variables. Consequently, a significantly higher number of iterations is required for the algorithm to converge in the former case, i.e. 943 iterations for

the array with arbitrary element positions compared to 195 iterations for the symmetric array, requiring the computational time of 320.35 s and 46.42 s. By utilizing arbitrary positions, somewhat lower objective function value is achieved, which results in only 0.1 dB higher directivity.

Table 6.26 shows the comparison of the proposed arrays and the array from [90]. Clearly, the proposed arrays provide up to 2 dB higher directivity and narrower main beam than does the array from [90]. Note that it was achieved by utilizing only one excitation level (and nonequidistant elements), whereas the array from [90] has a significantly higher dynamic range ratio of 11.8. Figures 6.24 and 6.25 show the positions of the proposed arrays together with the corresponding array factors. Element positions of the proposed arrays are given in Tables 6.27 6.28, for convenience.
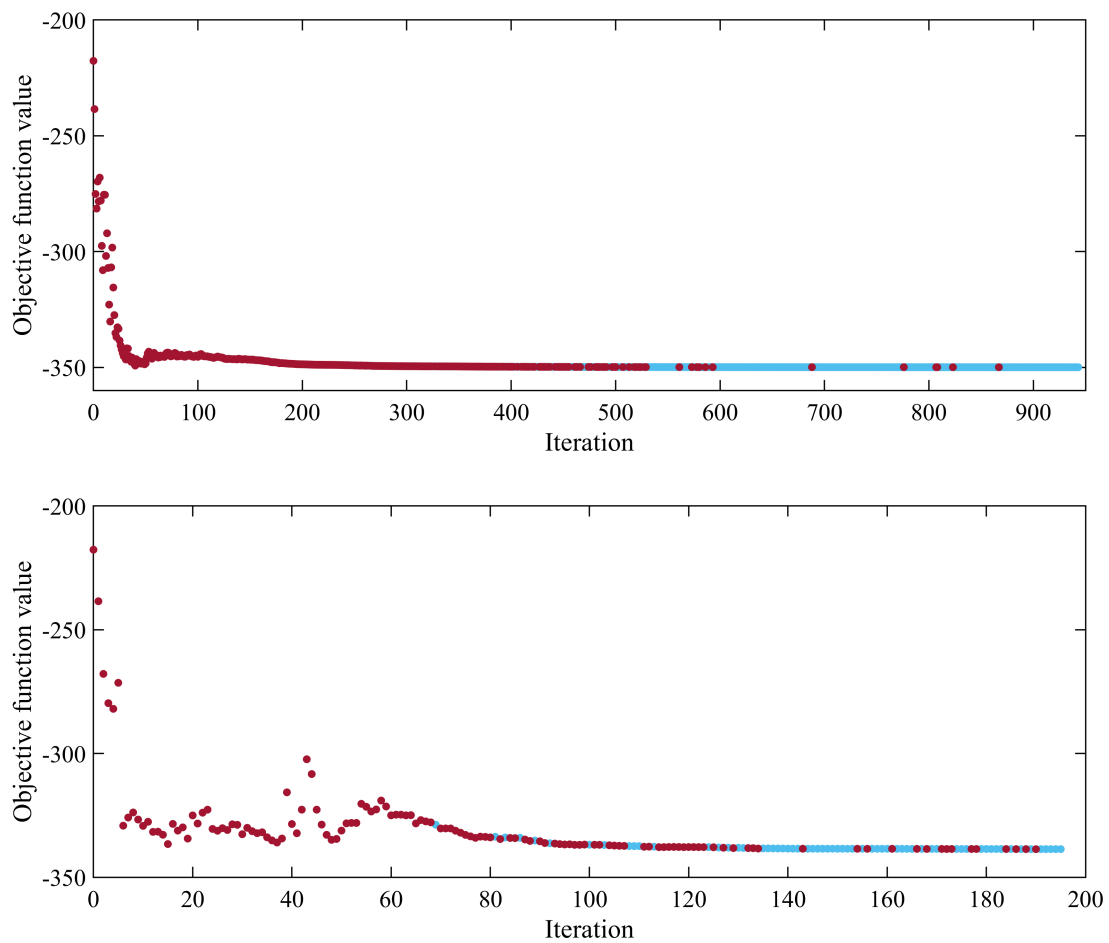
Figure 6.23: Convergence rates of optimizations performed for planar arrays with arbitrary (top) and symmetric (bottom) elements' positions. Red color indicates infeasible points, whereas cyan indicates feasible points.

Table 6.26: Directivity, D, 3dB cutoff, θ_{3dB}, and position of first zero, θ_z, of proposed arrays with arbitrary and symmetric element positions, and of array from [90], obtained for start of sidelobe region $\theta_s = 14°$.

Design method	D, dB	θ_{3dB}, deg	θ_z, deg
Proposed, arbitrary positions	25.4	5.0	12.0
Proposed, symmetric positions	25.3	5.0	12.0
Method from [90]	23.4	5.5	16.6
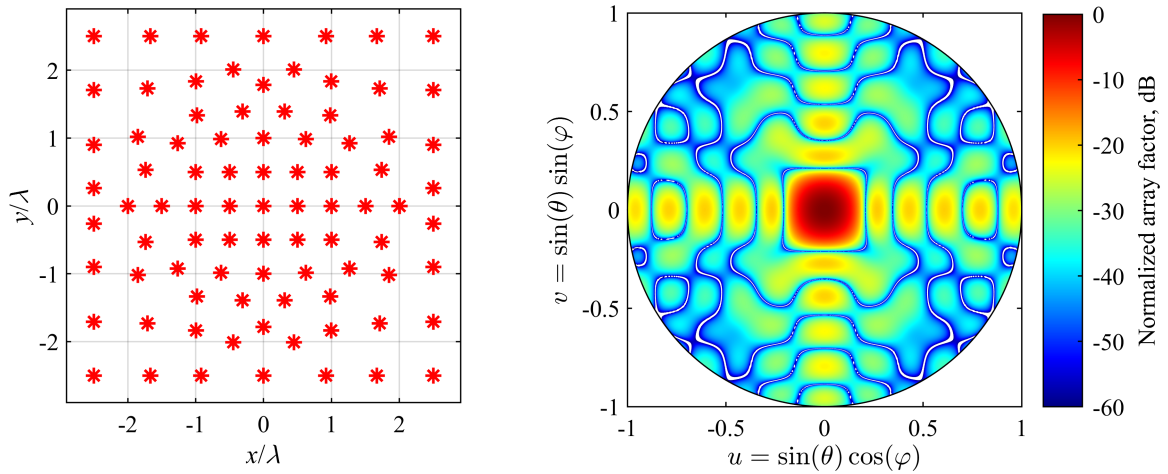
Figure 6.24: Element positions of optimum symmetric array with 85 elements (left) and corresponding normalized array factor (right).
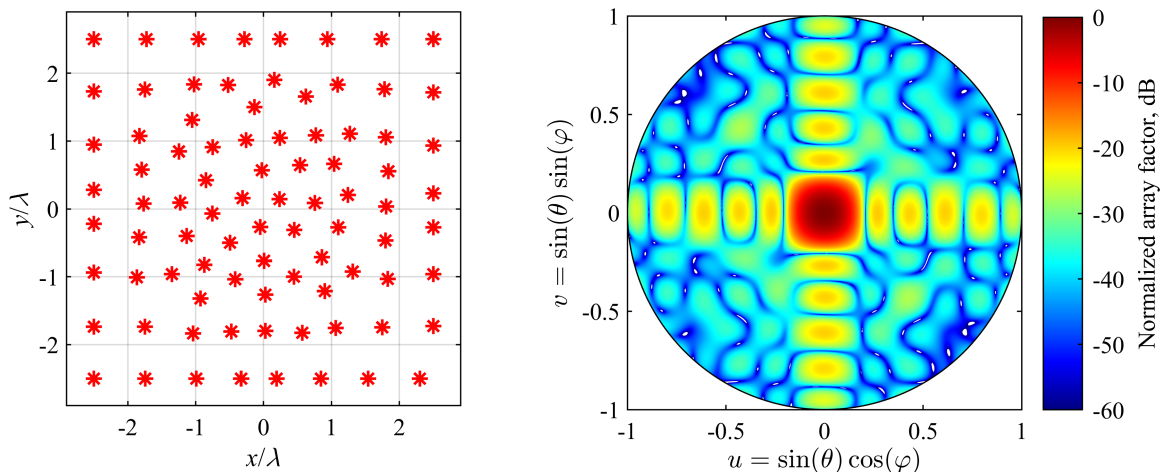
Figure 6.25: Element positions of optimum array with 85 elements and no symmetry requirement (left) and corresponding normalized array factor (right).

Table 6.27: Element positions of array with maximum directivity, 85 elements, and no symmetry requirement.

n	x_n, λ	y_n, λ	n	x_n, λ	y_n, λ	n	x_n, λ	y_n, λ
1	−1.7226	2.5000	30	−2.5000	0.9462	59	−1.8656	−1.0073
2	−0.9549	2.5000	31	−1.7935	0.5773	60	−0.8709	−0.8240
3	−0.2806	2.5000	32	−1.2446	0.8492	61	−0.4174	−1.0348
4	0.2418	2.5000	33	−0.7484	0.9107	62	0.0268	−1.2642
5	0.6232	1.6546	34	−0.0257	0.5707	63	0.4493	−0.9967
6	0.9373	2.5000	35	0.2352	0.1442	64	1.8281	−1.0340
7	1.7409	2.5000	36	0.7553	0.0886	65	2.5000	−0.9623
8	1.7823	1.7623	37	1.8404	0.5554	66	−2.5000	−0.9379
9	2.5000	2.5000	38	1.8064	0.0333	67	−1.3519	−0.9605
10	−2.5000	2.5000	39	−1.7663	0.0780	68	−0.9293	−1.3206
11	−1.0211	1.8330	40	−1.2261	0.0935	69	0.0264	−1.7986
12	−0.5211	1.8275	41	−0.8481	0.4207	70	1.7482	−1.7449
13	1.0918	1.8288	42	−0.3094	0.1589	71	−2.5000	−1.7339
14	1.2692	1.1062	43	−0.0484	−0.2676	72	−1.7478	−1.7343
15	2.5000	1.7146	44	0.4500	−0.3074	73	−1.0382	−1.8371
16	−1.7462	1.7574	45	1.1006	−0.2731	74	0.5699	−1.8269
17	0.1594	1.9008	46	1.2412	0.2068	75	1.0644	−1.7530
18	−0.1363	1.4976	47	1.7960	−0.4666	76	2.5000	−1.7265
19	0.7696	1.0856	48	−2.5000	0.2816	77	−2.5000	−2.5000
20	2.5000	0.9338	49	−1.1318	−0.3975	78	−1.7443	−2.5000
21	−2.5000	1.7310	50	−0.7537	−0.0703	79	−0.9912	−2.5000
22	−1.8289	1.0760	51	−0.4928	−0.4968	80	−0.3326	−2.5000
23	−1.0497	1.3097	52	0.0065	−0.7646	81	−0.4736	−1.8044
24	−0.2590	1.0129	53	0.8598	−0.7113	82	0.1934	−2.5000
25	0.2400	1.0445	54	0.9018	−1.2095	83	0.8435	−2.5000
26	0.5376	0.6427	55	1.3123	−0.9240	84	1.5385	−2.5000
27	1.0372	0.6633	56	2.5000	−0.2700	85	2.3014	−2.5000
28	1.7982	1.0536	57	−2.5000	−0.2184			
29	2.5000	0.2300	58	−1.8330	−0.4175			

Table 6.28: Element positions of symmetric array with maximum directivity and 85 elements. Only elements in first quadrant and on positive x and y axes are listed.

n	x_n, λ	y_n, λ	n	x_n, λ	y_n, λ	n	x_n, λ	y_n, λ
1	0.0000	0.0000	10	0.4456	2.0116	19	0.6245	0.9843
2	0.5000	0.0000	11	0.9206	2.5000	20	0.9801	1.3357
3	1.0000	0.0000	12	1.6684	2.5000	21	1.2644	0.9244
4	1.5000	0.0000	13	2.5000	2.5000	22	2.5000	0.9017
5	2.0000	0.0000	14	0.9947	1.8355	23	0.5000	0.5000
6	0.0000	2.5000	15	1.7081	1.7326	24	1.0000	0.5000
7	0.0000	1.7823	16	2.5000	1.7097	25	1.7379	0.5312
8	0.0000	1.0000	17	0.3115	1.3911	26	2.5000	0.2629
9	0.0000	0.5000	18	1.8492	1.0186			

6.3.5 Concluding Remarks

Extensive examples considering constrained optimization via SQP show that the proposed approach is suitable for designing linear and planar arrays with various requirements.

In the case of uniformly-excited unequally-spaced linear arrays with maximum beam efficiency, the same results are obtained as by the evolutionary methods. The application of the proposed approach in optimization of planar arrays improves directivity and beam efficiency. In optimization of beam efficiency, the improvement has been encountered in the design of square arrays with square and circular regions of interest, as well as in the design of circular arrays with circular region of interest. In optimization of directivity, the proposed method has been successfully applied in the design of uniformly-excited unequally-spaced antenna arrays with constrained minimum interelement spacing, maximum sidelobe level, and maximum array size.

The proposed method based on SQP is straightforward and it can be easily utilized in solving various optimization problems with different constraints. In addition, it exhibits fast convergence, which makes it suitable for experimenting with various design criteria.

Chapter 7

Conclusion

Three new methods for the design of pencil-beam antenna arrays with low dynamic range ratio of excitation coefficients have been presented in this dissertation.

The first method is based on convex optimization of linear pencil-beam arrays with minimum L_1-norm. Such optimization is performed for the arrays with predefined positions of antenna elements. If the elements are placed at the spacing of $\lambda/2$, the resulting optimum arrays exhibit maximum sidelobe level of approximately -21 dB for any number of antenna elements, with the sidelobes that monotonically decrease as the angle increases. Therefore, the L_1 pencil beams radiate very small amount of power in the sidelobe region. The corresponding antenna coefficients are bell-shaped with positive magnitudes. Their dynamic range ratio increases linearly as the number of elements increases and generally takes low values.

Even though the DRR of L_1 pencil beams is generally low, in some applications it could still be too high to be realized with available beamforming networks. This problem has been overcome by incorporating DRR constraints into the design. The second method proposed in this dissertation performs the optimization of L_1 pencil beams with constrained DRR and constrained maximum sidelobe level. The latter have been incorporated to prevent deterioration in the array factor caused by the DRR constraints. Since the DRR constraints are not convex, the proposed method utilizes global search based on branch and bound algorithm that employs convex optimization and feasibility test for tree pruning. The method supports real-valued coefficients with arbitrary signs as well as an independent control of DRR and SLL.

Finally, the design of uniformly-excited unequally-spaced arrays has been considered. The design of such arrays leads to nonlinear and nonconvex problems. For their solving, general-purpose methods for nonlinear optimization have been proposed. The application of these methods proved efficient in unconstrained and constrained design of linear and planar arrays with maximum beam efficiency and with maximum directivity. The proposed approach ensures fast convergence and enables very simple formulation of the design problems. Several examples have been provided, showing that the proposed approach is suitable for improving the results obtained by other methods.

Bibliography

[1] Balains, C. A., Antenna Theory: Analysis and Design, Fourth Edition. Hoboken, New Jersey: John Wiley & Sons, 2016.

[2] Kildal, P.-S., Foundations of Antenna Engineering: A Unified Approach for Line-of-Sight and Multipath. Gothenburg, Sweden: Kildal Antenn AB, 2015.

[3] Orfanidis, S. J., Electromagnetic Waves and Antennas. Piscataway, New Jersey: Rutgers University, 2016.

[4] Schmalenberg, P., Dede, E. M., Nomura, T., Nishiwaki, S., "Optimization of planar phased arrays for vehicles", IEEE Antennas and Wireless Propagation Letters, Vol. 21, No. 10, October 2022, pp. 2140-2144.

[5] Toso, G., Mangenot, C., Roederer, A. G., "Sparse and thinned arrays for multiple beam satellite applications", in Proceedings of 2nd European Conference on Antennas and Propagation, Edinburgh, UK, November 2007, pp. 1-4.

[6] Bucci, O. M., Isernia, T., Perna, S., Pinchera, D., "Isophoric sparse arrays ensuring global coverage in satellite communications", IEEE Transactions on Antennas and Propagation, Vol. 62, No. 4, April 2014, pp. 1607-1618.

[7] Sadhu, B., et al., "A 28 GHz 32-element phased array transceiver IC with concurrent dual polarized beams and 1.4 degree beam-steering resolution for 5G communication", in Proceedings of 2017 IEEE International Solid-State Circuits Conference, San Francisco, CA, USA, February 2017, pp. 128-129.

[8] Valkonen, R., "A 28 GHz 32-element phased array transceiver IC with concurrent dual polarized beams and 1.4 degree beam-steering resolution for 5G communication", in Proceedings of 2018 IEEE/MTT-S International Microwave Symposium - IMS, Philadelphia, PA, USA, June 2018, pp. 1334-1337.

[9] Shinohara, N., Zhou, J., Far-Field Wireless Power Transfer and Energy Harvesting. Norwood, Massachusetts: Artech House, 2022.

[10] Shinohara, N., Ed., Recent Wireless Power Transfer Technologies via Radio Waves. Gistrup, Denmark: River Publishers, 2018.

[11] Massa, A., Oliveri, G., Viani, F., Rocca, P., "Array designs for long-distance wireless power transmission: state-of-the-art and innovative solutions", Proceedings of the IEEE, Vol. 101, No. 6, June 2013, pp. 1464-1481.

[12] Dewdney, P. E., Hall, P. J., Schilizzi, R. T., Lazio, T. J. L. W., "The Square Kilometre Array", Proceedings of the IEEE, Vol. 97, No. 8, August 2009, pp. 1482-1496.

[13] de Vos, M., Gunst, A. W., Nijboer, R., "The LOFAR telescope: system architecture and signal processing", Proceedings of the IEEE, Vol. 97, No. 8, August 2009, pp. 1431-1437.

[14] Iero, D. A. M., Isernia, T., Morabito, A. F., Catapano, I., Crocco, L., "Optimal constrained field focusing for hyperthermia cancer therapy: a feasibility assessment on realistic phantoms", Progress In Electromagnetics Research, Vol. 102, 2010, pp. 125-141.

[15] Veen, B. D. V., Buckley, K. M., "Beamforming: a versatile approach to spatial filtering", IEEE Acoustics, Speech, and Signal Processing Magazine, Vol. 5, No. 2, April 1988, pp. 4-24.

[16] Mailloux, R. J., Phased Array Antenna Handbook, Third Edition. Norwood, Massachusetts: Artech House, 2018.

[17] Vescovo, R., "Consistency of constraints on nulls and on dynamic range ratio in pattern synthesis for antenna arrays", IEEE Transactions on Antennas and Propagation, Vol. 55, No. 10, October 2007, pp. 2662-2670.

[18] Skolnik, M. I., Nemhauser, G., Sherman, J. W., "Dynamic programming applied to unequally spaced arrays", IEEE Transactions on Antennas and Propagation, Vol. 12, No. 1, January 1964, pp. 35-43.

[19] Miao, Y., Liu, F., Lu, J., Li, K., "Synthesis of unequally spaced arrays with uniform excitation via iterative second-order cone programming", IEEE Transactions on Antennas and Propagation, Vol. 68, No. 8, August 2020, pp. 6013-6021.

[20] Bucci, O. M., D'Urso, M., Isernia, T., Angeletti, P., Toso, G., "Deterministic synthesis of uniform amplitude sparse arrays via new density taper techniques", IEEE Transactions on Antennas and Propagation, Vol. 58, No. 6, June 2010, pp. 1949-1958.

[21] Dolph, C. L., "A current distribution for broadside arrays which optimizes the relationship between beam width and sidelobe level", Proceedings of the IRE, Vol. 34, No. 6, June 1946, pp. 335-348.

[22] Buttazzoni, G., Vescovo, R., "Gaussian approach versus Dolph-Chebyshev synthesis of pencil beams for linear antenna arrays", Electronics Letters, Vol. 54, No. 1, January 2018, pp. 8-10.

[23] Santos, F. E. S., Azevedo, J. A. R., "Adapted raised cosine window function for array factor control with dynamic range ratio limitation", in Proceedings of 11th European Conference on Antennas and Propagation, Paris, France, March 2017, pp. 2020-2024.

[24] Molnar, G., Matijascic, M., "Gegenbauer arrays with minimum dynamic range ratio and maximum beam efficiency", in Proceedings of 2020 IEEE International Symposium on Antennas and Propagation and North American Radio Science Meeting (AP-S/URSI 2020), Montreal, Quebec, Canada, July 2020, pp. 234-244.

[25] Molnar, G., Babić, M., Šipuš, Z., "Closed-form design of optimum linear arrays based on raised-cosine beampattern", in Proceedings of 2020 IEEE International Symposium on Antennas and Propagation and North American Radio Science Meeting (AP-S/URSI 2020), Montreal, Quebec, Canada, July 2020, pp. 1889-1890.

[26] Molnar, G., Matijaščić, M., "Window-to-polynomial transform and its application in antenna array design", in Proceedings of 14th European Conference on Antennas and Propagation, Copenhagen, Denmark, March 2020, pp. 1-5.

[27] Molnar, G., Ljubenko, D., Jelavić-Šako, A., "Antenna array design based on Kaiser-Hamming polynomials", in Proceedings of 15th European Conference on Antennas and Propagation, Düsseldorf, Germany, March 2021, pp. 1-5.

[28] Keizer, W. P. M. N., "Low-sidelobe pattern synthesis using iterative fourier techniques coded in MATLAB [EM programmer's notebook]", IEEE Antennas and Propagation Magazine, Vol. 51, No. 2, April 2009, pp. 137-150.

[29] Nai, S. E., Ser, W., Yu, Z. L., Chen, H., "Beampattern synthesis for linear and planar arrays with antenna selection by convex optimization", IEEE Transactions on Antennas and Propagation, Vol. 58, No. 12, December 2007, pp. 3923-3930.

[30] Fuchs, B., Rondineau, S., "Array pattern synthesis with excitation control via norm minimization", IEEE Transactions on Antennas and Propagation, Vol. 64, No. 10, October 2016, pp. 4228-4234.

[31] Mahanti, G. K., Chakraborty, A., Das, S., "Design of fully digital controlled reconfigurable array antennas with fixed dynamic range ratio", Journal of Electromagnetic Waves and Applications, Vol. 21, January 2007, pp. 97-106.

[32] Fan, X., Liang, J., So, H. C., "Beampattern synthesis with minimal dynamic range ratio", Signal Processing, Vol. 152, November 2018, pp. 411–416.

[33] Fan, X., Liang, J., Zhang, Y., So, H. C., Zhao, X., "Shaped power pattern synthesis with minimization of dynamic range ratio", IEEE Transactions on Antennas and Propagation, Vol. 67, No. 5, May 2019, pp. 3067–3078.

[34] Zhang, X., Wang, X., So, H. C., "Linear arbitrary array pattern synthesis with shape constraints and excitation range control", IEEE Antennas and Wireless Propagation Letters, Vol. 20, No. 6, June 2021, pp. 1018-1022.

[35] Lin, Z., Hu, H., Lei, S., Li, R., Tian, J., Chen, B., "Low-sidelobe shaped-beam pattern synthesis with amplitude constraints", IEEE Transactions on Antennas and Propagation, Vol. 70, No. 4, April 2022, pp. 2717-2731.

[36] Wang, Y., Yin, W., Zheng, J., "Global convergence of ADMM in nonconvex nonsmooth optimization", Linear Algebra and Its Applications, Vol. 78, January 2019, pp. 29-63.

[37] Bellotti, M. J., Vucic, M., "Global optimization of pencil beams with constrained dynamic range ratio", in Proceedings of 14th European Conference on Antennas and Propagation, Copenhagen, Denmark, March 2020, pp. 1-5.

[38] Matijascic, M., Bellotti, M. J., Vucic, M., Molnar, G., "Optimum synthesis of pencil beams with constrained dynamic range ratio", International Journal of Antennas and Propagation, Vol. 2022, November 2022.

[39] Quijano, J. L. A., Vecchi, G., "Sparse array synthesis via alternating projections", in 2009 IEEE Antennas and Propagation Society International Symposium, Charleston, South Carolina, June 2009, pp. 1-4.

[40] Quijano, J. L. A., Righero, M., Vecchi, G., "Sparse 2-D array placement for arbitrary pattern mask and with excitation constraints: A simple deterministic approach", IEEE Transactions on Antennas and Propagation, Vol. 62, No. 4, April 2014, pp. 1652–1662.

[41] Bellotti, M. J., Vucic, M., "Global optimization of sparse pencil beams with constrained dynamic range ratio", in Proceedings of 2020 IEEE International Symposium on Antennas and Propagation and North American Radio Science Meeting (AP-S/URSI 2020), Montreal, Quebec, Canada, July 2020, pp. 129-130.

[42] Cheng, M., Wu, Q., Yu, C., Wang, H., Hong, W., "Synthesis of a thinned prephased electronically steered phased array using excitation control of both the small amplitude dynamic range ratio and low-resolution phase", IEEE Transactions on Antennas and Propagation, Vol. 72, No. 1, January 2024, pp. 600-613.

[43] Sun, J., Li, H., Jin, C., Cao, A., Zhou, J., "A hybrid algorithm for sparse circular array SLL suppression under the constraint of ADRR", in Proceedings International Conference on Radar Systems (Radar 2017), Belfast, UK, October 2017, pp. 1-5.

[44] Buttazzoni, G., Vescovo, R., "Pencil beam constrained synthesis of linear sparse arrays in presence of coupling effects", in Proceedings of 2018 IEEE International Symposium on Antennas and Propagation USNC/URSI National Radio Science Meeting (AP-S/URSI 2018), Boston, MA, USA, July 2018, pp. 2197-2198.

[45] Buttazzoni, G., Vescovo, R., "Density tapering of linear arrays radiating pencil beams: a new extremely fast gaussian approach", IEEE Transactions on Antennas and Propagation, Vol. 65, No. 12, December 2017, pp. 7372-7377.

[46] Buttazzoni, G., Vescovo, R., "Synthesis of co-polar and cross-polar patterns with dynamic range ratio reduction for phase-only reconfigurable arrays", in Proceedings of 12th European Conference on Antennas and Propagation, Prague, Czech Republic, March 2012, pp. 26-30.

[47] Goudos, S. K., Siakavara, K., Samaras, T., Vafiadis, E. E., Sahalos, J. N., "Self-adaptive differential evolution applied to real-valued antenna and microwave design problems", IEEE Transactions on Antennas and Propagation, Vol. 59, No. 4, April 2011, pp. 1286-1298.

[48] Fuchs, B., Skrivervik, A., Mosig, J. R., "Synthesis of uniform amplitude focused beam arrays", IEEE Antennas and Wireless Propagation Letters, Vol. 11, 2012, pp. 1178-1181.

[49] Zhang, F., Jia, W., Yao, M., "Linear aperiodic array synthesis using differential evolution algorithm", IEEE Antennas and Wireless Propagation Letters, Vol. 12, 2013, pp. 797-800.

[50] Clavier, T., Razavi-Ghods, N., Glineur, F., Gonzalez-Ovejero, D., de Lera Acedo, E., Craeye, C., Alexander, P., "A global-local synthesis approach for large non-regular arrays", IEEE Transactions on Antennas and Propagation, Vol. 62, No. 4, April 2014, pp. 1596-1606.

[51] Gangwar, V. S., Singh, A. K., Singh, S. P., "An effective approach for the synthesis of unequally spaced antenna array by estimating optimum elements density on the aperture", IEEE Antennas and Wireless Propagation Letters, Vol. 16, June 2017, pp. 2278-2282.

[52] Echeveste, J. I., de Aza, M. A. G., Rubio, J., Craeye, C., "Gradient-based aperiodic array synthesis of real arrays with uniform amplitude excitation including mutual coupling", IEEE Transactions on Antennas and Propagation, Vol. 65, No. 2, February 2017, pp. 541-551.

[53] Lei, S., Hu, H., Chen, B., Tang, P., Tian, J., Qiu, X., "An array position refinement algorithm for pencil beam pattern synthesis with high-order Taylor expansion", IEEE Antennas and Wireless Propagation Letters, Vol. 18, No. 9, September 2019, pp. 1766-1770.

[54] Aslan, Y., Puskley, J., Roederer, A., Yarovoy, A., "Multiple beam synthesis of passively cooled 5g planar arrays using convex optimization", IEEE Transactions on Antennas and Propagation, Vol. 68, No. 5, May 2020, pp. 3557-3566.

[55] Pinchera, D., Migliore, M. D., Panariello, G., "Isophoric inflating deflating exploration algorithm (I-IDEA) for equal-amplitude aperiodic arrays", IEEE Transactions on Antennas and Propagation, Vol. 70, No. 11, November 2022, pp. 10 405-10 416.

[56] Li, X., Guo, Y.-X., "The grey wolf optimizer for antenna optimization designs: continuous, binary, single-objective, and multiobjective implementations", IEEE Antennas and Propagation Magazine, Vol. 64, No. 6, December 2022, pp. 29-40.

[57] Yan, C., Xing, P. Y. Z., Huang, S. Y., "Synthesis of planar sparse arrays with minimum spacing constraint", IEEE Antennas and Wireless Propagation Letters, Vol. 17, No. 6, June 2018, pp. 1095-1098.

[58] Lin, Z., Hu, H., Chen, B., Lei, S., Tian, J., Gao, Y., "Shaped-beam pattern synthesis with sidelobe level minimization via nonuniformly-spaced sub-array", IEEE Transactions on Antennas and Propagation, Vol. 70, No. 5, May 2022, pp. 3421-3436.

[59] Yang, J., Yang, P., Yang, F., Xing, Z., "A hybrid approach for the synthesis of nonuniformly spaced and excited linear arrays with strict element spacing constraints", IEEE Transactions on Antennas and Propagation, Vol. 70, No. 7, July 2022, pp. 5521-5533.

[60] Li, X., Duan, B., Zhou, J., Song, L., Zhang, Y., "Planar array synthesis for optimal microwave power transmission with multiple constraints", IEEE Antennas and Wireless Propagation Letters, Vol. 16, February 2017, pp. 70-73.

[61] Buttazzoni, G., Vescovo, R., "Reducing the sidelobe power pattern of linear broadside arrays by refining the element positions", IEEE Antennas and Wireless Propagation Letters, Vol. 17, No. 8, August 2018, pp. 1464-1468.

[62] Zhou, H.-W., Yang, X.-X., Rahim, S., "Synthesis of the sparse uniform-amplitude concentric ring transmitting array for optimal microwave power transmission", International Journal of Antennas and Propagation, Vol. 2018, 2018, pp. 1-8.

[63] Liu, G. X., Qin, Q., Zhang, Q. H., "Linear array synthesis for wireless power transmission based on brain storm optimization algorithm", International Journal of Antennas and Propagation, Vol. 2021, February 2021, pp. 1-8.

[64] Vodvarka, K., Bellotti, M. J., Vucic, M., "Design of unequally spaced antenna arrays with minimum sidelobe power via Quasi-Newton method", in Proceedings of 17th European Conference on Antennas and Propagation, Florence, Italy, March 2023, pp. 1-5.

[65] Vodvarka, K., Bellotti, M. J., Vucic, M., "Design of uniformly-excited unequally-spaced antenna arrays by using nonlinear optimization", IEEE Antennas and Wireless Propagation Letters, Vol. 23, No. 5, May 2024, pp. 1463-1467.

[66] Morabito, A. F., "Synthesis of maximum-efficiency beam arrays via convex programming and compressive sensing", IEEE Antennas and Wireless Propagation Letters, Vol. 16, 2017, pp. 2404-2407.

[67] Poli, L., Oliveri, G., Rocca, P., Salucci, M., Massa, A., "Long-distance WPT unconventional arrays synthesis", Journal of Electromagnetic Waves and Applications, Vol. 31, No. 14, 2017, pp. 1399-1420.

[68] Costa, B. F., Abrao, T., "GA-aided directivity in volumetric and planar massive-antenna array design", Signal Processing, Vol. 405, April 2023.

[69] Antoniou, A., Lu, W.-S., Practical Optimization. New York, NY, USA: Springer, 2007.

[70] Nocedal, J., Wright, S. J., Numerical Optimization. New York, NY, USA: Springer, 1999.

[71] Boyd, S., Vandenberghe, L., Convex Optimization. Cambridge, UK: Cambridge University Press, 2004.

[72] Lobo, M. S., Vandenberghe, L., Boyd, S., Lebret, H., "Applications of second-order cone programming", Linear Algebra and Its Applications, Vol. 284, No. 1, November 1998, pp. 193-228.

[73] Sturm, J. F., "Using SeDuMi1.02, a MATLAB toolbox for optimization over symmetric cones", Optimization Methods and Software, Vol. 11, 1999, pp. 625-653.

[74] MOSEK ApS, "MOSEK Optimization Toolbox for MATLAB, Release 9.2.29", 2020.

[75] Grant, M., Boyd, S., "CVX: Matlab software for disciplined convex programming, version 2.1", 2014.

[76] Lofberg, J., "YALMIP: a toolbox for modeling and optimization in MATLAB", in Proceedings of IEEE International Conference on Robotics and Automation, Taipei, Taiwan, September 2004, pp. 284-289.

[77] Fletcher, R., Practical Methods of Optimization. New York: Wiley, 1987.

[78] Morrison, D. R., Jacobson, S. H., Sauppe, J. J., Sewell, W. C., "Branch-and-bound algorithms: A survey of recent advances in searching, branching, and pruning", Discrete Optimization, Vol. 19, February 2016, pp. 79-102.

[79] Vodvarka, K., Vucic, M., Molnar, G., "Synthesis of Pencil Beams Optimum in L1-Sense", in Proceedings of 2021 IEEE International Symposium on Antennas and Propagation and USNC-URSI Radio Science Meeting, Singapore, Singapore, December 2021, pp. 307-308.

[80] Prasad, S., "On the index for array optimization and the discrete prolate spheroidal functions", IEEE Transactions on Antennas and Propagation, Vol. 30, No. 5, 1982, pp. 1021-1023.

[81] Grossmann, L. D., Eldar, Y. C., "An L_1-method for the design of linear-phase FIR digital filters", IEEE Transactions on Signal Processing, Vol. 55, No. 11, November 2007, pp. 5253-5266.

[82] Vodvarka, K., Bellotti, M. J., Vucic, M., "Synthesis of L1 pencil beams with constrained sidelobe level and dynamic range ratio", in Proceedings of 16th European Conference on Antennas and Propagation, Madrid, Spain, March 2022, pp. 1-5.

[83] Song, Y.-S., Lee, Y. H., "Design of sparse FIR filters based on branch-and-bound algorithm", in Proceedings of the 1997 40th Midwest Symposium on Circuits and Systems, Sacramento, CA, USA, August 1997, pp. 1445-1447.

[84] Oliveri, G., Poli, L., Massa, A., "Maximum efficiency beam synthesis of radiating planar arrays for wireless power transmission", IEEE Transactions on Antennas and Propagation, Vol. 61, No. 5, May 2013, pp. 2490-2499.

[85] MATLAB R2023a, The MathWorks Inc., Natick, MA, USA, 2023.

[86] Lee, M. J., Song, L., Yoon, S., Park, S. R., "Evaluation of directivity for planar antenna arrays", IEEE Antennas and Propagation Magazine, Vol. 42, No. 3, June 2000, pp. 64-67.

[87] Virtanen, P., et. al, "SpiPy 1.0: Fundamental algorithms for scientific computing in python", Nature Methods, Vol. 17, 2020, pp. 261-272.

[88] Constrained Nonlinear Optimization Algorithms, The MathWorks Inc., Natick, MA, USA, February 2024, available at: https://www.mathworks.com/help/optim/ug/constrained-nonlinear-optimization-algorithms.html#brnox0o

[89] Choosing the Algorithm, The MathWorks Inc., Natick, MA, USA, February 2024, available at: https://www.mathworks.com/help/optim/ug/choosing-the-algorithm.html#bsbwxm7

[90] Zhang, Y.-X., Jiao, Y.-C., Zhang, L., "Antenna array directivity maximization with side-lobe level constraints using convex optimization", IEEE Transactions on Antennas and Propagation, Vol. 69, No. 4, April 2021, pp. 2041-2052.

Biography

Katarina Vodvarka was born in 1997. in Zagreb, Croatia. She received the MSc degree in Electronic and Computer Engineering from the University of Zagreb Faculty of Electrical Engineering and Computing, Zagreb, Croatia, in 2020.

Since 2020 she has been employed as a Research Assistant at the University of Zagreb Faculty of Electrical Engineering and Computing. At the same faculty, she enrolled in Doctoral study in winter 2020. The scope of her research covers the optimization methods and the design of antenna arrays. She participated as a researcher on the project HRZZ IP-2019-04-4189 - Efficient Signal Processing Systems for Software Defined Radio, funded by Croatian Science Foundation and led by Prof. Mladen Vučić, PhD. She has been involved in teaching activities in the following courses: Embedded Systems, Embedded System Design and Tools for Digital Design.

She is a member of IEEE Antennas and Propagation Society and IEEE Signal Processing Society.

List of publications

Journal papers

1. Vodvarka, K., Jurisic Bellotti, M., Vucic, M., "Design of uniformly-excited unequally-spaced antenna arrays by using nonlinear optimization", IEEE Antennas and Wireless Propagation Letters, Vol. 23, No. 5, May 2024, pp. 1463-1467.

Papers in conference proceedings

1. Vucic, M., Jurisic Bellotti, M., Vodvarka, K., "Synthesis of flat-top beampattern with minimax sidelobes and constrained dynamic range ratio", in Proceedings of 2023 IEEE International Symposium on Antennas and Propagation and USNC-URSI Radio Science Meeting (AP-S/URSI 2023), Portland, OR, USA, July 2023, pp. 385-386.

2. Vodvarka, K., Jurisic Bellotti, M., Vucic, M., "Design of unequally spaced antenna arrays with minimum sidelobe power via quasi-Newton method", in Proceedings of 17th European Conference on Antennas and Propagation (EuCAP 2023), Florence, Italy, March 2023, pp. 1249-1253.

3. Vodvarka, K., Jurisic Bellotti, M., Vucic, M., "Synthesis of L1 pencil beams with constrained sidelobe level and dynamic range ratio", in Proceedings of 16th European Conference on Antennas and Propagation (EuCAP 2022), Madrid, Spain, March 2022, pp. 1-5.

4. Vodvarka, K., Vucic, M., Molnar G., "Synthesis of pencil beams optimum in L1-sense", in Proceedings of 2021 IEEE International Symposium on Antennas and Propagation and USNC-URSI Radio Science Meeting (AP-S/URSI 2021), Singapore, Singapore, December 2021, pp. 307-308.

Abstracts in conference proceedings

1. Vodvarka, K., Jurisic Bellotti, M., Vucic, M., "Design of unequally spaced antenna arrays via general-purpose optimization methods", Abstract book of 8th International Workshop on Data Science (IWDS 2023), Zagreb, Croatia, 25th October 2023, pp. 62-64.

2. Vodvarka, K., Jurisic Bellotti, M., Vucic, M., "Global design of L1 pencil beams with multiple constraints", Abstract book of 7th International Workshop on Data Science (IWDS 2022), Zagreb, Croatia, 26th October 2022, pp. 15-17.

3. Vodvarka, K., Jurisic Bellotti, M., Vucic, M., "Global design of linear antenna arrays with constrained dynamic range ratio", Abstract book of 6th International Workshop on Data Science (IWDS 2021), Zagreb, Croatia, 24th November 2021, pp. 14-16.

Životopis

Katarina Vodvarka rođena je 1997. godine u Zagrebu, Republika Hrvatska. Diplomirala je 2020. godine na Sveučilištu u Zagrebu Fakultetu elektrotehnike i računarstva, smjer Elektroničko i računalno inženjerstvo.

Od 2020. zaposlena je kao znanstveni novak na Sveučilištu u Zagrebu Fakultetu elektrotehnike i računarstva. Na istom fakultetu upisuje doktorski studij elektrotehnike u zimskom semestru 2020. godine. U sklopu istraživanja bavi se optimizacijskim postupcima i dizajnom antenskih nizova. Kao istraživač sudjelovala je u projektu HRZZ IP-2019-04-4189 - Učinkoviti sustavi za obradu signala namijenjeni programski definiranom radiju, financiranom od Hrvatske zaklade za znanost, pod vodstvom prof. dr. sc. Mladena Vučića. Sudjelovala je u nastavnim aktivnostima na kolegijima Ugradbeni računalni sustavi, Projektiranje ugradbenih računalnih sustava te Alati za razvoj digitalnih sustava.

Članica je udruženja *IEEE Antennas and Propagation Society* i *IEEE Signal Processing Society*.